united nations
educational, scientific
and cultural
organization

international atomic
energy agency

the
abdus salam
international centre for theoretical physics

SMR.1148 - 49

COLLEGE ON MEDICAL PHYSICS
AND
WORKSHOP ON
NUCLEAR DATA FOR SCIENCE AND TECHNOLOGY:
MEDICAL APPLICATIONS
(20 SEPTEMBER - 15 OCTOBER 1999)

"Physics and Applications of ETRAN and ITS Electron-Photon Transport Monte Carlo Codes"

Stephen M. SELTZER
National Institute for Standards & Technology
Radp C-312
Gaithersburg MD-20899-0001
U.S.A.

Physics and Applications of ETRAN and ITS Electron-Photon Transport Monte Carlo Codes

Stephen M. Seltzer
National Institute of Standards and Technology
Gaithersburg, MD 20899 USA

Workshop on Nuclear Data for Science and Technology
Medical Applications
International Center for Theoretical Physics
Trieste, October 4-15, 1999

Development of Radiation Interaction Data and Transport Calculations

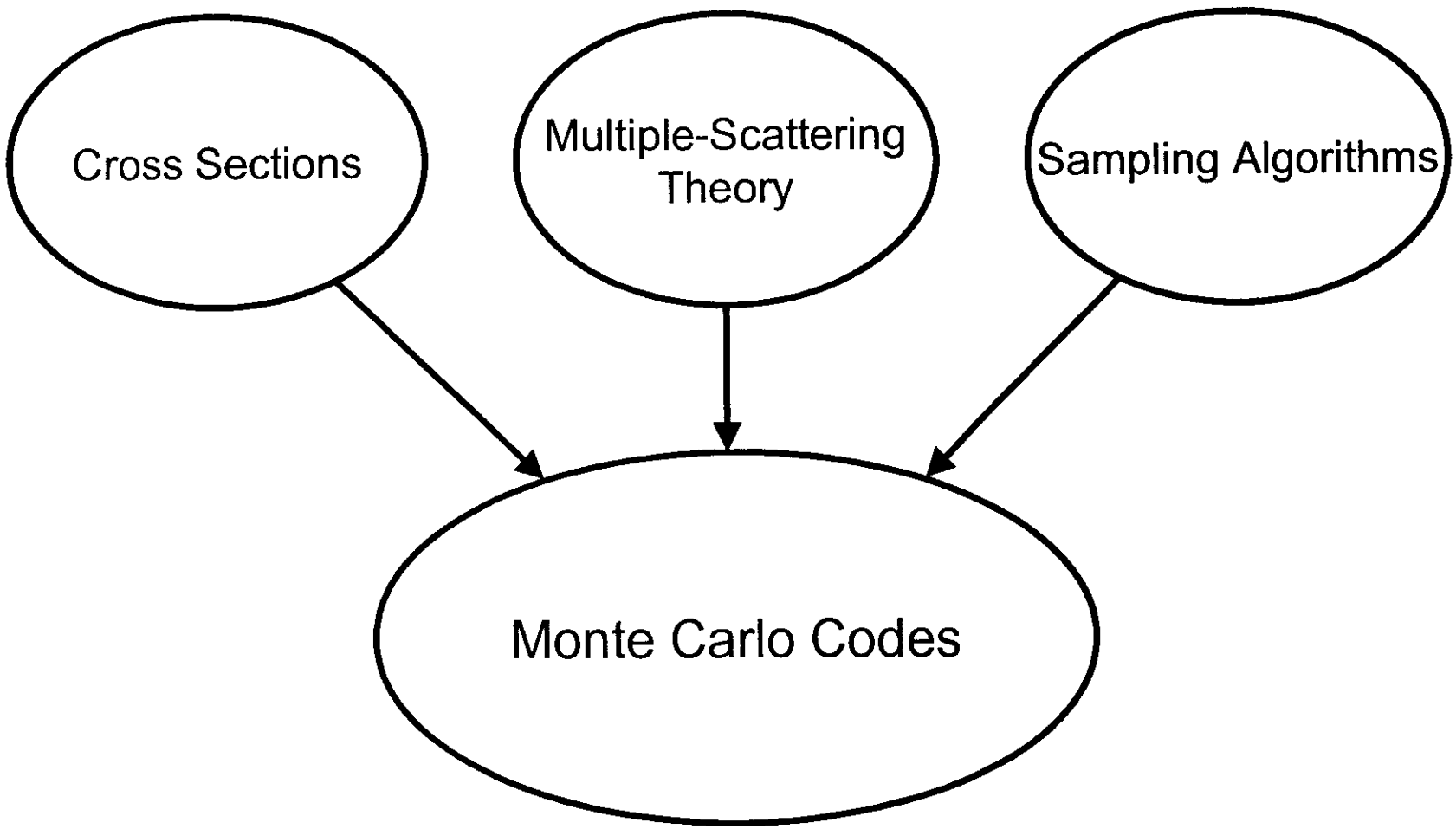

Coupled Electron-Photon Monte Carlo Calculations

- **PHOTON TRANSPORT (Analog)**
  - **Photon Interactions**
    - **Coherent (Rayleigh) scattering**
    - **Incoherent (Compton) scattering**
      - **Binding corrections**
    - **Photoelectric absorption**
    - **Pair production (screened nuclear field)**
    - **Triplet production (field of atomic electrons)**
    - **Photonuclear absorption**

- **ELECTRON TRANSPORT (Condensed History)**
  - **Energy-loss**
    - **Multiple-scattering treatment**
      - **Class I (complete grouping)**
        - **CSDA**
        - **Energy-loss straggling**
      - **Class II (catastrophic+CSDA)**
    - **Electronic stopping power (mean energy loss)**
      - **Density effect**
    - **Radiative stopping power (mean energy loss)**
    - **Bremsstrahlung production (single scattering)**
      - **Energy distribution**
        - **Analytical theory**
        - **"Exact"**
  - **Elastic scattering**
    - **Multiple-scattering treatment**
      - **Goudsmit-Saunderson (exact)**
      - **Moliére (small-angle approximation)**
    - **Single-scattering cross sections**
      - **Screened Rutherford**
      - **"Exact"**
    - **Spatial displacements ("wiggliness" corrections)**
      - ***e.g.*, PRESTA (transverse)**
      - ***e.g.*, TLC (transverse and longitudinal)**
      - ***e.g.*, Random hinging**

Coupled Electron-Photon Monte Carlo Calculations

SECONDARY RADIATIONS

- **Bremsstrahlung photons**
  - **Energy distribution**
    - **Analytical theory**
    - **"Exact"**
  - **Intrinsic angular distribution**
    - **Analytical theory**
    - **"Exact"**
- **Knock-on electrons (Møller or Bhabha cross section)**
- **Compton electrons**
  - **Binding corrections**
- **Photoelectrons**
  - **Angular distribution**
- **Pair "electrons"**
  - **Energy distribution**
  - **Angular distribution**
- **Annihilation quanta**
  - **Positron at rest**
  - **Positron in flight**
- **Atomic relaxation**
  - **Characteristic x rays**
  - **Auger electrons**

ALGORITHM CONSIDERATIONS

- **Boundary crossing**
- **Track-end disposition**
- **Variance reduction**
- **Geometry**
  - **Generality**
  - **Speed**
  - **Ease of use**
- **Sampling**
  - **Numerical distributions**
  - **Analytical formulae**
  - **Ersatz functions**

PHOTON TRANSPORT

PHOTON TRANSPORT

Single-scattering treatment

- pair (and triplet) production
- photo-electric absorption
- incoherent scattering
- coherent scattering

Production and transport of secondary radiation

- electron-positron pairs
- photoelectrons, characteristic x rays, Auger electrons
- Compton electrons

ELECTRON AND POSITRON TRANSPORT

ELECTRON AND POSITRON TRANSPORT

Basically "condensed"-history or path-segment model

Multiple-scattering treatment of all collision for:

- ionization and excitation energy loss (including fluctuations)
- elastic scattering

Sample individual interactions for production of secondary radiations:

- bremsstrahlung photons (contributes also to energy-loss straggling)
- knock-on electrons (Møller [or Bhabha] cross section)
- characteristic x rays and Auger electrons from ionization events
- photons from annihilation of positrons at rest [and in flight]

STEP SIZE

CONDENSED-HISTORY STEP SIZE

- **Should be *short* enough: energy loss and angular deflection is small**

- **Should be *long* enough: enough collisions for multiple scattering treatment; not too many steps per history**

CONDENSED-HISTORY STEP SIZE

- **Compromise:**

  (a) **Major step length for mean fractional energy loss of** $2^{-1/k}$, **i.e.,** $T_{n+1} = 2^{-1/k} T_n$

$$s_n = \int_{T_{n+1}}^{T_n} \left[\frac{1}{\rho} S(T') \right]^{-1} dT' = r_o(T_n) - r_o(T_{n+1})$$

  Typically $k = 8$; **mean fractional energy loss** $= 8.3\%$

  (b) **Divide major step into m sub-steps for small angular deflections. Typically** $m = 2$ **to** 20

Mean deflection cosines for typical electron steps in the ETRAN random walk. Pathlengths for energy reduction by factor $2^{1/8}$ (= 0.917), further subdivided into m equal sub-steps.

	C	A	Cu	Ag	Pb
m =	2	3	7	11	18
T(MeV)					
64	0.9989	0.9990	0.9994	0.9995	0.9996
32	0.9975	0.9973	0.9982	0.9985	0.9988
16	0.9948	0.9939	0.9952	0.9959	0.9963
8	0.9901	0.9876	0.9893	0.9901	0.9904
4	0.9825	0.9776	0.9793	0.9796	0.9788
2	0.9720	0.9634	0.9648	0.9640	0.9604
1	0.9597	0.9463	0.9477	0.9451	0.9375
0.5	0.9478	0.9297	0.9313	0.9271	0.9158
0.25	0.9382	0.9164	0.9185	0.9134	0.9014
0.125	0.9316	0.9072	0.9101	0.9056	0.8969
0.0625	0.9273	0.9012	0.9054	0.9033	0.9010
0.03125	0.9246	0.8975	0.9039	0.9057	0.9092
0.015625	0.9226	0.8951	0.9054	0.9117	0.9183
0.0078125	0.9209	0.8939	0.9096	0.9190	0.9280

ANGULAR DEFLECTIONS

GOUDSMIT-SAUNDERSON DISTRIBUTION

Disadvantages

- **Sampling more complicated than from Molière**
- **Cannot evaluate on the fly. Need to pre-store distributions for pre-selected set of pathlengths**

Advantages

- **Not in small-angle approximation, good for all scattering angles**
- **Formally exact for any cross section (e.g., e^- and e^+ differences)**
- **Can apply to smaller pathlengths**

MULTIPLE ELASTIC-SCATTERING ANGULAR DEFLECTIONS

Goudsmit-Saunderson Distribution

$$A_{GS}(\vartheta, s) \;=\; \sum_{\ell=0}^{\infty} \frac{2\ell+1}{2}\, e^{-sG_\ell}\, P_\ell(\cos\theta)$$

$$G_\ell \;=\; 2\pi N \int_{-1}^{+1} \frac{d\sigma(\theta,T)}{d\Omega}\,[1 - P_\ell(\cos\theta)]\, d(\cos\theta)$$

Energy loss included by $sG_\ell \rightarrow \int_o^s G_\ell(s')\, ds'$ evaluated in CSDA

ELASTIC-SCATTERING CROSS SECTION

Factored cross section

$$\frac{d\sigma(\theta)}{d\Omega} = \frac{d\sigma_{Ruth}(\theta)}{d\Omega} K_{scr}(\theta) K_{rel}(\theta)$$

Spin-relativistic correction

$$K_{rel}(\theta) = \frac{d\sigma_{Mott}}{d\Omega} \Big/ \frac{d\sigma_{Ruth}}{d\Omega}$$

Screening correction

$$K_{scr}(\theta) = \left(\frac{1 - \cos\theta}{1 - \cos\theta + 2\eta} \right)^2$$

Molière screening angle

$$\eta = \tfrac{1}{4} \left(\frac{\alpha mc}{0.885\, p} \right)^2 Z^{2/3} \left[1.13 + 3.76 \left(\alpha Z/\beta \right)^2 \right]$$

ELASTIC-SCATTERING CROSS SECTION

Transport (or momentum-transfer) cross section

$$\sigma_t = 2\pi \int_{-1}^{+1} \frac{d\sigma(\theta)}{d\Omega} (1 - \cos\theta)\, d(\cos\theta)$$

has dominant influence on multiple-scattering process

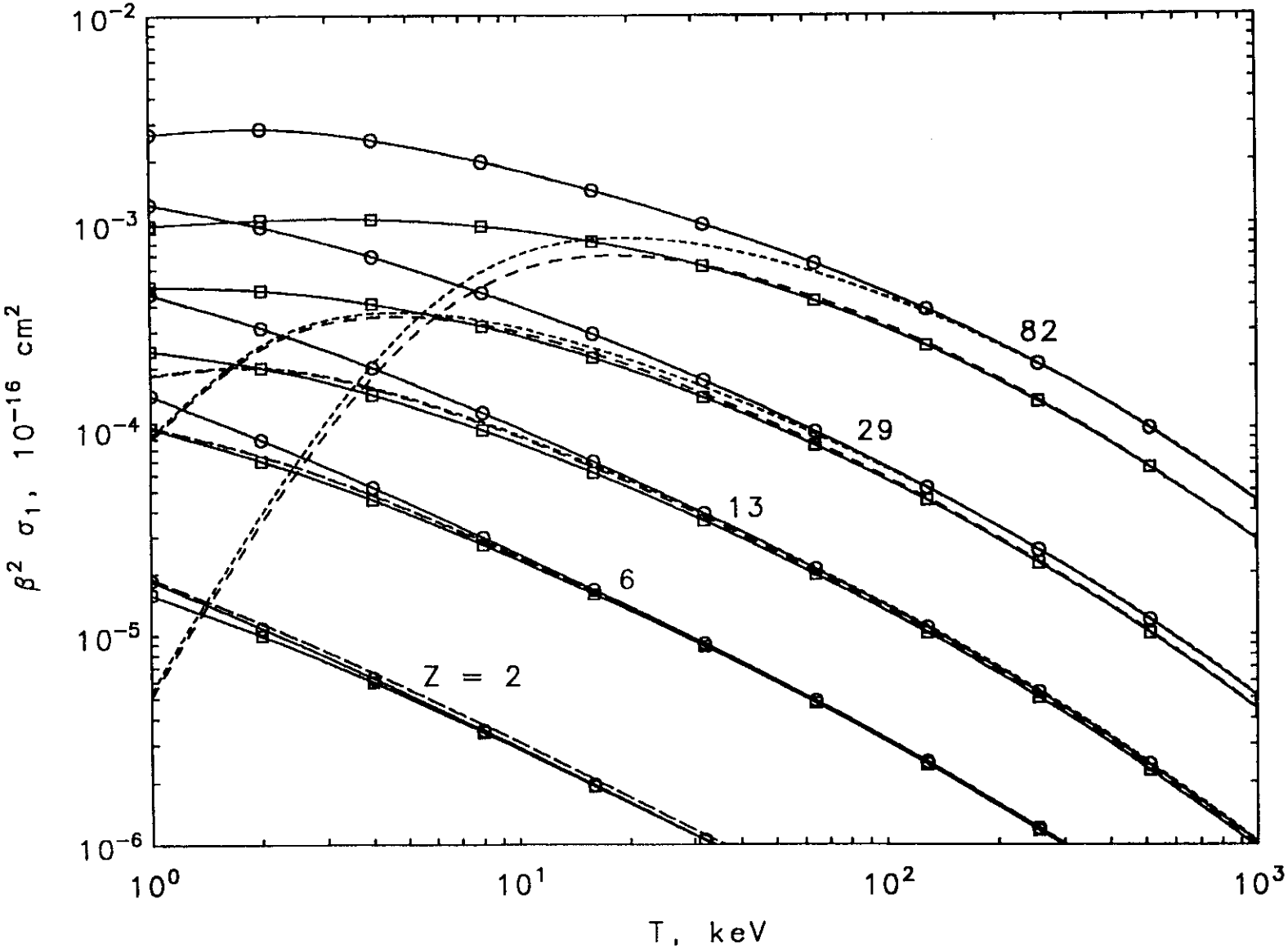
10^{-2}
10^{-3}
10^{-4}
10^{-5}
10^{-6}
$\beta^2\ \sigma_1,\ 10^{-16}\ cm^2$
10^0
10^1
10^2
10^3
T, keV
82
29
13
6
Z = 2

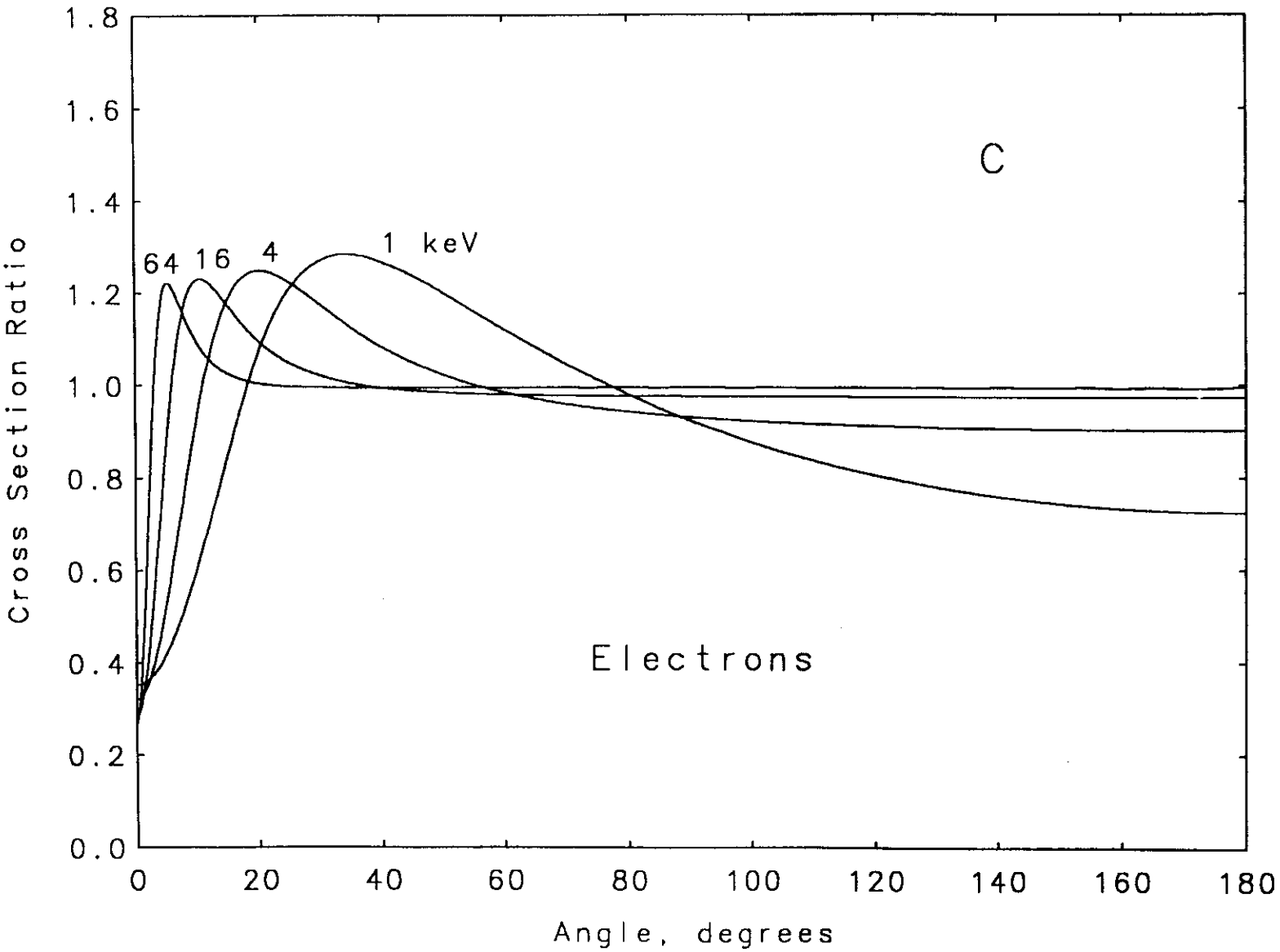
C
64
16
4
1 keV
Electrons
Cross Section Ratio
Angle, degrees
0.0
0.2
0.4
0.6
0.8
1.0
1.2
1.4
1.6
1.8
0
20
40
60
80
100
120
140
160
180

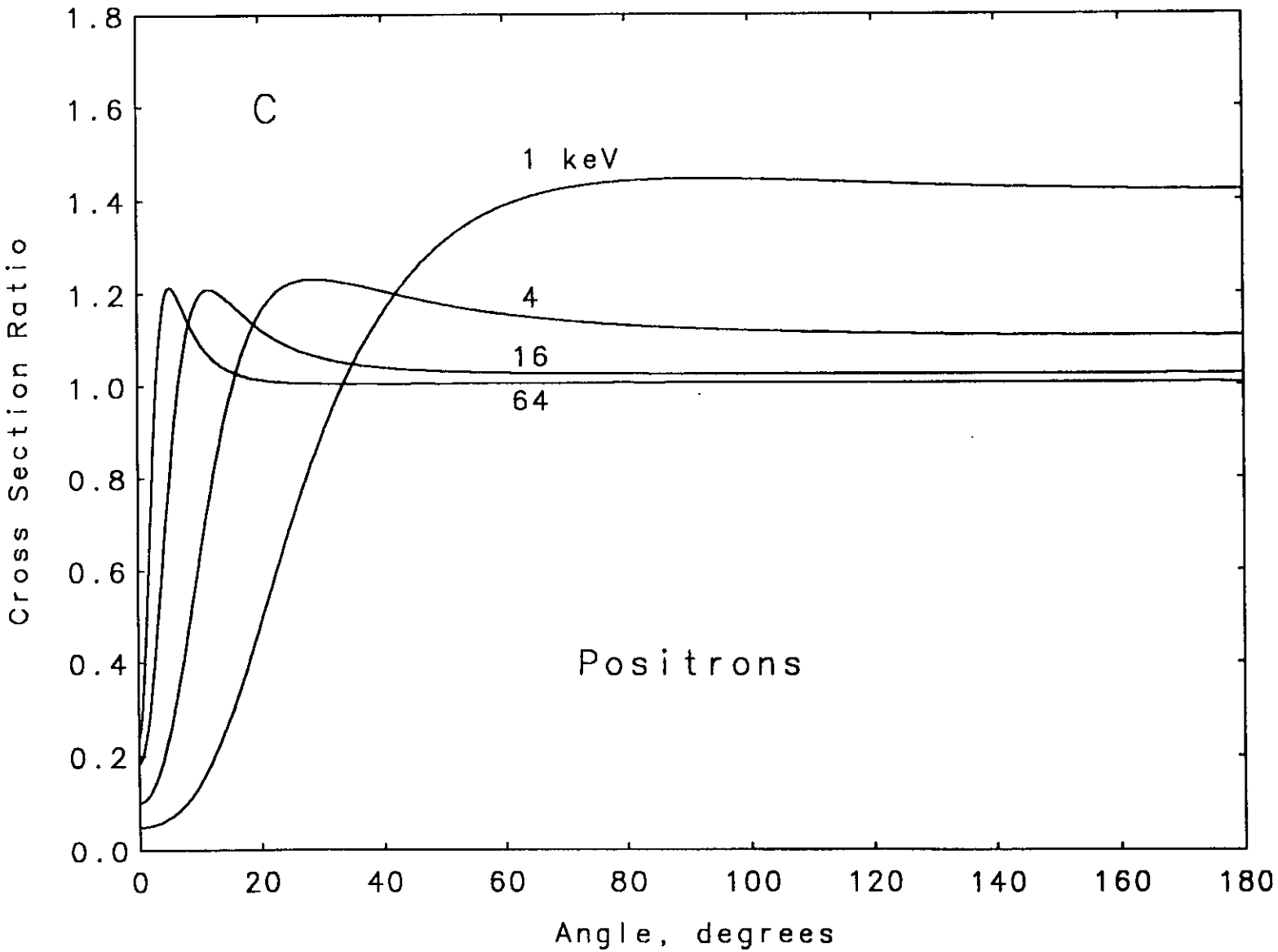
C
1 keV
4
16
64
Positrons
Cross Section Ratio
Angle, degrees
0.0
0.2
0.4
0.6
0.8
1.0
1.2
1.4
1.6
1.8
0
20
40
60
80
100
120
140
160
180

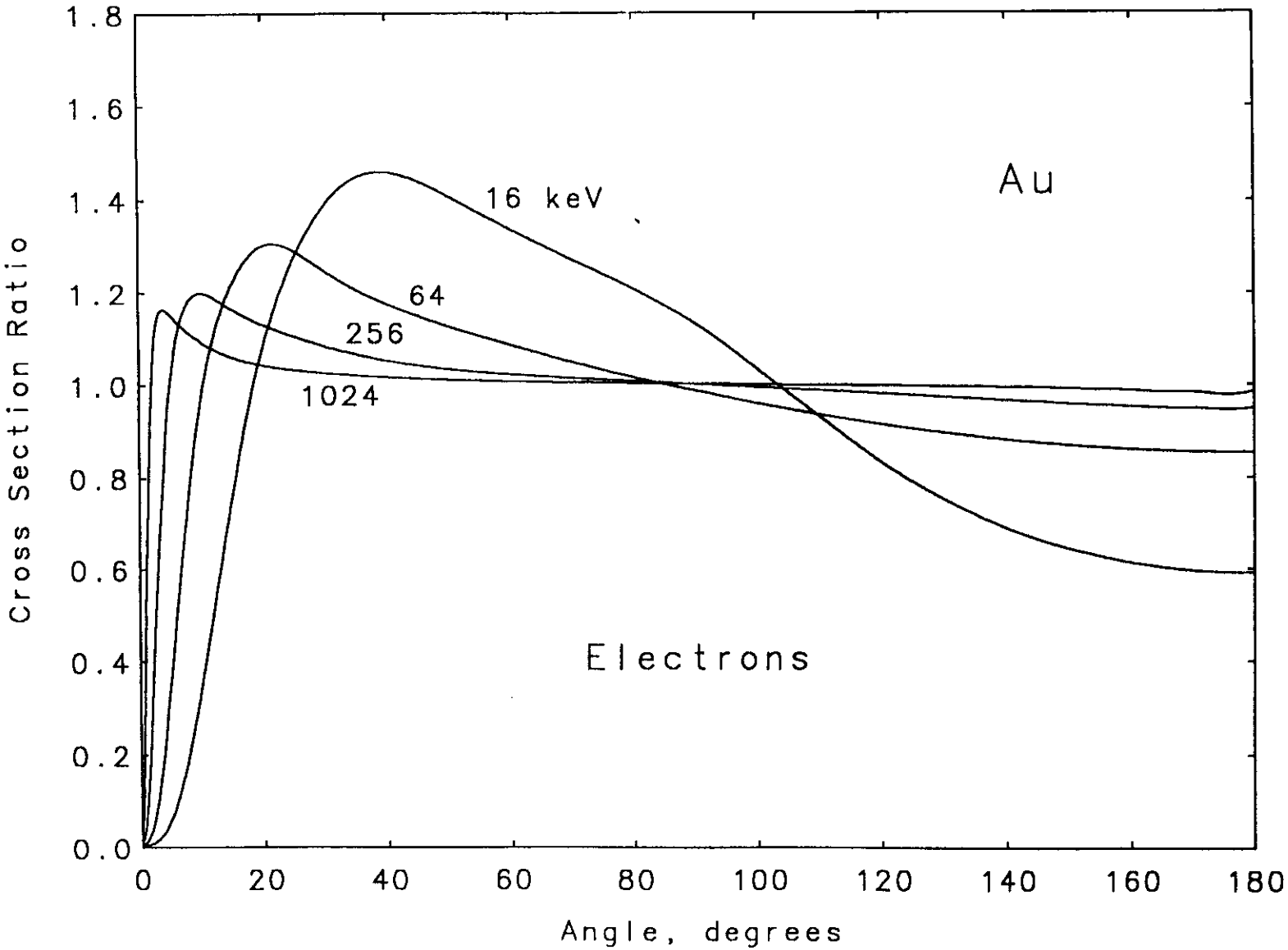
Au
16 keV
64
256
1024
Electrons
Cross Section Ratio
Angle, degrees
0.0
0.2
0.4
0.6
0.8
1.0
1.2
1.4
1.6
1.8
0
20
40
60
80
100
120
140
160
180

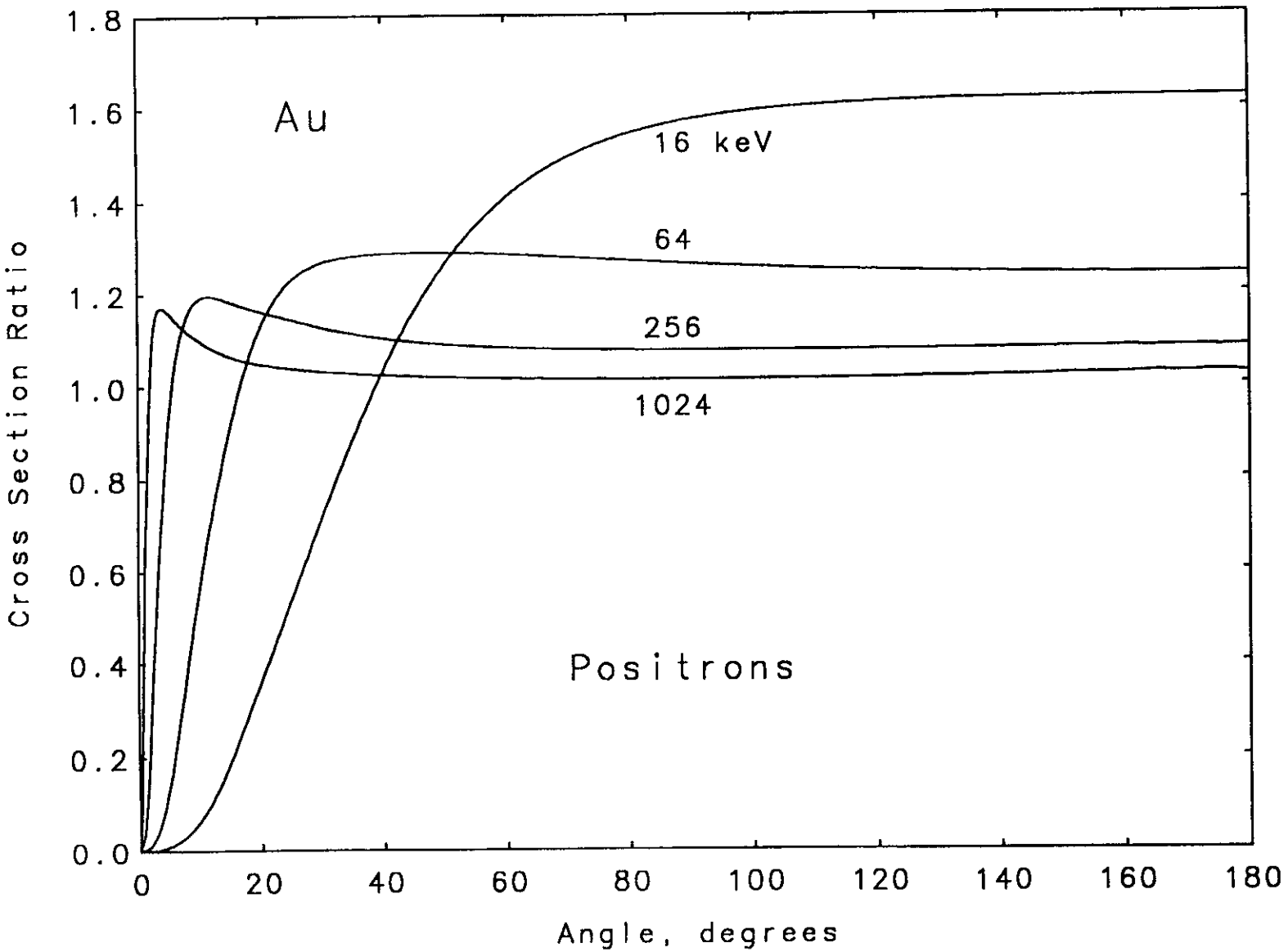
Au
16 keV
64
256
1024
Positrons
Cross Section Ratio
Angle, degrees
0.0
0.2
0.4
0.6
0.8
1.0
1.2
1.4
1.6
1.8
0
20
40
60
80
100
120
140
160
180

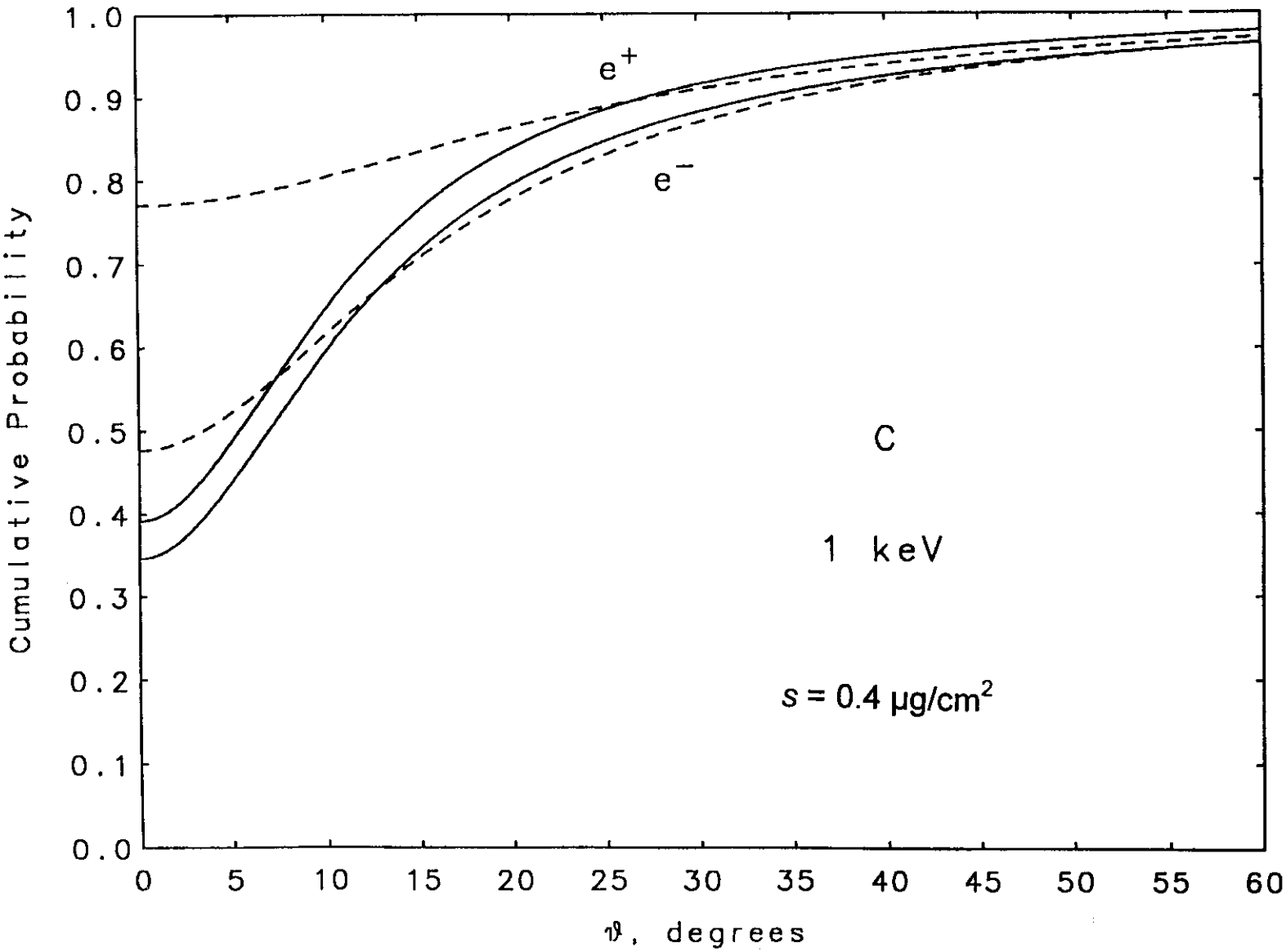
1.0
0.9
0.8
0.7
0.6
0.5
0.4
0.3
0.2
0.1
0.0
Cumulative Probability
0
5
10
15
20
25
30
35
40
45
50
55
60
ϑ, degrees
e+
e−
C
1 keV
s = 0.4 µg/cm2

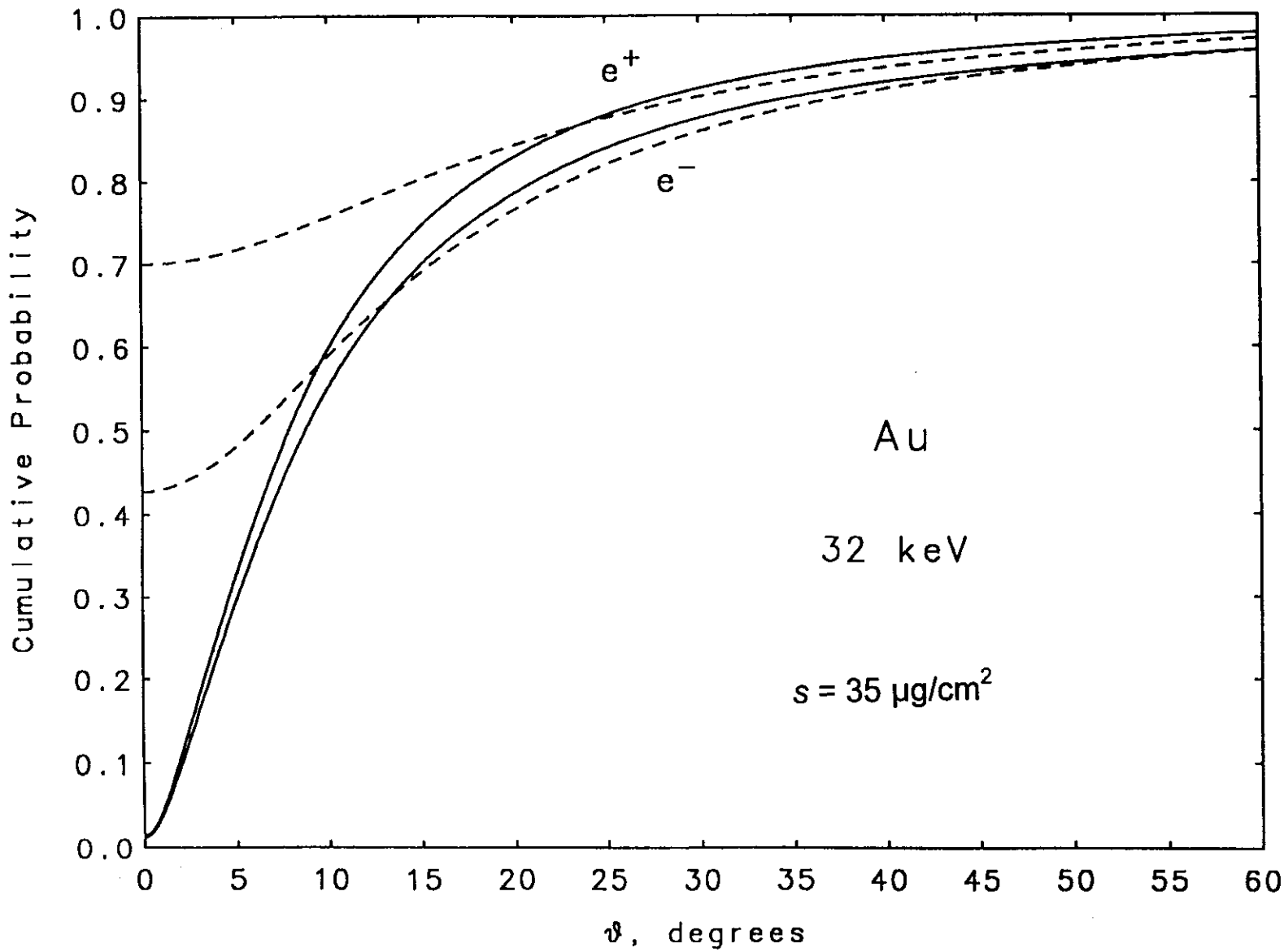
1.0
0.9
0.8
0.7
0.6
0.5
0.4
0.3
0.2
0.1
0.0
Cumulative Probability
0
5
10
15
20
25
30
35
40
45
50
55
60
ϑ, degrees
e+
e−
Au
32 keV
s = 35 µg/cm2

Dependence of foil transmission and reflection coefficients on the elastic-scattering cross sections used in ETRAN calculations. The results pertain to 32-keV electrons normally incident on tantalum foils of thickness z, expressed in units of the csda range r_o = 4.61 mg/cm^2.

Fraction Transmitted

	Number			Energy		
z/r_o	Riley[a]	Factored[b]	b/a	Riley[a]	Factored[b]	b/a
0.05	0.823	0.826	1.004	0.776	0.778	1.003
0.10	0.647	0.649	1.003	0.560	0.562	1.004
0.15	0.492	0.483	1.002	0.385	0.385	1.000
0.20	0.346	0.350	1.012	0.246	0.249	1.012
0.25	0.226	0.227	1.004	0.147	0.148	1.007
0.30	0.135	0.135	1.000	0.0813	0.0815	1.002
0.35	0.0745	0.0744	0.999	0.0421	0.0418	0.993

Fraction Reflected

	Number			Energy		
z/r_o	Riley[a]	Factored[b]	b/a	Riley[a]	Factored[b]	b/a
0.35	0.490	0.490	1.000	0.378	0.378	1.000

[a] Using elastic-scattering cross sections from partial-wave calculations with the Riley code.

[b] Using elastic-scattering cross sections from the factored cross section, with the screening angle chosen to give the same transport cross section as from the partial-wave calculations.

SPATIAL DISPLACEMENT CORRECTIONS

Transverse and Longitudinal Corrections (TLC)

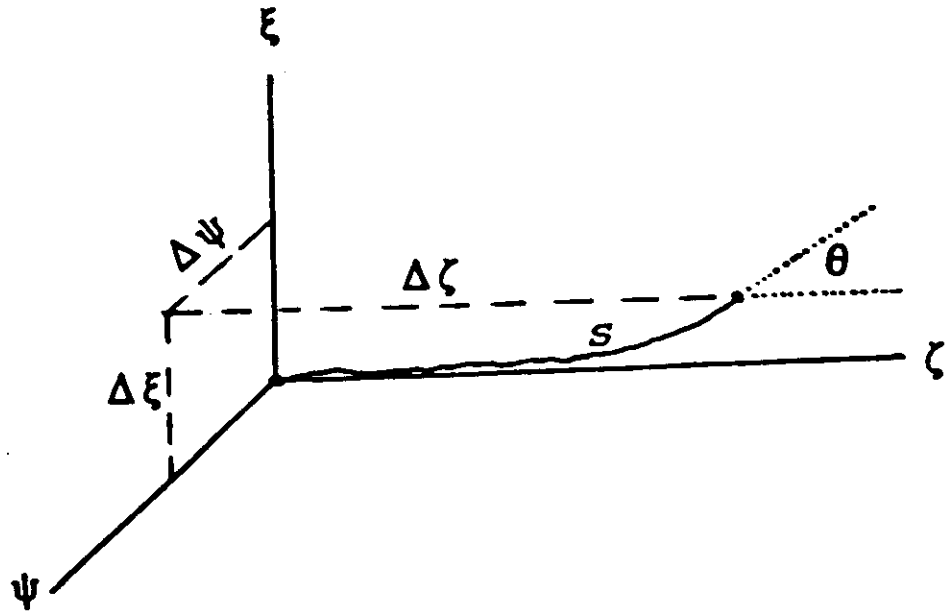

$$\Delta\zeta = s\,\frac{1+cos\theta}{2}$$

$$\Delta\xi = \frac{s}{2}\left[sin\theta\, cos\Delta\varphi + \nu_x \left(\frac{<\theta^2>}{6}\right)^{1/2}\right]$$

$$\Delta\psi = \frac{s}{2}\left[sin\theta\, sin\Delta\varphi + \nu_y \left(\frac{<\theta^2>}{6}\right)^{1/2}\right]$$

ν_x and ν_y are normally distributed random numbers

Transverse and Longitudinal Corrections (TLC)

$$< \theta^2 > = 4\pi Ns \int_{cos\theta_c}^{1} \left[\frac{d\sigma_{Ruth}}{d\Omega} K_{scr}(\theta) \right] (1 - cos\theta)\, d(cos\theta)$$

$$2\pi Ns \int_{-1}^{cos\theta_c} \left[\frac{d\sigma_{Ruth}}{d\Omega} K_{scr}(\theta) \right] d(cos\theta) = n \sim 1$$

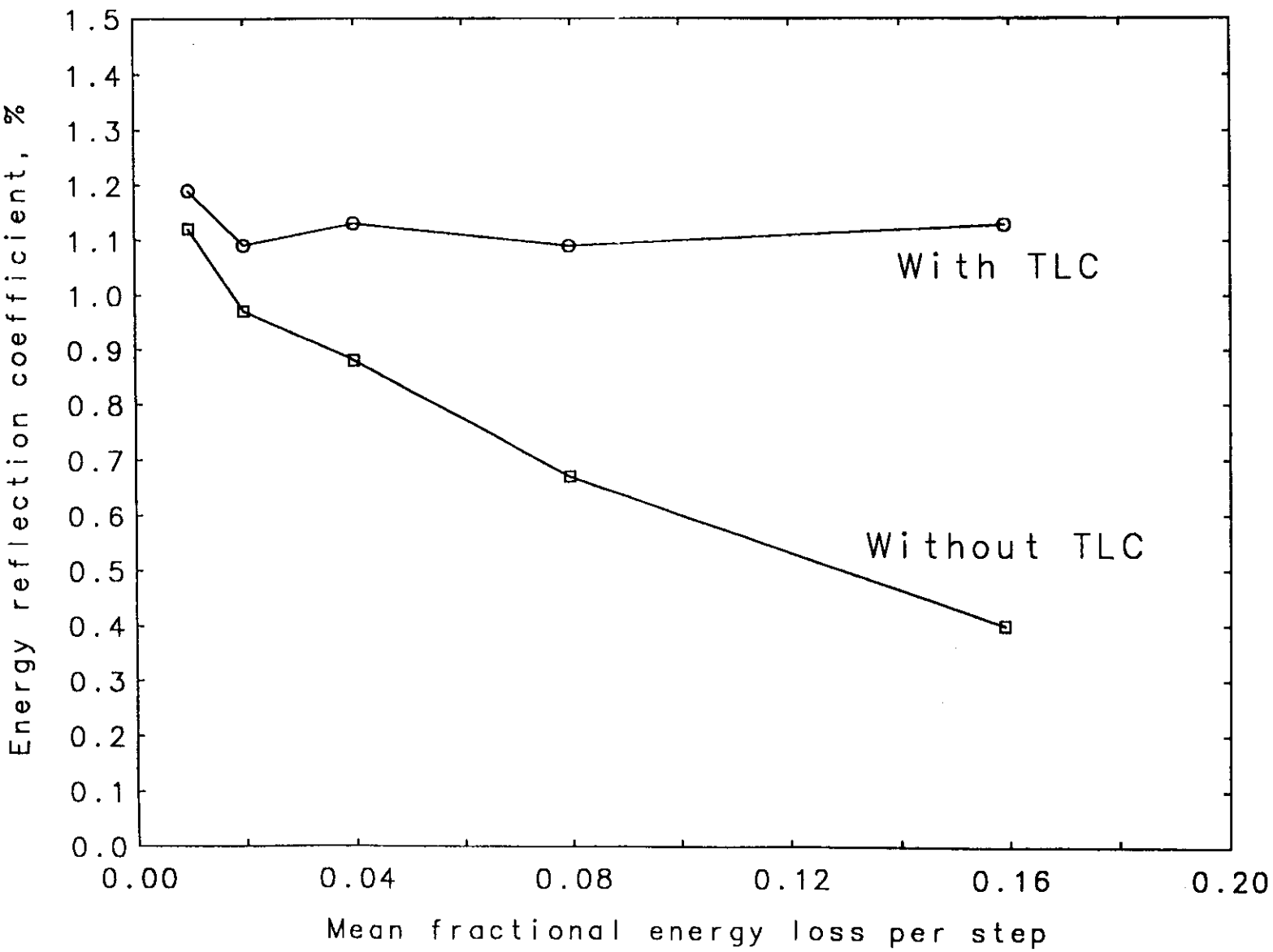
Energy reflection coefficient, %
1.5
1.4
1.3
1.2
1.1
1.0
0.9
0.8
0.7
0.6
0.5
0.4
0.3
0.2
0.1
0.0
0.00
0.04
0.08
0.12
0.16
0.20
Mean fractional energy loss per step
With TLC
Without TLC

ENERGY LOSS

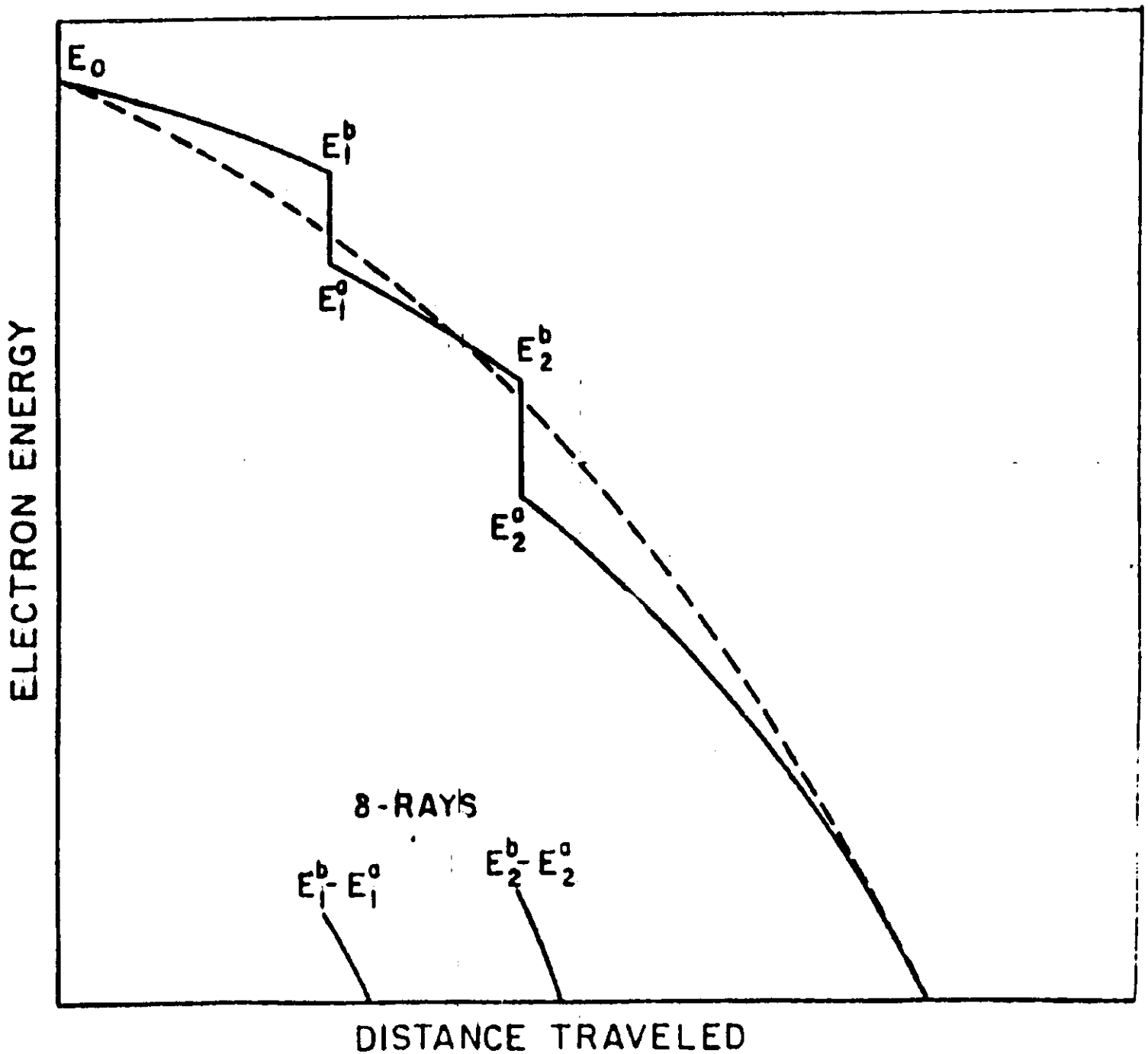
E_0
E_1^b
E_1^a
E_2^b
E_2^a
ELECTRON ENERGY
δ-RAYS
$E_1^b - E_1^a$
$E_2^b - E_2^a$
DISTANCE TRAVELED

IONIZATION ENERGY-LOSS FLUCTUATIONS

Landau theory

- Many collisions
- One velocity (small mean energy loss)
- Rutherford energy-transfer cross section, $\sim \epsilon^{-2}$ (for $\epsilon >> \mathrm{I}$)
- First moment of cross section for small energy transfers from Bethe theory
- Maximum energy transfer $\epsilon_{max} = \infty$

Distribution of energy loss Δ in terms of universal function

$$f(\Delta, s)\, d\Delta \;=\; \phi(\lambda)\, d\lambda$$

$$\lambda \;=\; \frac{\Delta}{\xi} \;-\; ln\left[\frac{2\xi\, mc^2\, \beta^2}{(1-\beta^2)I^2}\right] \;+\; \beta^2 \;+\; \delta \;-\; 0.42278$$

$$\xi \;=\; \frac{2\pi\, r_e^2\, mc^2\, N\, Z}{\beta^2}\; s$$

$$\phi(\lambda) \;=\; \frac{1}{2\pi i} \int_{a-i\infty}^{a+i\infty} exp(u\, ln\, u \;+\; \lambda u)\, du$$

Valid for $T \;>>\; \xi \;>>\; I$

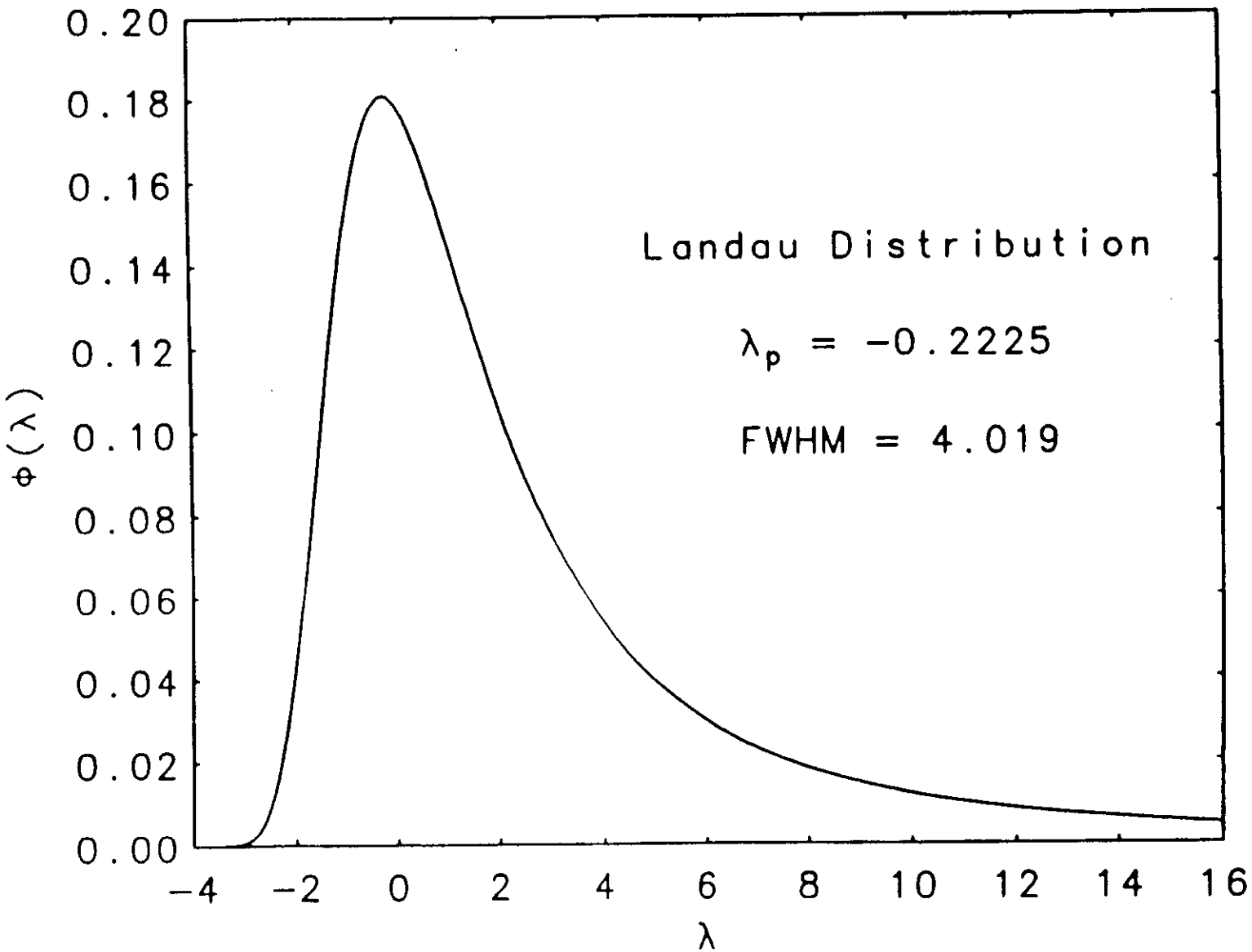
0.20
0.18
0.16
0.14
0.12
0.10
0.08
0.06
0.04
0.02
0.00
$\phi(\lambda)$
−4
−2
0
2
4
6
8
10
12
14
16
λ
Landau Distribution
λ_p = −0.2225
FWHM = 4.019

IONIZATION ENERGY-LOSS FLUCTUATIONS

Because $\epsilon_{max} = \infty$, $< \Delta > = \int_0^\infty \Delta f(\Delta, s)\, d\Delta = \infty$

Need to impose correct mean energy loss.

Re-write Landau variable in terms of $\overline{\Delta}$ from stopping-power,

$$\lambda = \frac{\Delta - \overline{\Delta}}{\xi} + \nu^{\pm}$$

$$\nu^{-} = ln\left(\frac{T}{\xi}\right) - 0.80907 + \left[\frac{\tau^2}{8} - (2\tau + 1)\, ln2\right]/(\tau + 1)^2$$

$$\nu^{+} = ln\left(\frac{T}{\xi}\right) - 0.422784 - \frac{\beta^2}{12}\left[11 + \frac{14}{\tau + 2} + \frac{10}{(\tau + 2)^2} + \frac{4}{(\tau + 2)^3}\right]$$

Define λ_{cut} such that

$$\overline{\lambda} = \nu^{\pm}$$

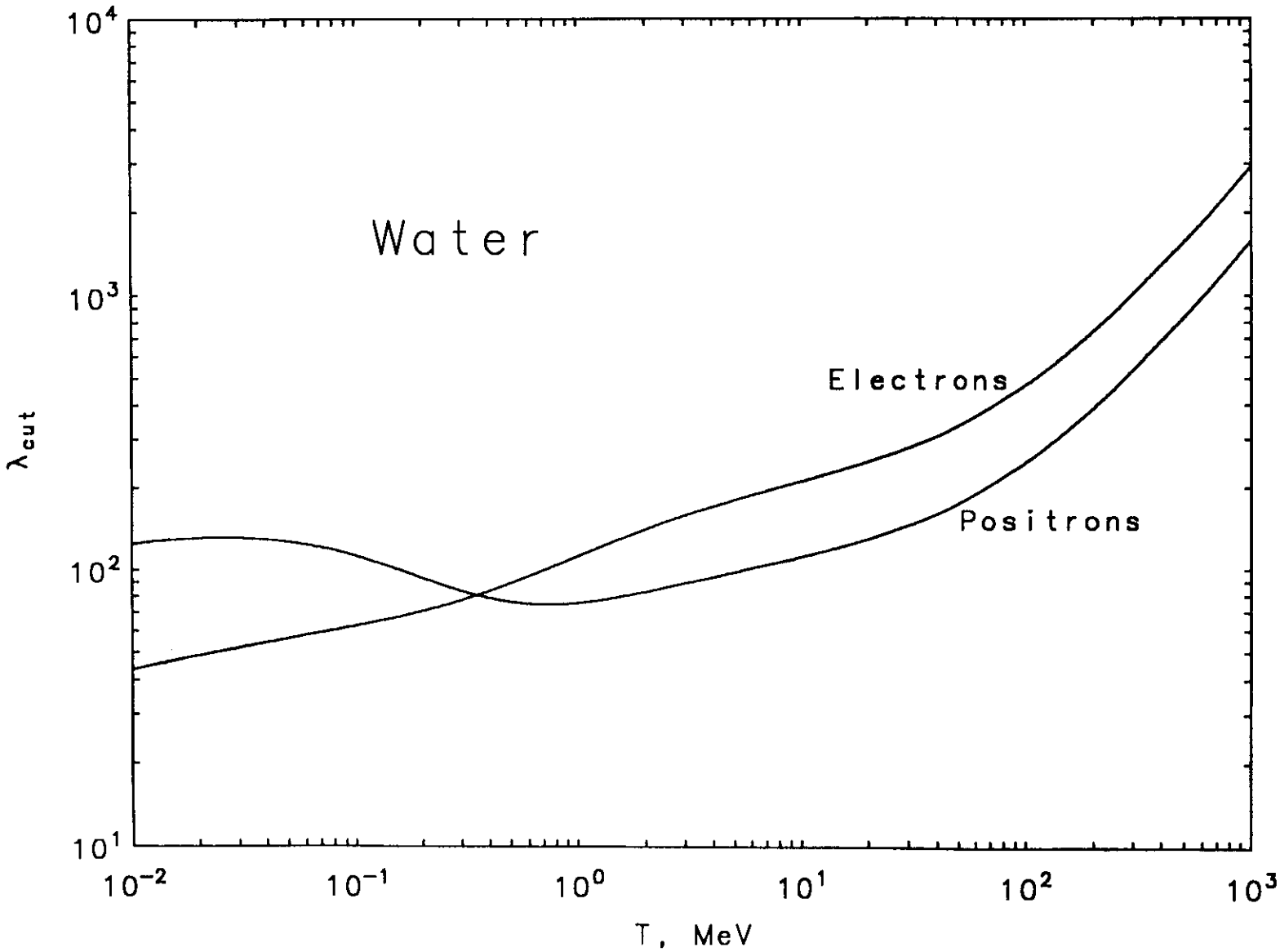
Water
Electrons
Positrons
λ_{cut}
10^4
10^3
10^2
10^1
10^{-2}
10^{-1}
10^0
10^1
10^2
10^3
T, MeV

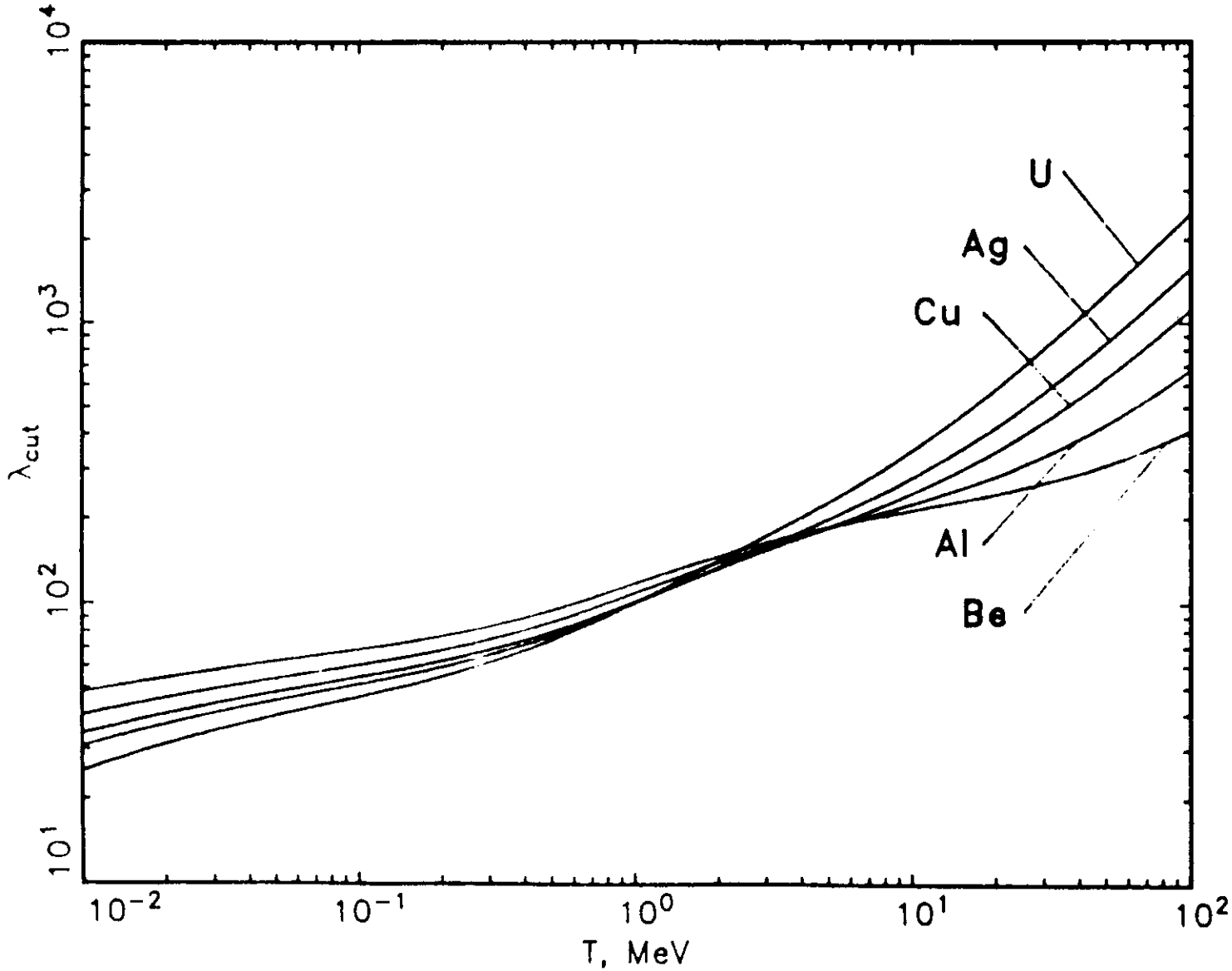
10^4
10^3
10^2
10^1
λ_{cut}
U
Ag
Cu
Al
Be
10^{-2}
10^{-1}
10^0
10^1
10^2
T, MeV

IONIZATION ENERGY-LOSS FLUCTUATIONS

Blunck & Leisegang included second moment of the cross section for small energy transfers

$$f_{BL}(\Delta, s) = \frac{1}{\sqrt{2\pi}\,\sigma} \int_{-\infty}^{+\infty} f(\Delta', s)\, exp\left[\frac{(\Delta - \Delta')^2}{2\sigma^2}\right] d\Delta'$$

Blunck & Westphal:

$$\sigma_{BW}^2 = 10eV \cdot Z^{4/3}\,\overline{\Delta}$$

Chechin & Ermilova estimate relative error of Landau-Blunck-Leisegang distribution (rather, its Laplace transform)

$$\varepsilon \sim \left[10\,\frac{\xi}{I}\left(1 + \frac{1}{10}\frac{\xi}{I}\right)^3\right]^{-1/2}$$

e.g.,

$$\varepsilon \lesssim 10\% \quad for \quad \frac{\xi}{I} \gtrsim 4$$

Values of ξ/I for typical ETRAN pathlengths in which mean total energy loss is 8.3%

T(MeV)	H	C	Al	Cu	Ag	Gd	Au	U
1000		3421	907	241	111	68.6	44.0	35.0
100		2091	687	215	104	66.4	43.2	34.7
10	1481	434	195	92.1	55.4	39.7	27.9	23.4
5	806	238	111	57.2	36.5	27.3	19.8	16.8
2	360	106	51.2	27.9	18.9	14.7	10.9	9.44
1	196	56.9	28.3	15.7	10.9	8.68	6.54	5.75
0.5	106	30.7	15.6	8.73	6.20	5.00	3.82	3.40
0.2	46.8	13.6	7.05	4.00	2.89	2.37	1.84	1.66
0.1	25.2	7.42	3.89	2.23	1.63	1.35	1.06	0.96
0.05	13.6	4.08	2.17	1.26	0.93	0.78	0.62	0.56
0.02	6.15	1.89	1.02	0.61	0.46	0.39	0.32	0.29
0.01	3.40	1.07	0.60	0.36	0.28	0.24	0.20	0.18

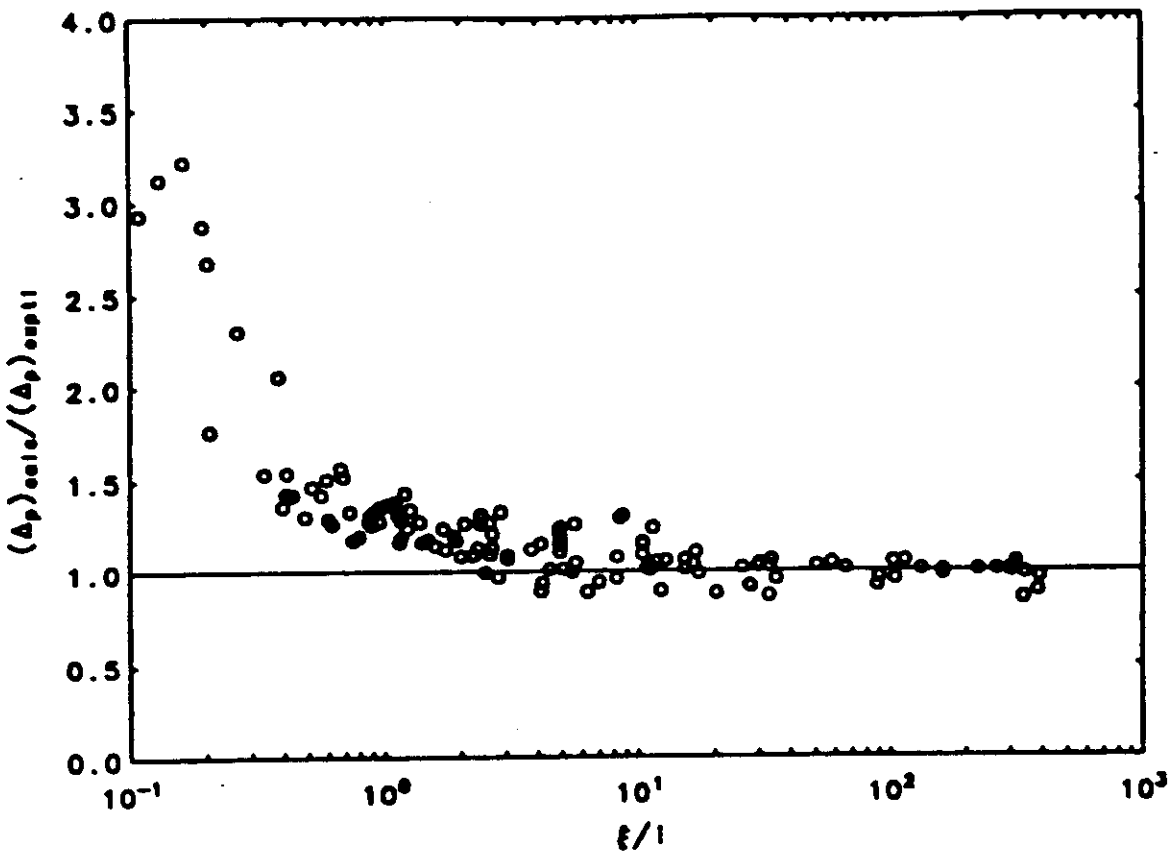
4.0
3.5
3.0
2.5
2.0
1.5
1.0
0.5
0.0
10^{-1}
10^{0}
10^{1}
10^{2}
10^{3}
$(\Delta\rho)_{calc}/(\Delta\rho)_{expt}$
ℓ/l

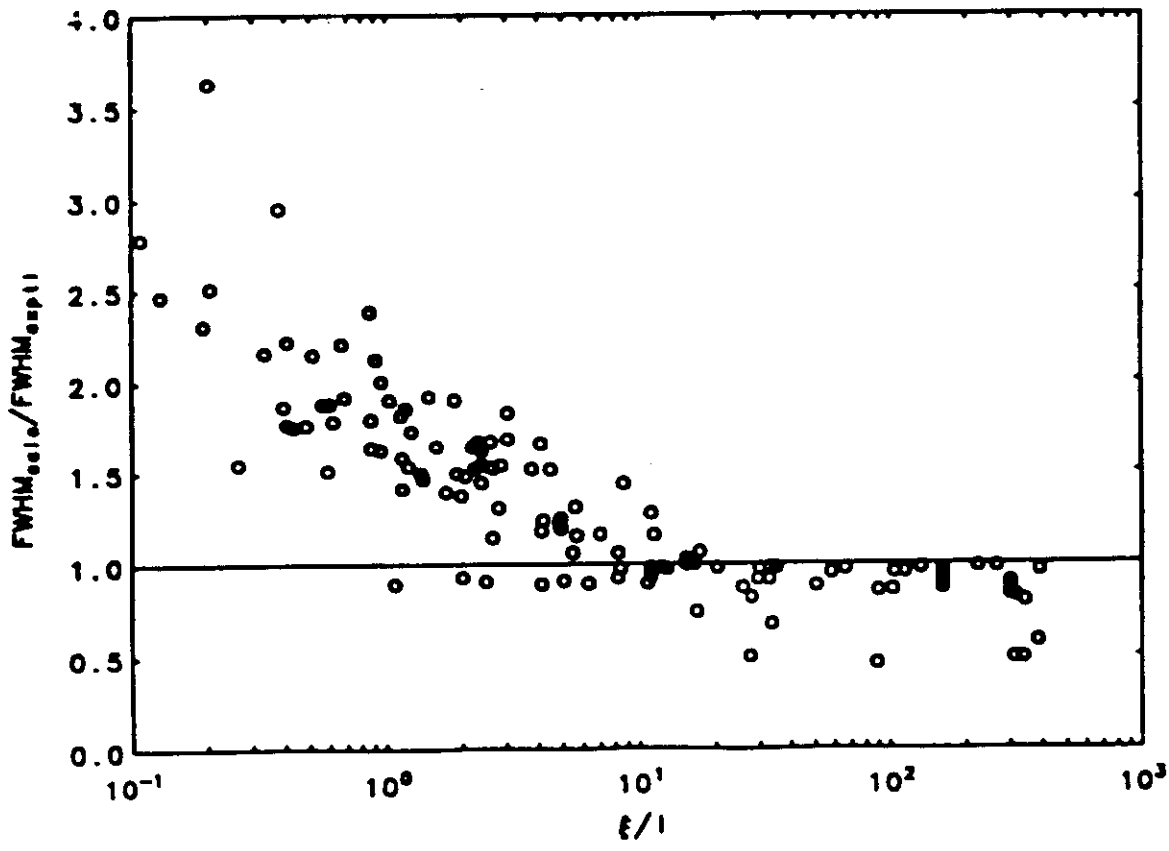
4.0
3.5
3.0
2.5
2.0
1.5
1.0
0.5
0.0
10^{-1}
10^{0}
10^{1}
10^{2}
10^{3}
$FWHM_{calc}/FWHM_{expt}$
ℓ/l

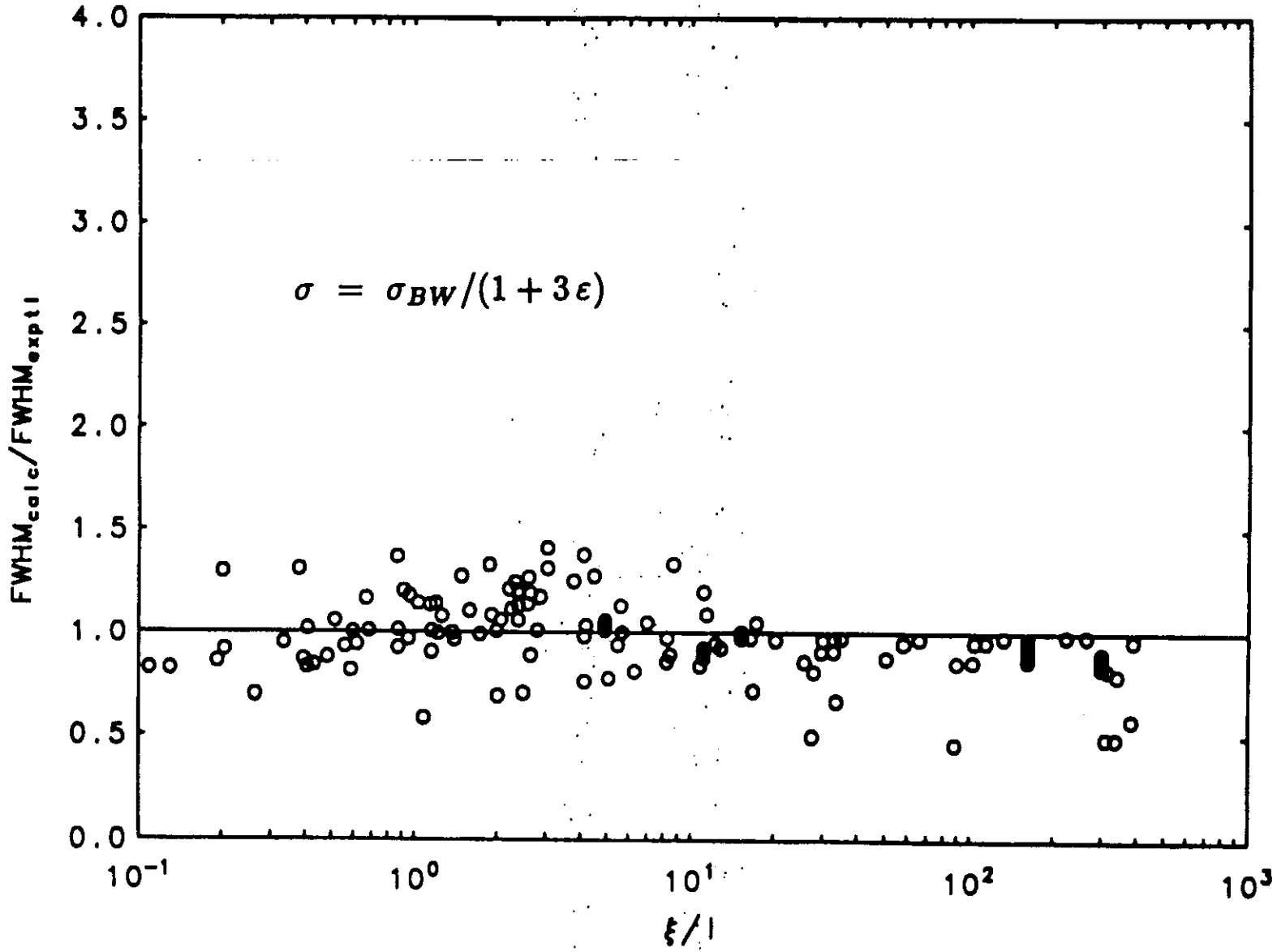
4.0
3.5
3.0
2.5
2.0
1.5
1.0
0.5
0.0
$\sigma = \sigma_{BW}/(1+3\epsilon)$
$FWHM_{calc}/FWHM_{exptl}$
10^{-1}
10^{0}
10^{1}
10^{2}
10^{3}
ξ/l

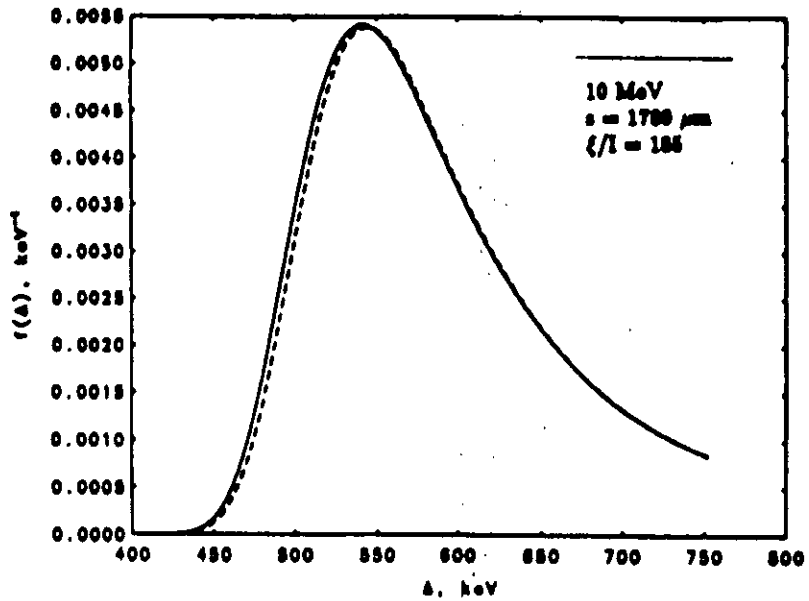
10 MeV
s = 1700 μm
ξ/I = 186
f(Δ), keV⁻¹
Δ, keV

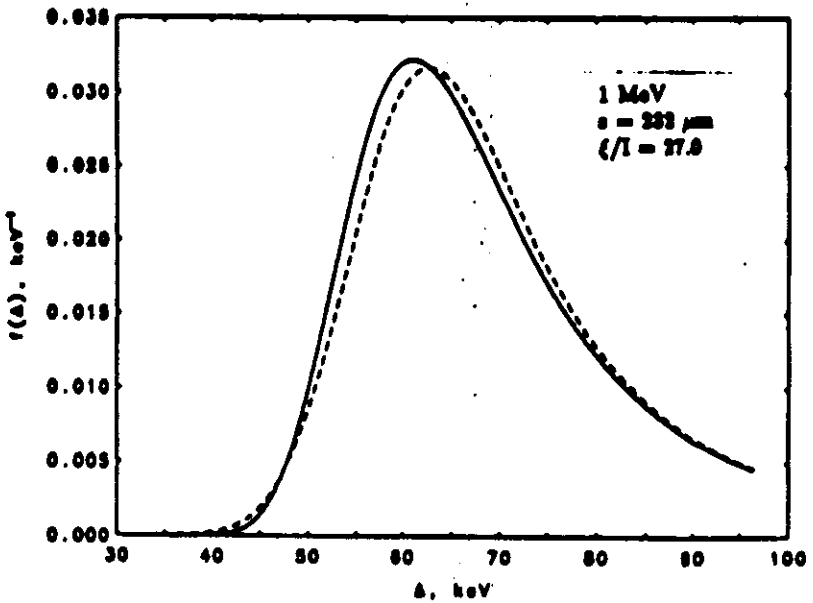
1 MeV
s = 282 μm
ξ/I = 27.8
f(Δ), keV⁻¹
Δ, keV

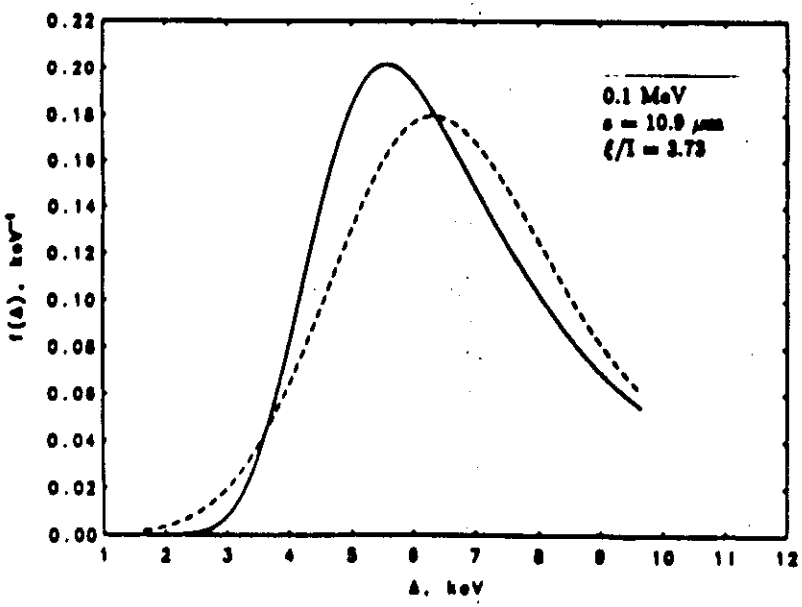
0.1 MeV
s = 10.9 μm
ξ/I = 1.73
f(Δ), keV⁻¹
Δ, keV

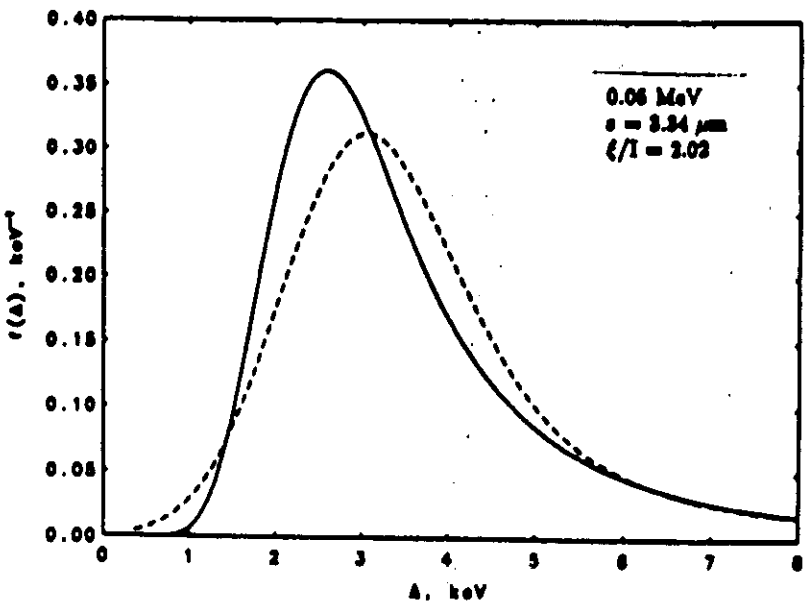
0.06 MeV
s = 3.84 μm
ξ/I = 1.02
f(Δ), keV⁻¹
Δ, keV

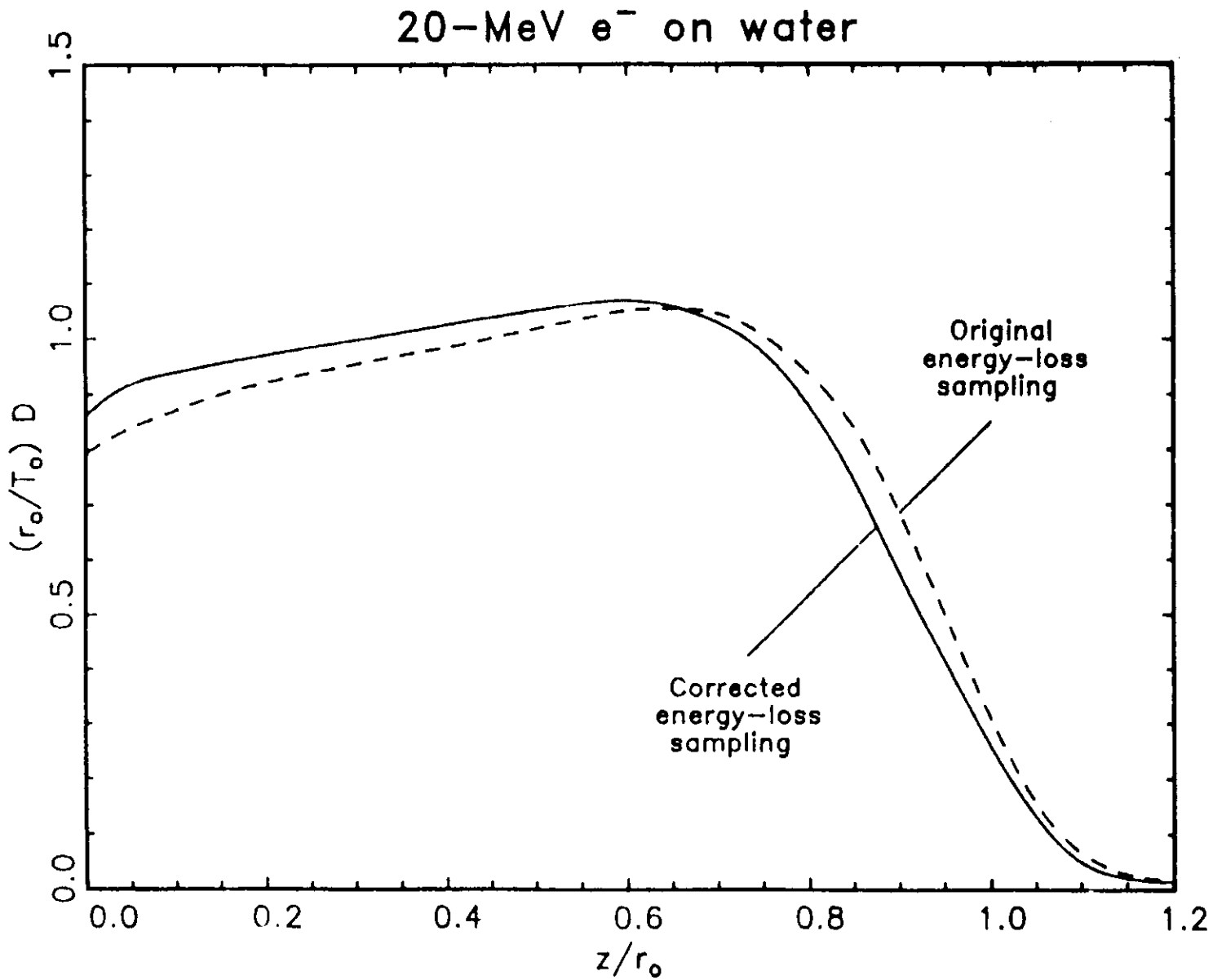
20–MeV e⁻ on water
1.5
1.0
0.5
0.0
(r_o/T_o) D
0.0
0.2
0.4
0.6
0.8
1.0
1.2
z/r_o
Original energy–loss sampling
Corrected energy–loss sampling

BREMSSTRAHLUNG

BREMSSTRAHLUNG ENERGY SPECTRA

$$\frac{d\sigma}{dk} = \frac{d\sigma_n}{dk} + \frac{Z\,d\sigma_e}{dk} = \left(1 + \frac{\eta}{Z}\right)\frac{d\sigma_n}{dk}$$

- Electron-nucleus cross section

  T > 50 MeV, high-energy analytical theory with screening and Coulomb corrections

  T $\leq$ 2 MeV, results of phase-shift calculations

- Electron-electron cross section

  Haug's theory with screening corrections

- Positron bremsstrahlung

  Spectral shape of electron cross section, but normalized to positron radiative stopping power

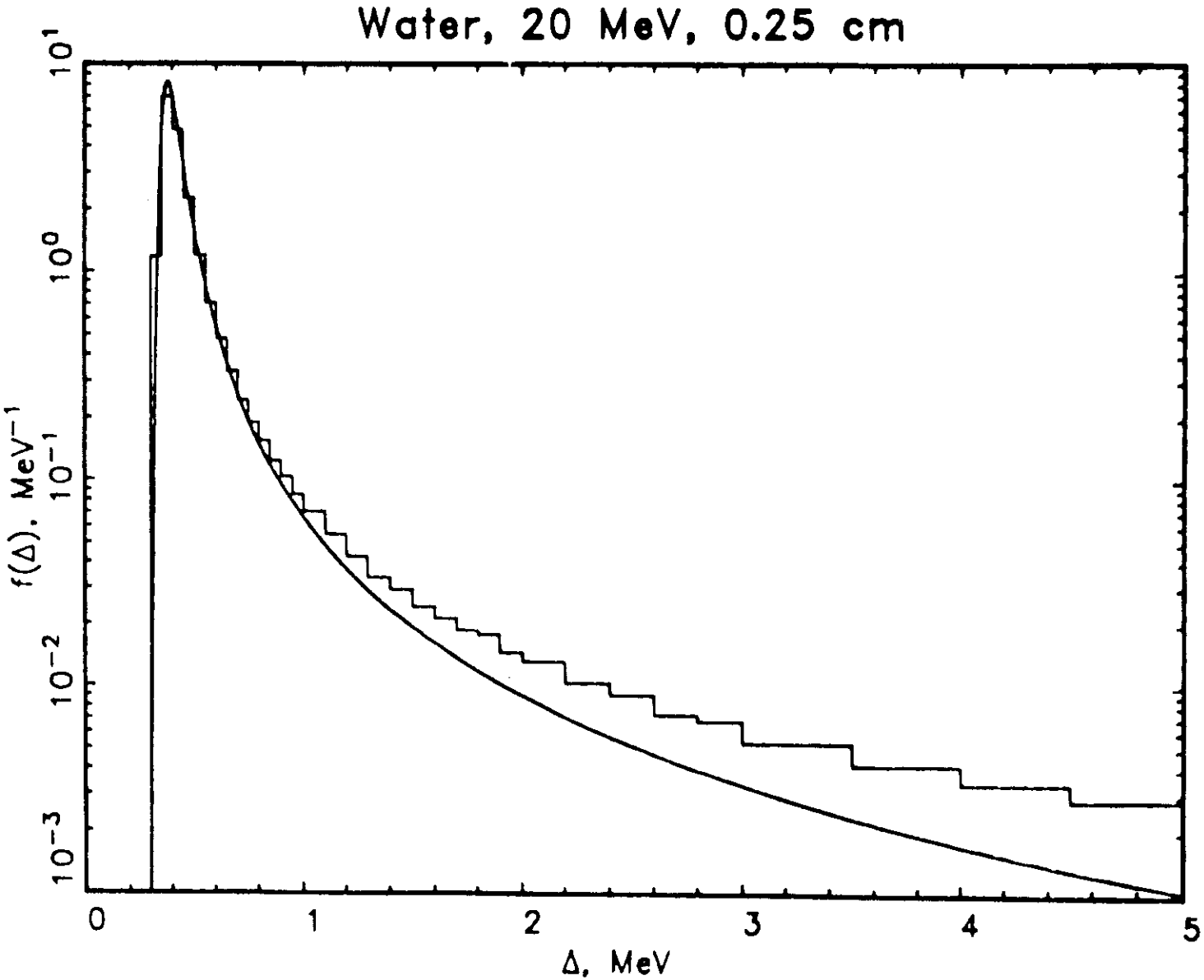
Water, 20 MeV, 0.25 cm
f(Δ), MeV⁻¹
10¹
10⁰
10⁻¹
10⁻²
10⁻³
0
1
2
3
4
5
Δ, MeV

BREMSSTRAHLUNG ANGULAR DISTRIBUTIONS

$$f(\theta) = \frac{d^2\sigma}{d\Omega dk} \Big/ \frac{d\sigma}{dk}$$

High energies: Olsen-Maximon formula with screening and Coulumb corrections

Low energies: Sauter formula (no screening)

Should utilize information from Kissel-Pratt phase-shift calculations, 1 - 500 keV.

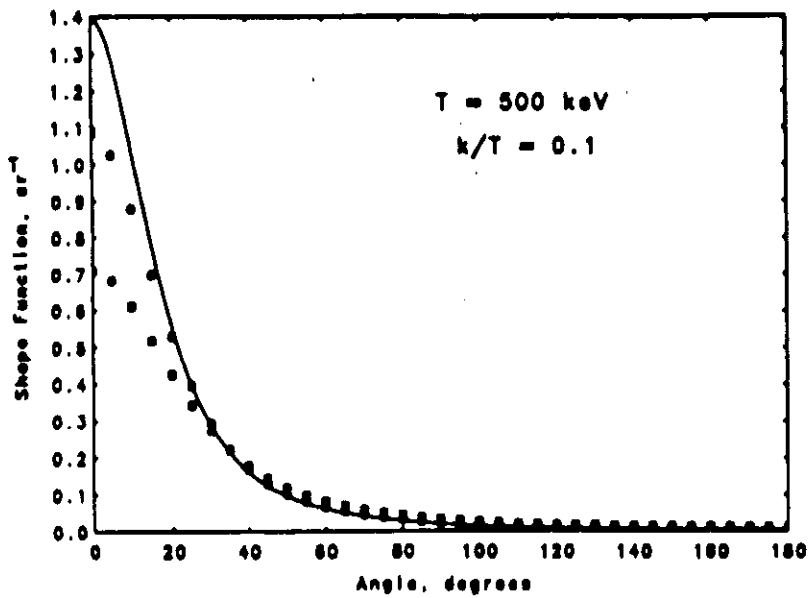
T = 500 keV
k/T = 0.1
Shape Function, sr⁻¹
Angle, degrees

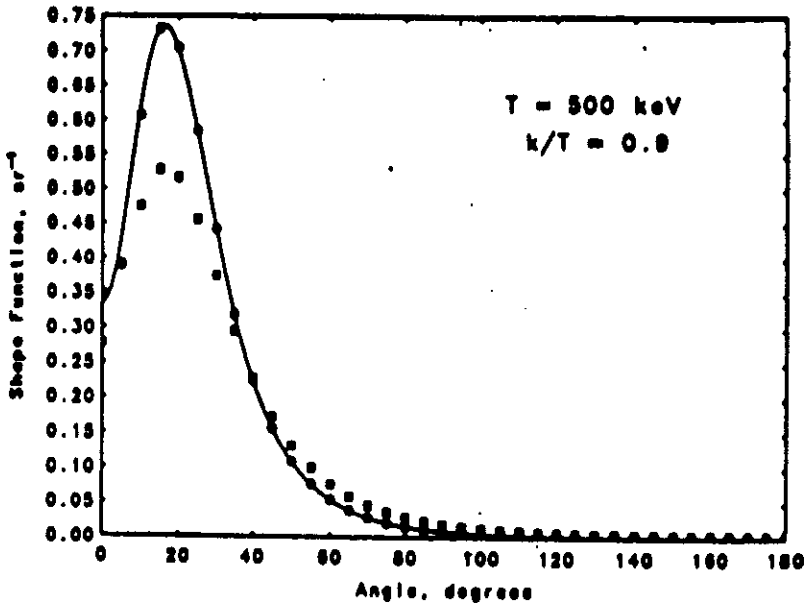
T = 500 keV
k/T = 0.9
Shape Function, sr⁻¹
Angle, degrees

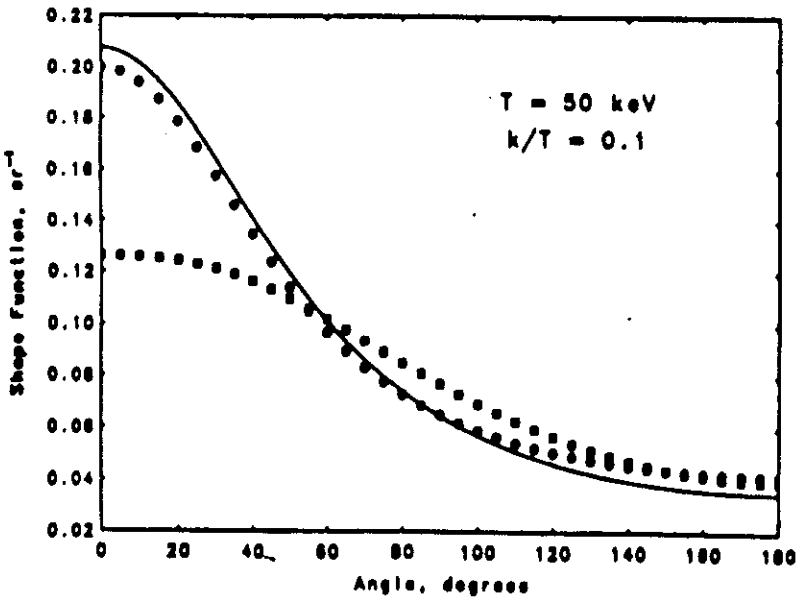
T = 50 keV
k/T = 0.1
Shape Function, sr⁻¹
Angle, degrees

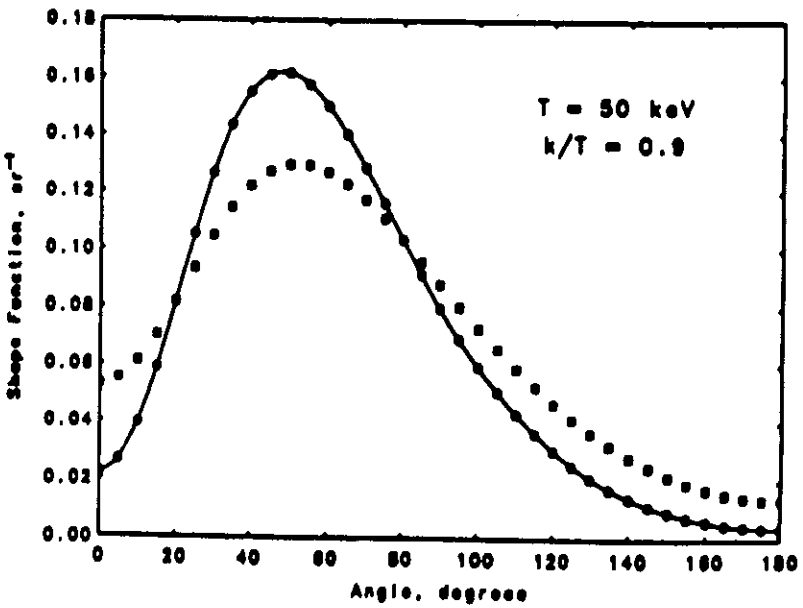
T = 50 keV
k/T = 0.9
Shape Function, sr⁻¹
Angle, degrees

OTHER FEATURES

HISTORY TERMINATION

Electrons

$T > T_{cut}$	follow
$T_{save} > T > T_{cut}$	follow if scoring boundary can be reached (if electron fluence is scored, $T_{save} = T_{cut}$)
$T \leq T_{cut}$	terminate; residual energy deposited along straight path of length = residual range × detour factor

Photons

$T \leq T_{cut}$	terminate

VARIANCE REDUCTION OPTIONS

- **To improve statistics for secondary photons, can artificially scale up:**

  bremsstrahlung production cross sections

  electron-impact ionization cross sections

  Compensating weights are assigned to the histories

- **Numbers of histories of secondary electrons from the large number of scaled-up photons can be controlled**

- **Emergent photon scoring by collision-density method (i.e., score uncollided escape probability after each scattering)**

LIMITATIONS

- Covers energies only down to 1 keV

- No electron or photon diffraction, no electron channeling, no intense-beam collective effects

- No interactions with fields of nucleons (no electron elastic scattering from nucleons, no electro- and photo-disintegration of nucleus)

- Lack of correlation between sampled primary electron energy loss and sampled knock-on electron energy

- Short pathlength and low-energy electron worries
  - general inapplicability of multiple-scattering treatment
  - some approximate boundary-crossing algorithms
  - failure of Bethe-theory stopping power

GENERAL PURPOSE ELECTRON-PHOTON MONTE CARLO CODES

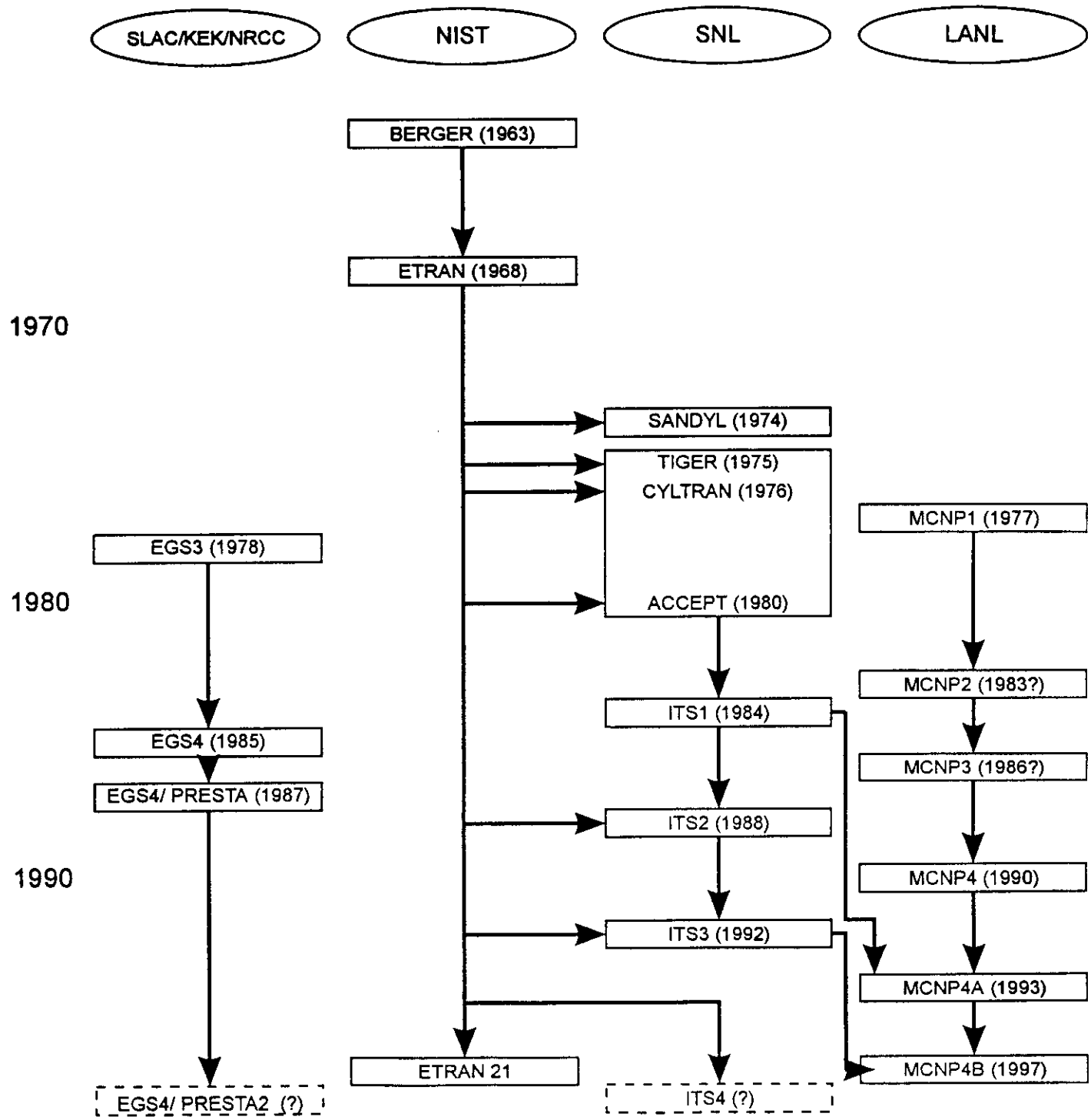

Integrated TIGER Series (ITS): Eight Codes, One Library

	STANDARD	PCODES	MCODES
1D	TIGER	TIGERP	
2.5D	CYLTRAN	CYLTRANP	CYLTRANM
3D	ACCEPT	ACCEPTP	ACCEPTM

K shell ionization

K - N shell ionization and relaxation

Macroscopic magnetic and electric fields

PHOTON TRANSPORT

PROCESS	ETRAN	ITS v. 3	MCNP4B	EGS4
Coherent scattering	yes	yes	yes	yes
Incoherent scattering	with binding	with binding	approx. binding	no binding*
Photoabsorption	yes (K relaxation)	yes (complete relax)	yes (K, L relaxation)	yes (K x rays)*
Pair production	yes	yes	yes	yes
Triplet production	included	included	no	?
Photonuclear abs.	no	no	no	no
Cross Sections	current NIST	current NIST	ENDF/B-IV (1975)	Storm&Israel (1975)

*/ Special versions developed at KEK include incoherent binding and atomic relaxation.

ELECTRON TRANSPORT

PROCESS	ETRAN	ITS v. 3	MCNP4B	EGS4
Energy-loss multiple scattering	Class I	Class I	Class I	Class II
Stopping powers	ICRU 37	ICRU 37	old B&S	ICRU 37
Collision straggling	adjusted Landau/BL	adjusted Landau/BL	adjusted Landau/BL	only above Ecut
Brems production spectrum	"exact"	"exact"	old B&S/K-M analytical package	renorm HE limit theory
Brems angular distribution	analytical theory package	analytical theory package	analytical theory package	Schiff theory
Elastic multiple scattering	Goudsmit-Saunderson	Goudsmit-Saunderson	Goudsmit-Saunderson	Moliere
Elastic single scattering	factored (correct σ_1)	"exact"	"exact"	screened Rutherford
Spatial displacement correction	TLC (1^{st} order)	none	none	PRESTA (0^{th} order)

SECONDARY RADIATIONS

Process	ETRAN	ITS v. 3	MCNP4B	EGS4
Brems production spectrum	"exact"	"exact"	old B&S/K-M analytical package	renorm HE limit theory
Brems angular distribution	analytical theory package	analytical theory package	analytical theory package	Schiff theory
Knock-ons	Moller/free	Moller/free	Moller/free	Moller/free
Compton electrons	with binding	with binding	approx. binding	no binding*
Photoelectrons	yes	yes	yes	yes
Electron-positron pairs	both treated as electrons	both treated as electrons	both treated as electrons	both treated as electrons
Annihilation quanta	at rest	at rest	at rest	in flight, at rest
X rays (photoabsorption)	K-shell	all shells	all shells	K-shell
Auger electrons (photo absorption)	K-shell	all shells	all shells (?)	none
X rays (electron impact)	K-shell	all shells	all shells (?)	none
Auger electrons (electron impact)	K-shell	all shells	all shells (?)	none

GEOMETRIES TREATED

	ETRAN	ITS v. 3	MCNP4B	EGS4
Materials	single	multiple	multiple	multiple
Slab geometry	(included)	TIGER	-	available
Cylindrical geometry	simple, but many simultaneously	CYLTRAN	-	available
General geometry	no	ACCEPT	only	*

*/ User code available for a number of geometries: rectangular, conical, cylindrical, spherical. In general, geometry is written by user.

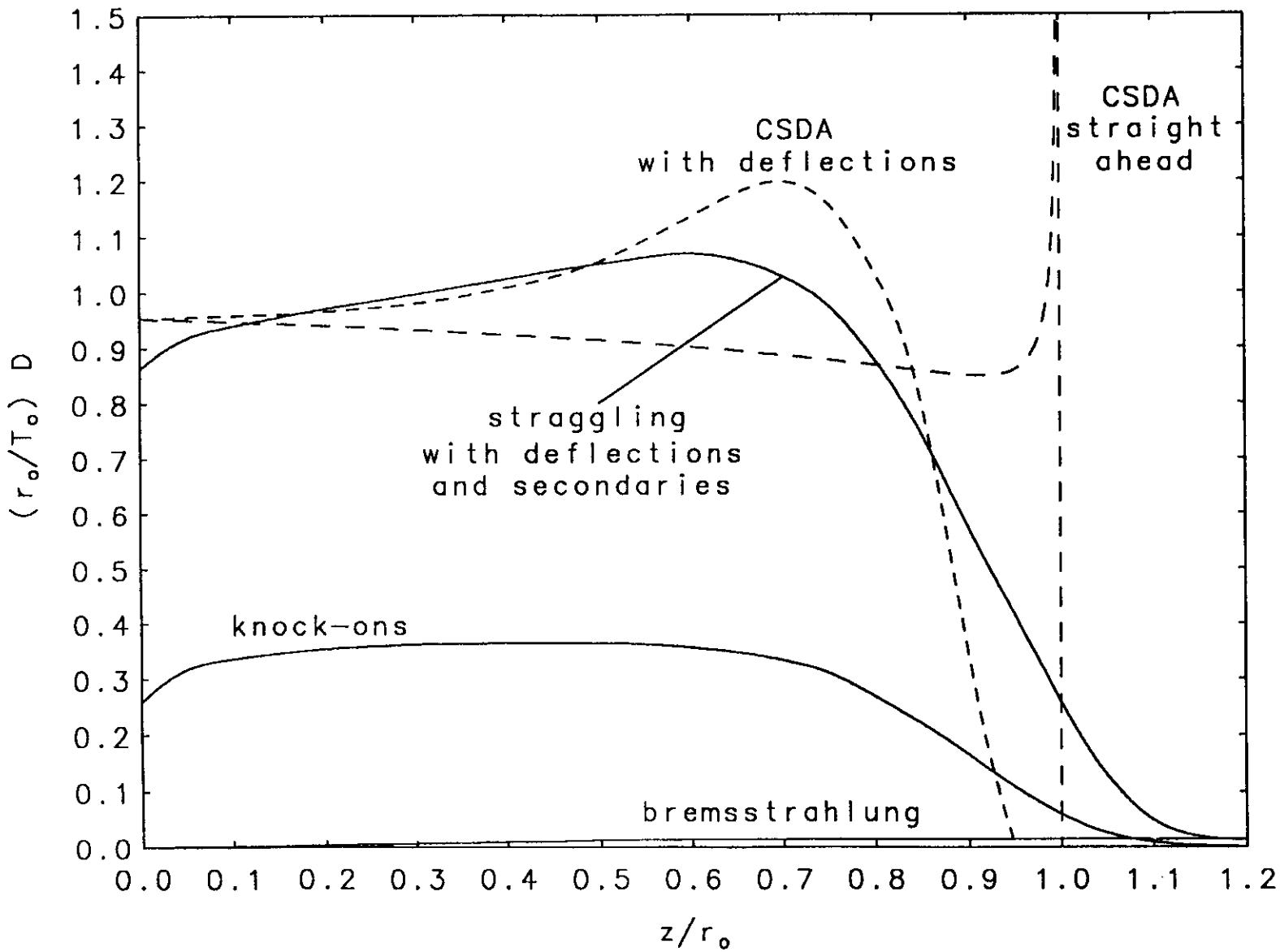
CSDA
with deflections
CSDA
straight
ahead
straggling
with deflections
and secondaries
knock-ons
bremsstrahlung
(r_o/T_o) D
z/r_o
0.0
0.1
0.2
0.3
0.4
0.5
0.6
0.7
0.8
0.9
1.0
1.1
1.2
1.3
1.4
1.5

Some Examples

Example of Monte Carlo calculations for high-energy photon therapy beams: scaling theorem

- Scaling: all dimensions scaled by electron density, $\varepsilon = \rho\, N_A\, Z/A$
  - $x' = (\varepsilon/\varepsilon')\, x$
  - Holds to extent that cross sections are proportional to Z, such as in Compton scattering

- Example: 24 MV photon beam (no electron contamination)
  - Parallel beams of circular area, $1 cm^{-2}$
  - Phantoms of water and of graphite ($1.7\ g/cm^3$), surrounded by vacuum
  - $\varepsilon_{graphite}/\varepsilon_{water} = 1.53$

- Monte Carlo calculations with ITSv3.0 (with slight modifications)
  - Results for central axis ($0.03\ mm^2$)

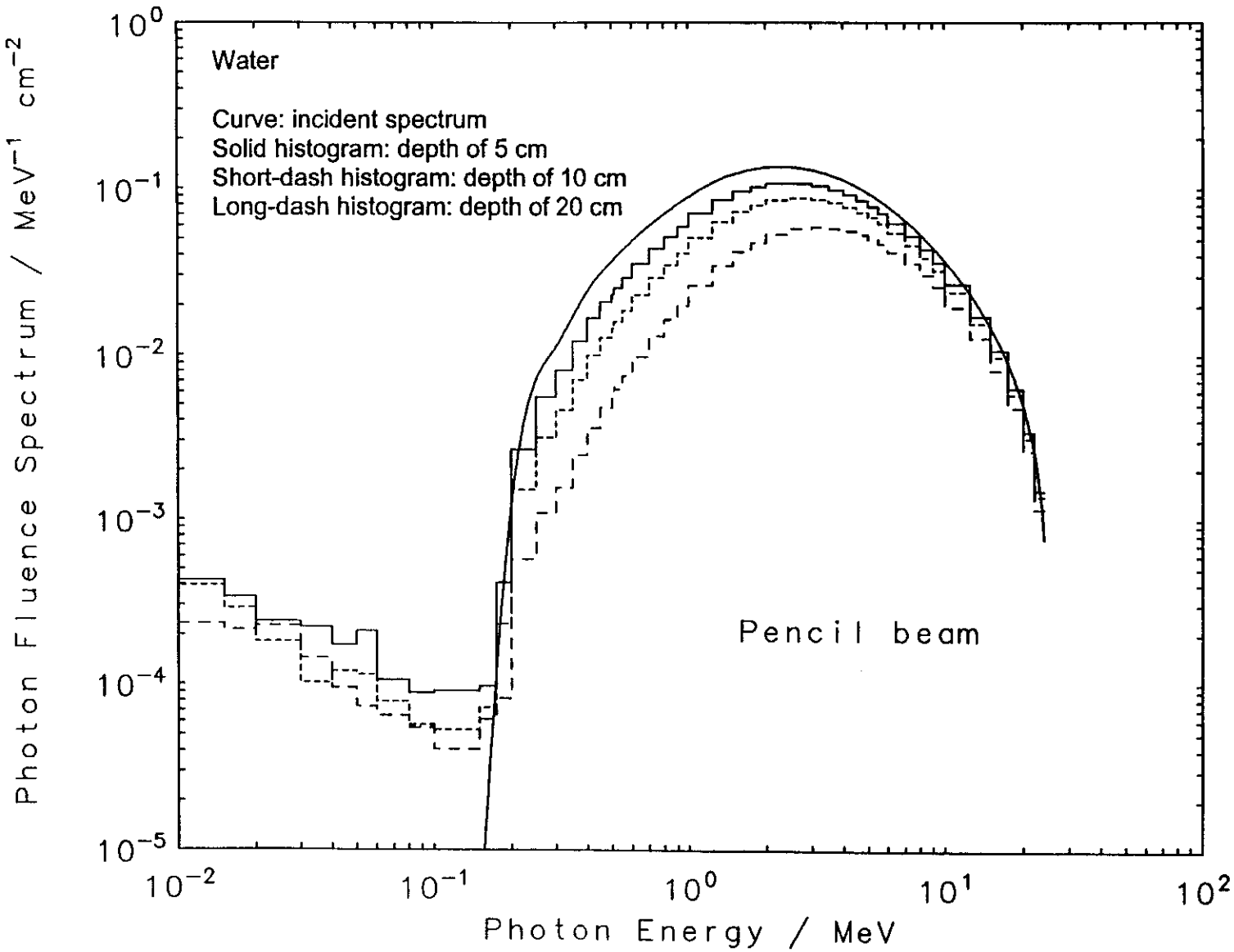
Water
Curve: incident spectrum
Solid histogram: depth of 5 cm
Short-dash histogram: depth of 10 cm
Long-dash histogram: depth of 20 cm
Pencil beam
Photon Fluence Spectrum / MeV^{-1} cm^{-2}
Photon Energy / MeV
10^{0}
10^{-1}
10^{-2}
10^{-3}
10^{-4}
10^{-5}
10^{-2}
10^{-1}
10^{0}
10^{1}
10^{2}

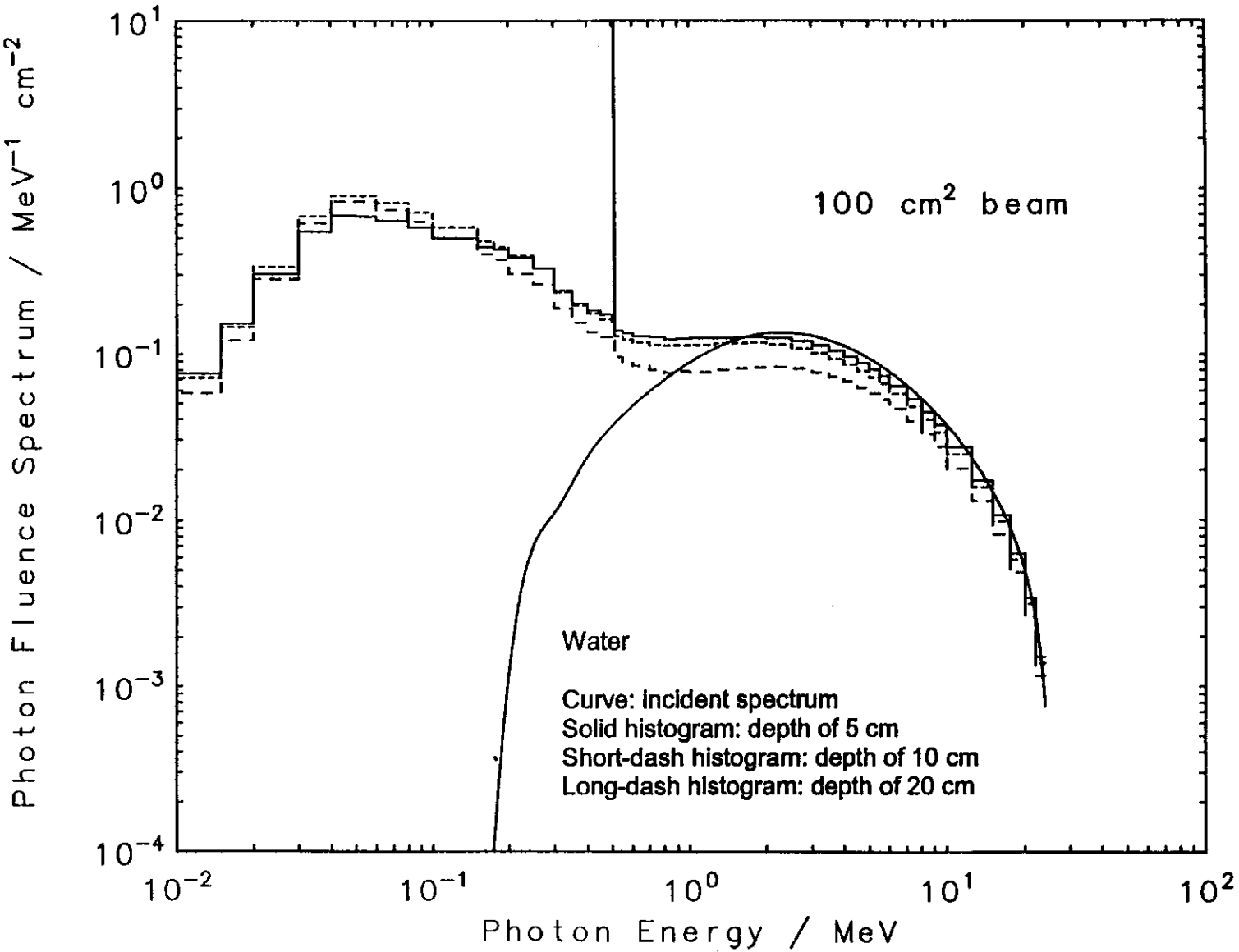
Photon Fluence Spectrum / MeV^{-1} cm^{-2}
10^{1}
10^{0}
10^{-1}
10^{-2}
10^{-3}
10^{-4}
10^{-2}
10^{-1}
10^{0}
10^{1}
10^{2}
Photon Energy / MeV
100 cm^2 beam
Water
Curve: incident spectrum
Solid histogram: depth of 5 cm
Short-dash histogram: depth of 10 cm
Long-dash histogram: depth of 20 cm

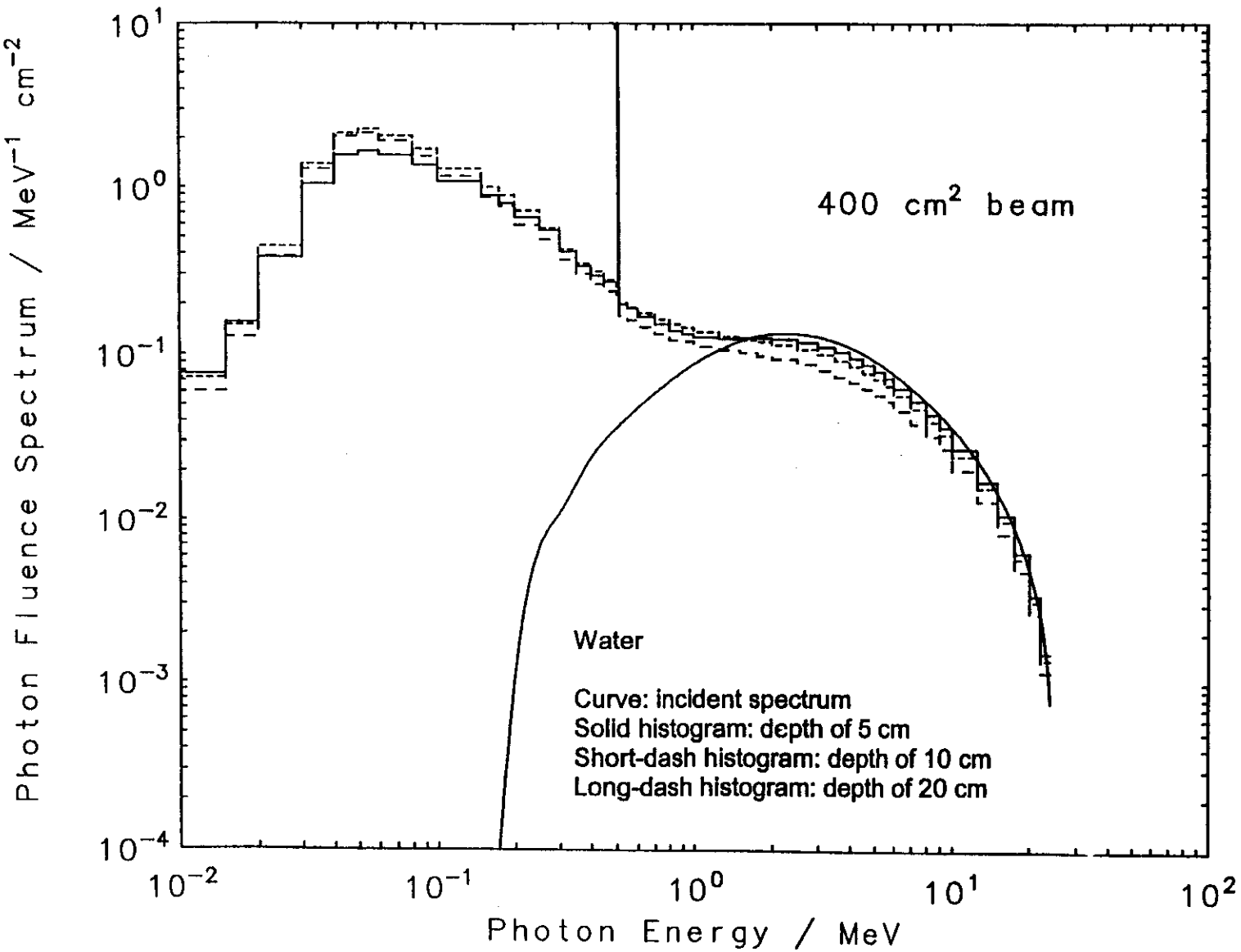
Photon Fluence Spectrum / MeV^{-1} cm^{-2}
10^{1}
10^{0}
10^{-1}
10^{-2}
10^{-3}
10^{-4}
10^{-2}
10^{-1}
10^{0}
10^{1}
10^{2}
Photon Energy / MeV
400 cm^2 beam
Water
Curve: incident spectrum
Solid histogram: depth of 5 cm
Short-dash histogram: depth of 10 cm
Long-dash histogram: depth of 20 cm

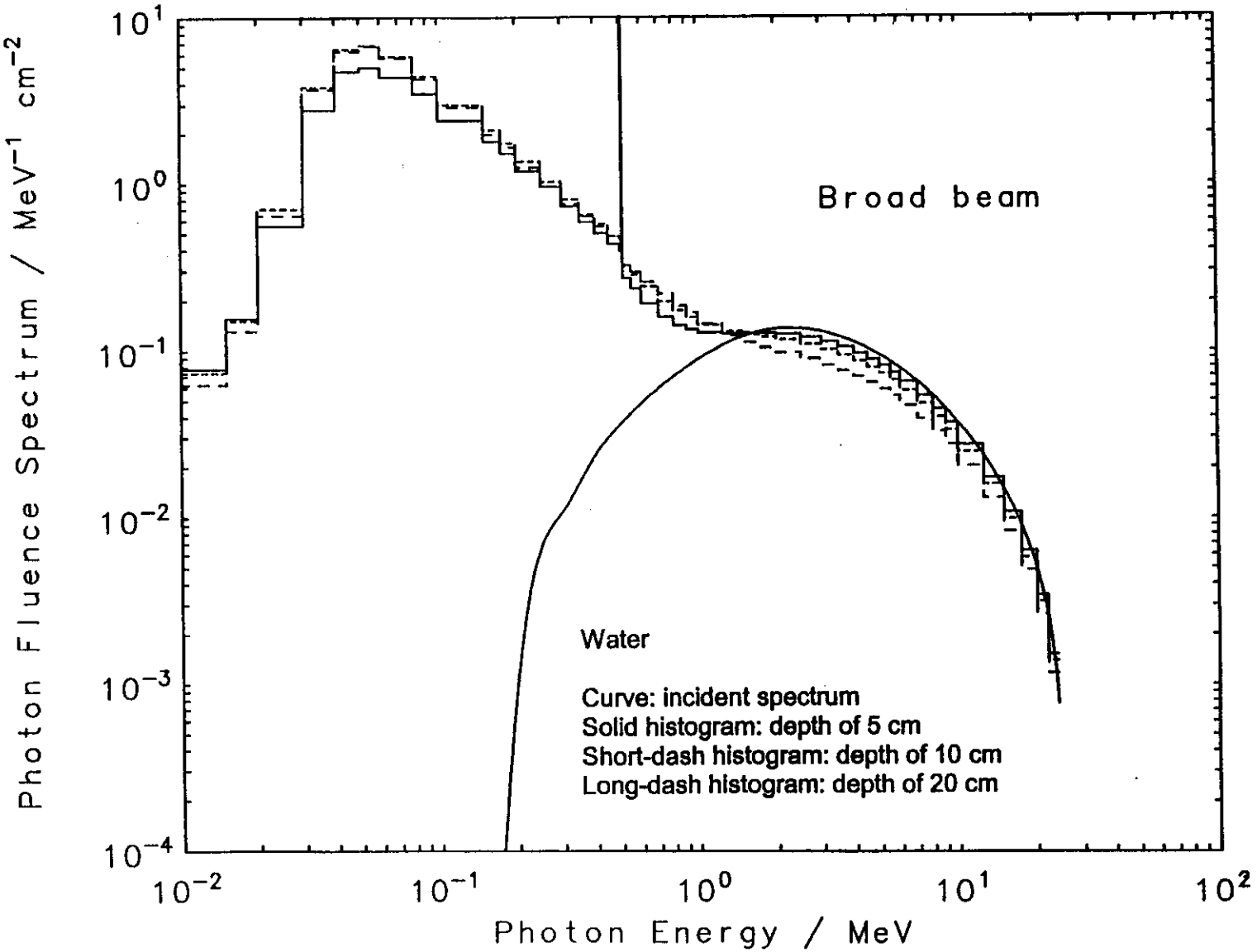
Photon Fluence Spectrum / MeV^{-1} cm^{-2}
10^{1}
10^{0}
10^{-1}
10^{-2}
10^{-3}
10^{-4}
10^{-2}
10^{-1}
10^{0}
10^{1}
10^{2}
Photon Energy / MeV
Broad beam
Water
Curve: incident spectrum
Solid histogram: depth of 5 cm
Short-dash histogram: depth of 10 cm
Long-dash histogram: depth of 20 cm

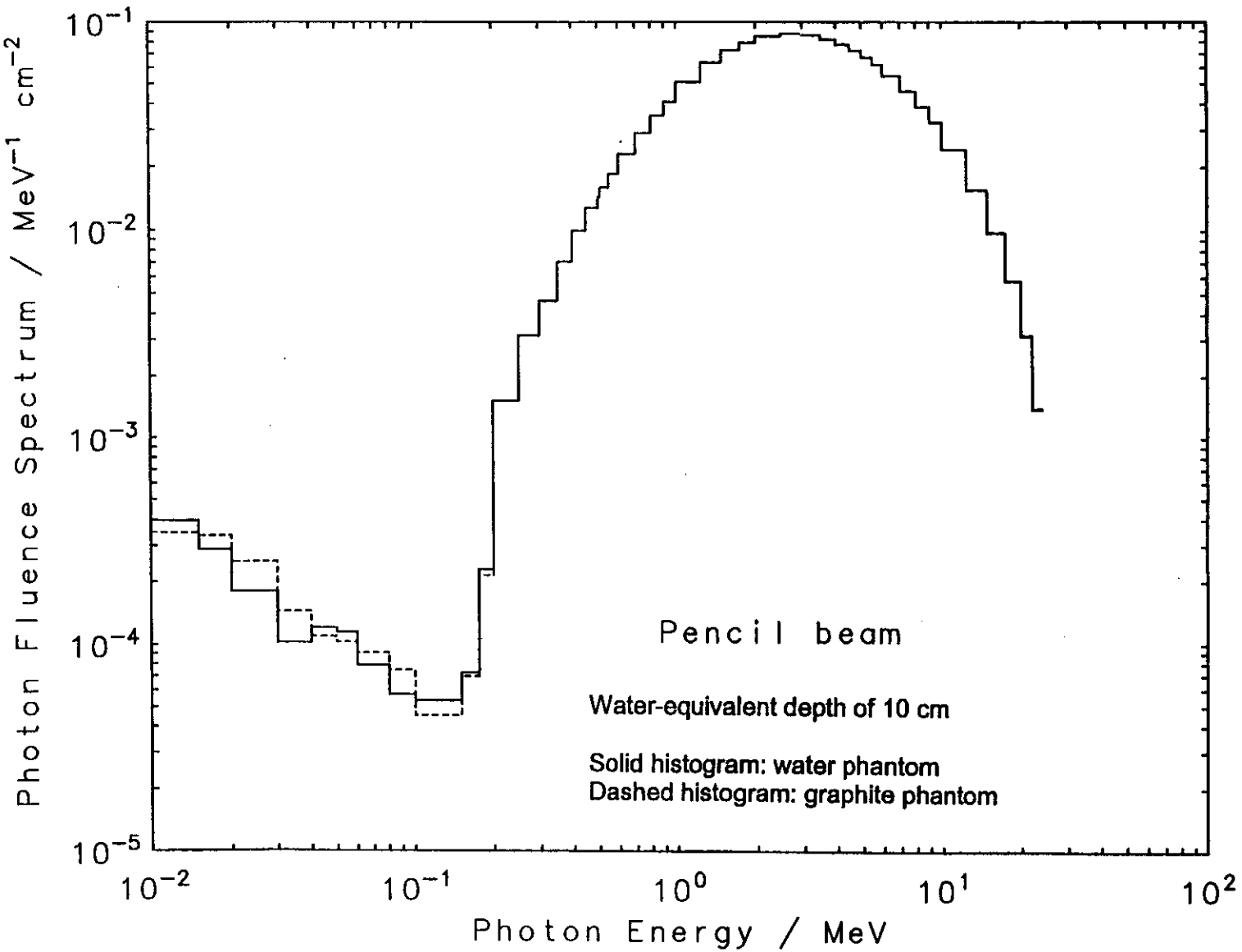
Photon Fluence Spectrum / MeV^{-1} cm^{-2}
10^{-1}
10^{-2}
10^{-3}
10^{-4}
10^{-5}
10^{-2}
10^{-1}
10^{0}
10^{1}
10^{2}
Photon Energy / MeV
Pencil beam
Water-equivalent depth of 10 cm
Solid histogram: water phantom
Dashed histogram: graphite phantom

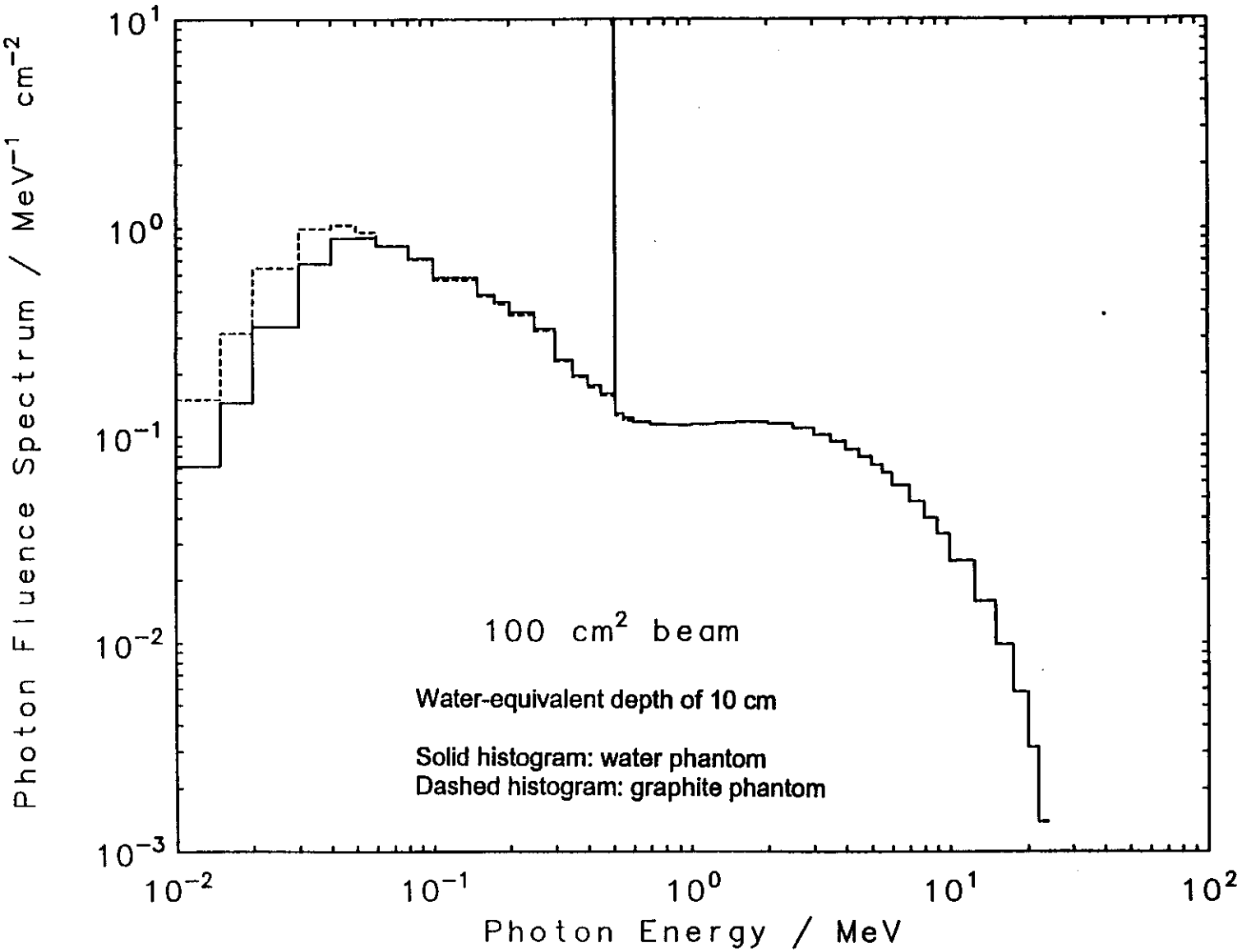
Photon Fluence Spectrum / MeV^{-1} cm^{-2}
10^{1}
10^{0}
10^{-1}
10^{-2}
10^{-3}
10^{-2}
10^{-1}
10^{0}
10^{1}
10^{2}
Photon Energy / MeV
100 cm^2 beam
Water-equivalent depth of 10 cm
Solid histogram: water phantom
Dashed histogram: graphite phantom

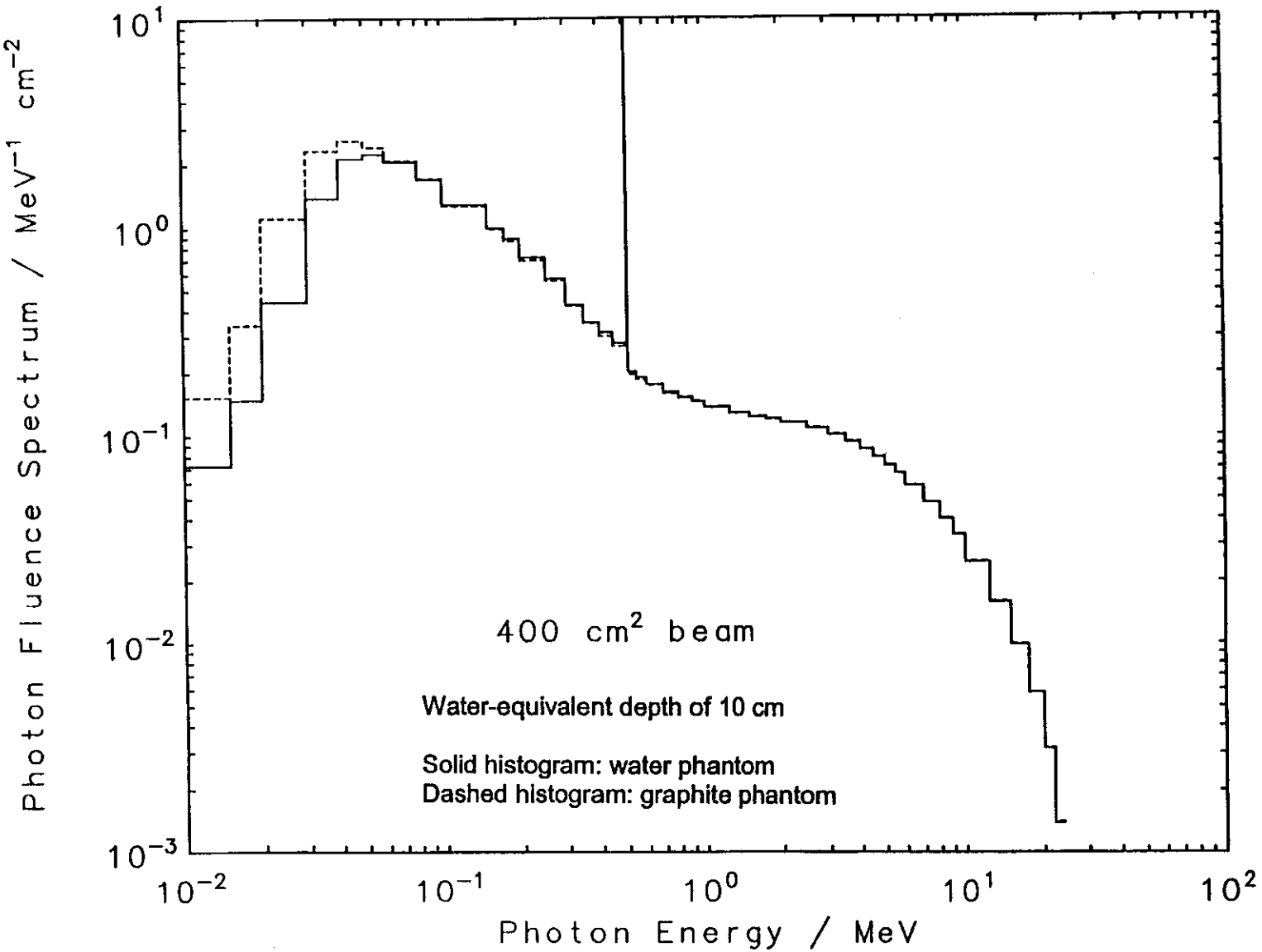
Photon Fluence Spectrum / MeV^{-1} cm^{-2}
10^{1}
10^{0}
10^{-1}
10^{-2}
10^{-3}
10^{-2}
10^{-1}
10^{0}
10^{1}
10^{2}
Photon Energy / MeV
400 cm^2 beam
Water-equivalent depth of 10 cm
Solid histogram: water phantom
Dashed histogram: graphite phantom

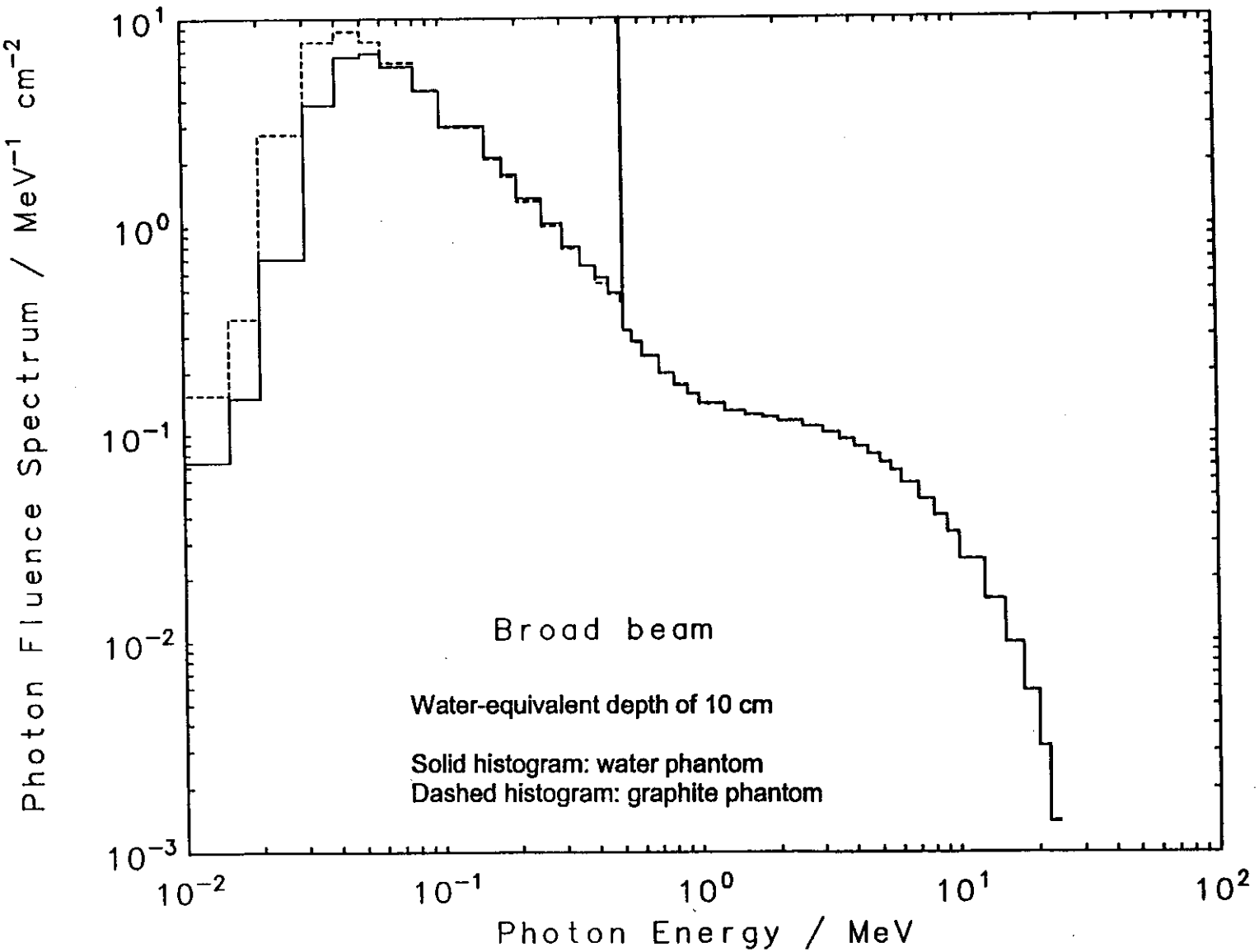
Photon Fluence Spectrum / MeV^{-1} cm^{-2}
10^{1}
10^{0}
10^{-1}
10^{-2}
10^{-3}
10^{-2}
10^{-1}
10^{0}
10^{1}
10^{2}
Photon Energy / MeV
Broad beam
Water-equivalent depth of 10 cm
Solid histogram: water phantom
Dashed histogram: graphite phantom

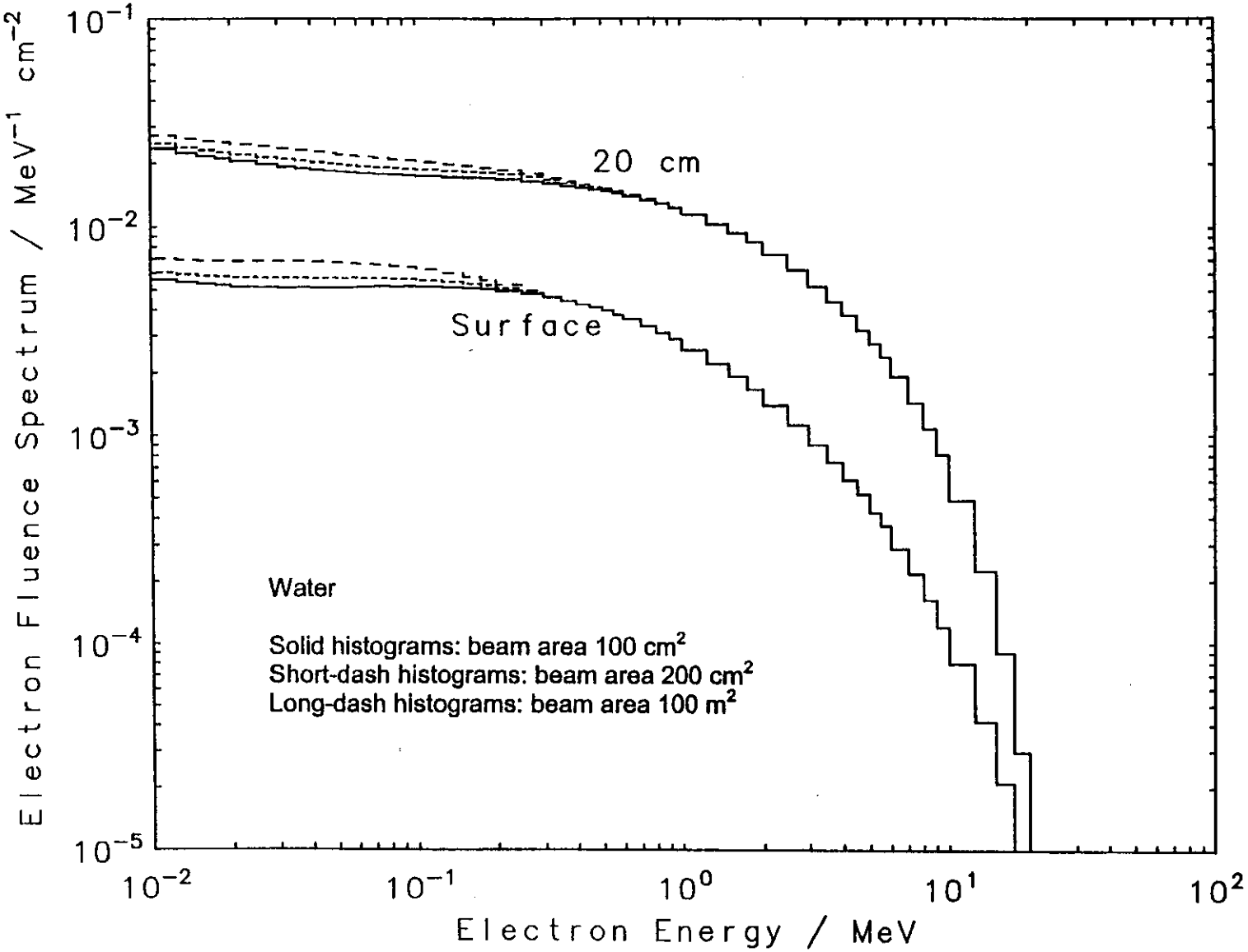
Electron Fluence Spectrum / MeV^{-1} cm^{-2}
10^{-1}
10^{-2}
10^{-3}
10^{-4}
10^{-5}
20 cm
Surface
Water
Solid histograms: beam area 100 cm^2
Short-dash histograms: beam area 200 cm^2
Long-dash histograms: beam area 100 m^2
10^{-2}
10^{-1}
10^{0}
10^{1}
10^{2}
Electron Energy / MeV

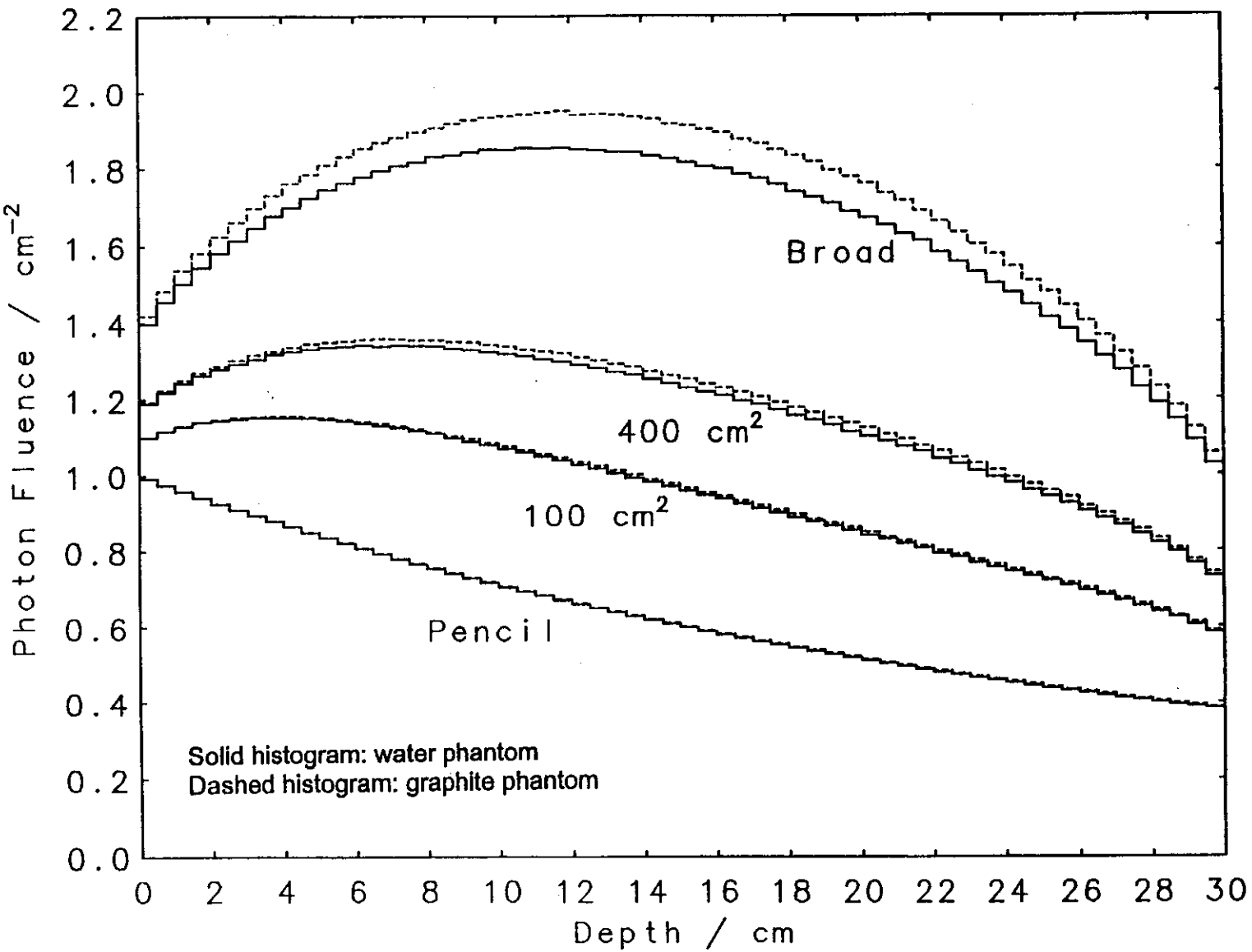
Photon Fluence / cm^{-2}
2.2
2.0
1.8
1.6
1.4
1.2
1.0
0.8
0.6
0.4
0.2
0.0
Broad
400 cm^2
100 cm^2
Pencil
Solid histogram: water phantom
Dashed histogram: graphite phantom
0 2 4 6 8 10 12 14 16 18 20 22 24 26 28 30
Depth / cm

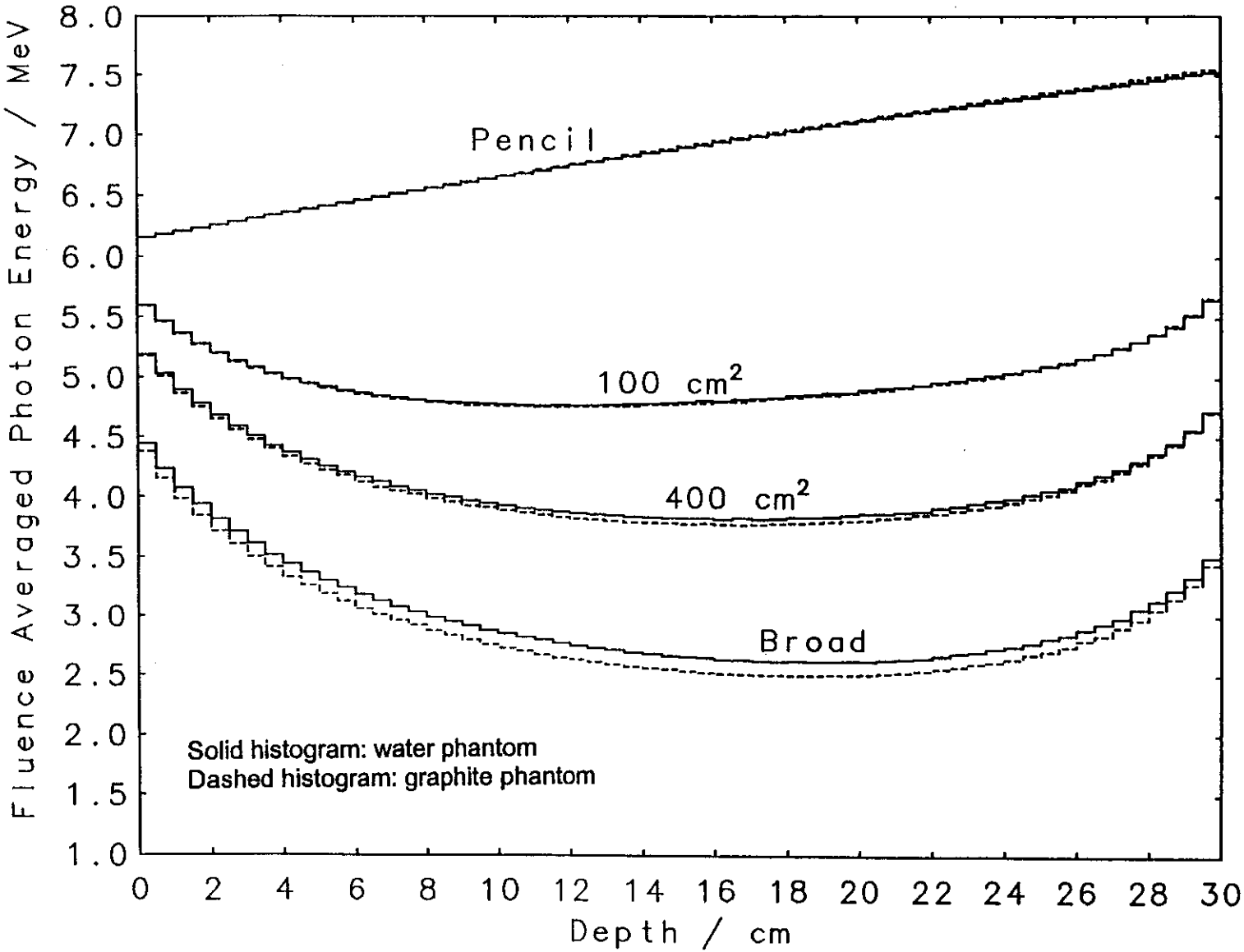
Fluence Averaged Photon Energy / MeV
8.0
7.5
7.0
6.5
6.0
5.5
5.0
4.5
4.0
3.5
3.0
2.5
2.0
1.5
1.0
Pencil
100 cm²
400 cm²
Broad
Solid histogram: water phantom
Dashed histogram: graphite phantom
0
2
4
6
8
10
12
14
16
18
20
22
24
26
28
30
Depth / cm

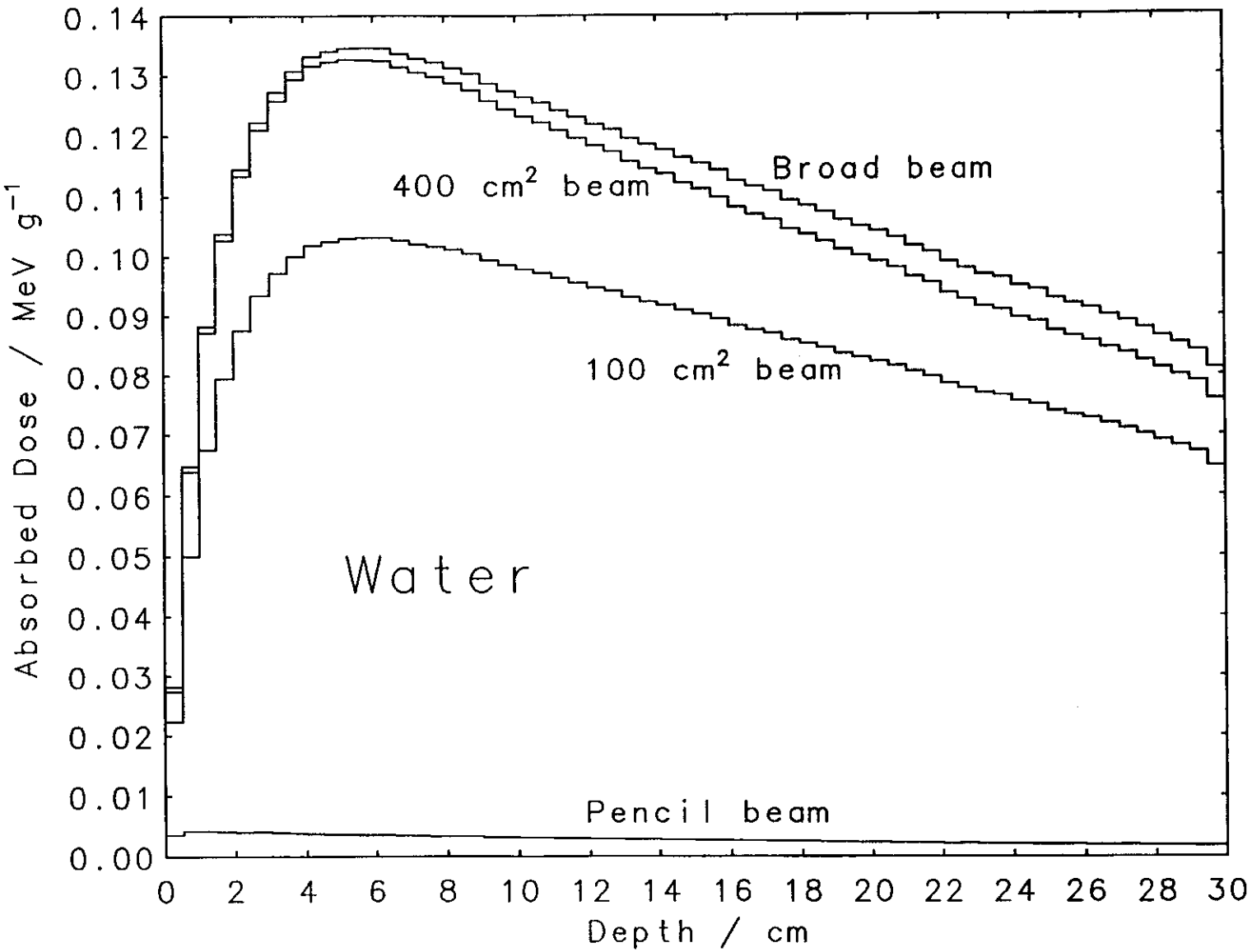
0.14
0.13
0.12
0.11
0.10
0.09
0.08
0.07
0.06
0.05
0.04
0.03
0.02
0.01
0.00
Absorbed Dose / MeV g^{-1}
Broad beam
400 cm^2 beam
100 cm^2 beam
Water
Pencil beam
0 2 4 6 8 10 12 14 16 18 20 22 24 26 28 30
Depth / cm

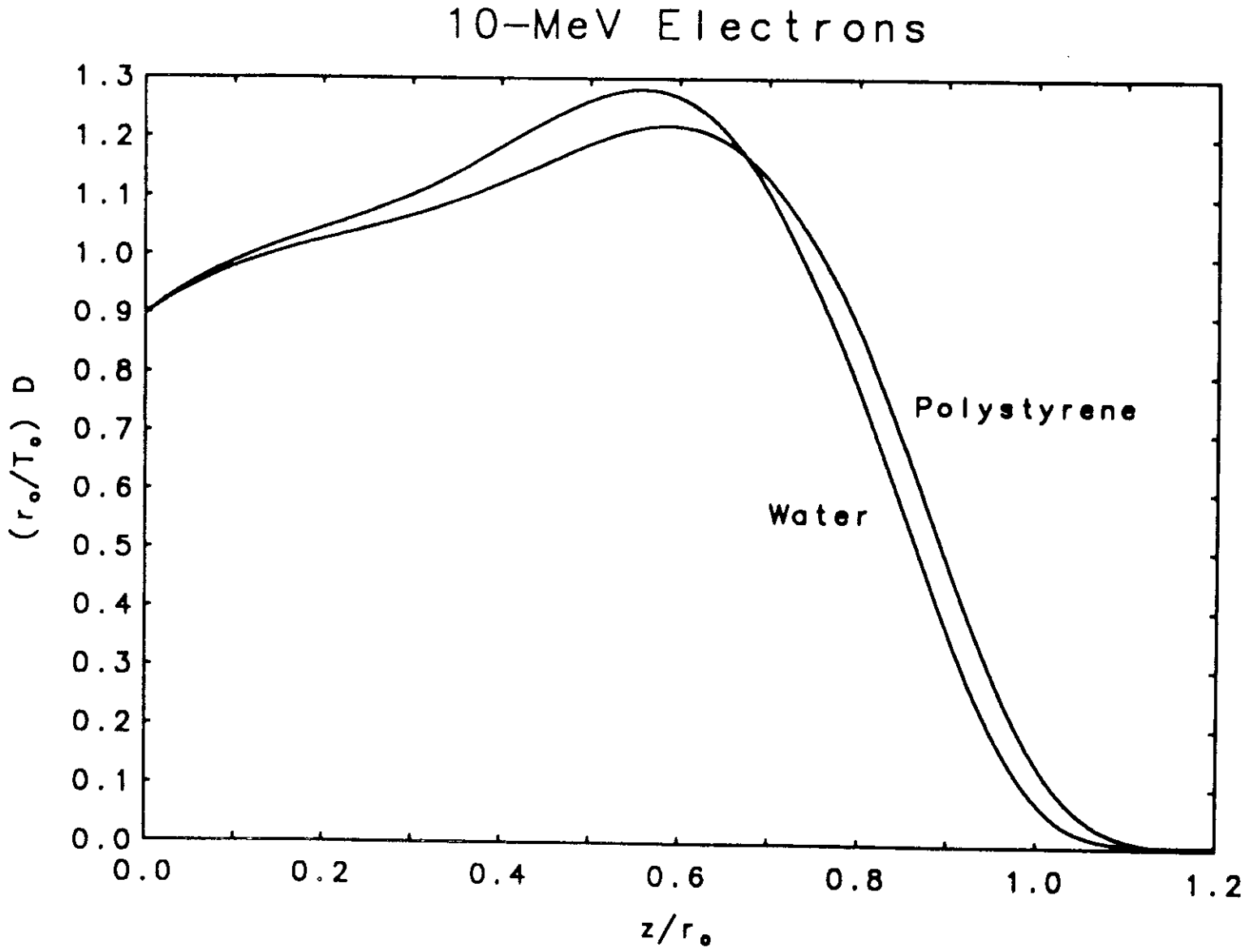
10-MeV Electrons
1.3
1.2
1.1
1.0
0.9
0.8
0.7
0.6
0.5
0.4
0.3
0.2
0.1
0.0
(r_o/T_o) D
0.0
0.2
0.4
0.6
0.8
1.0
1.2
z/r_o
Polystyrene
Water

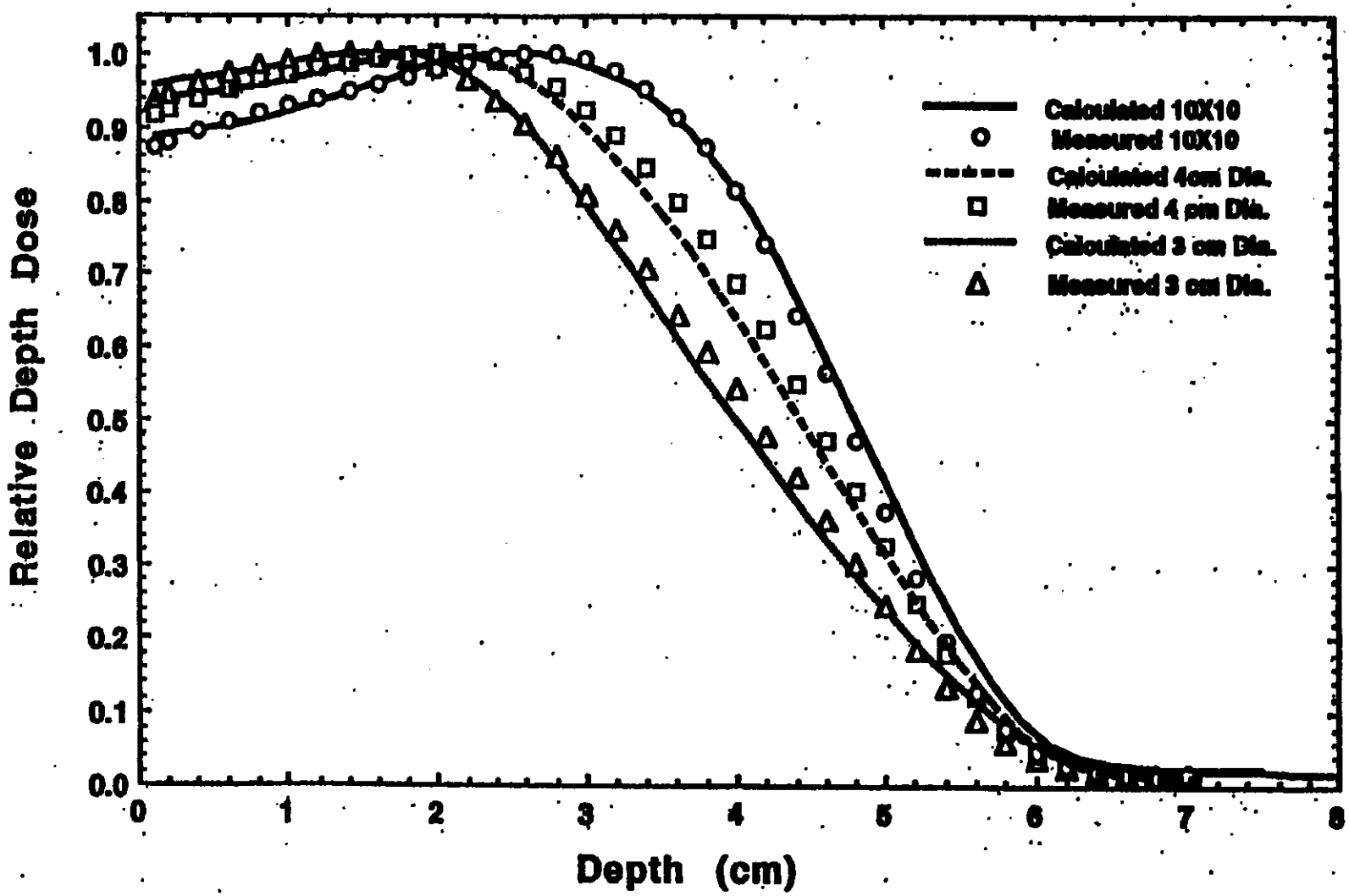

Comparison of central-axis depth-dose distributions from measurement (ion chamber) and Monte Carlo calculations (ITSv3.0) for an electron beam with a nominal energy of 12 MeV (Varian 2100C), after estimation of the actual electron spectrum emerging from the cone applicator. (From Kassaee et al., 1994).

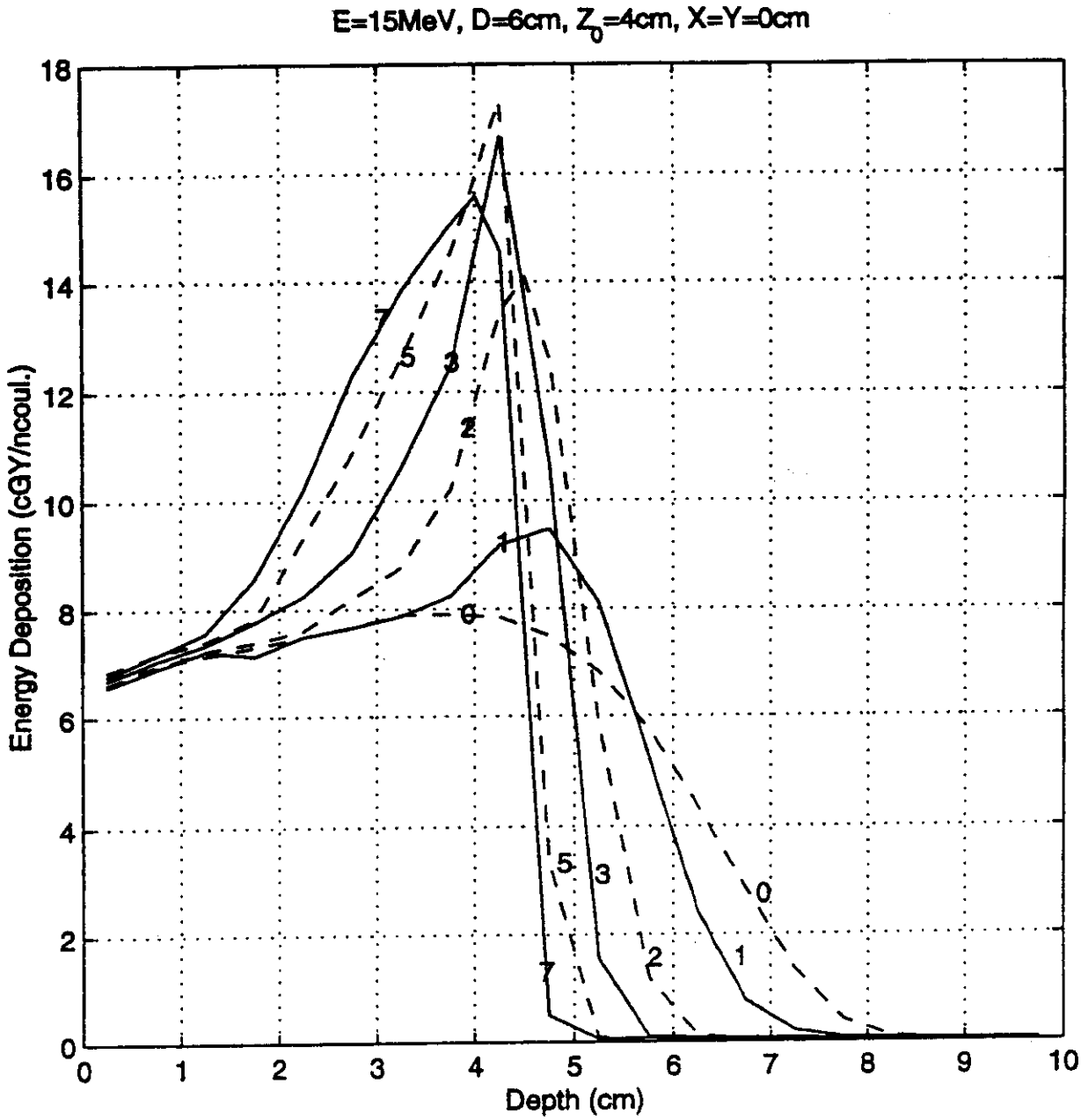

Central-axis depth-dose curves for electron beams incident with an energy of 15 MeV and a beam diameter of 6 cm. The initial 4 cm layer of tissue is field-free, after which there is applied a uniform magnetic field perpendicular to the beam axis. Results are from the ITS v. 3 Monte Carlo code ACCEPTM, and are shown for magnetic fields of 0, 1, 2, 3, 5 and 7 T. From Nardi and Barnea (1999).

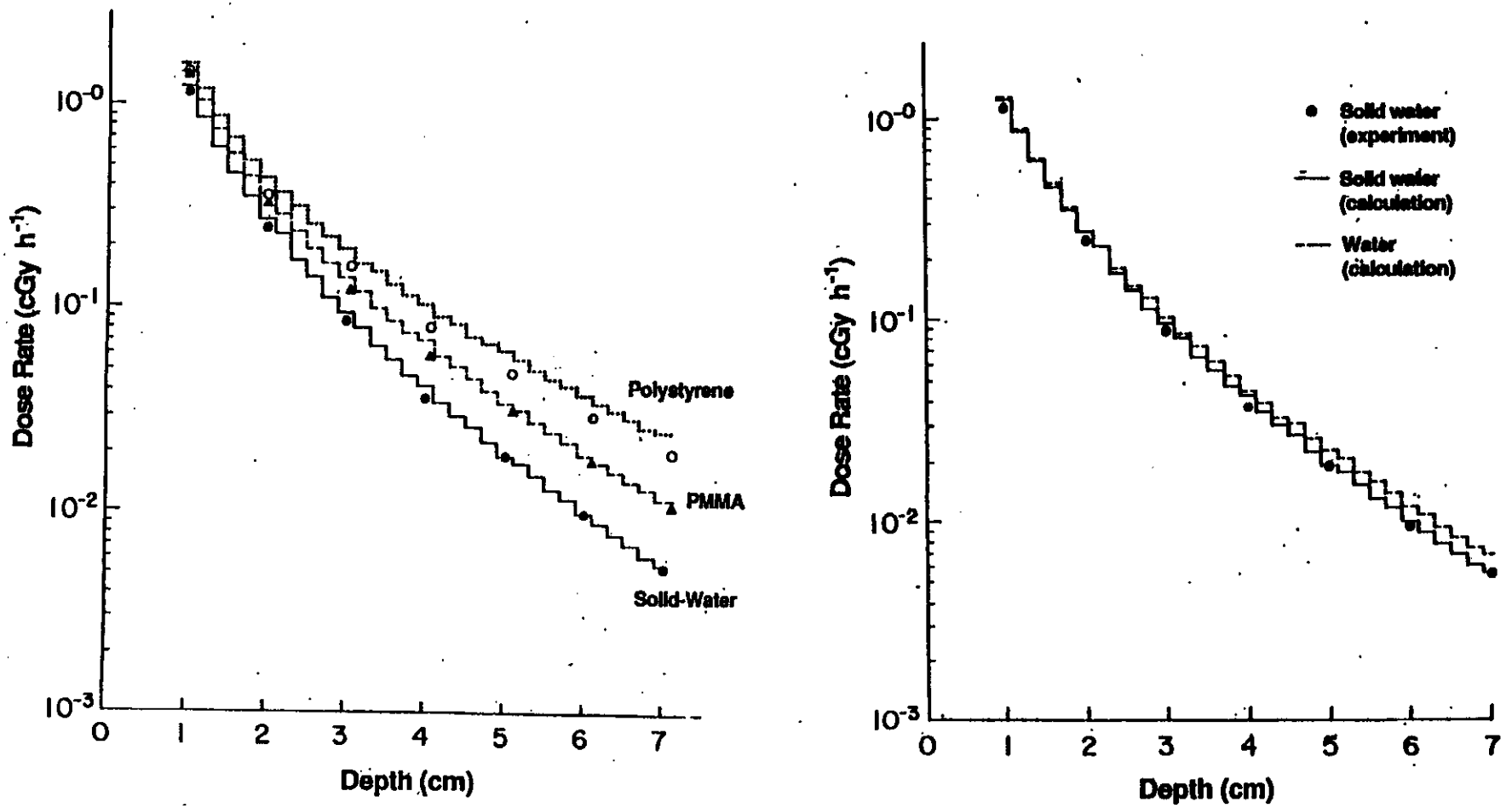

Comparison of results from measurement (TLD) and from Monte Carlo calculation (ITSv1.0) for the absorbed-dose rate along the perpendicular bisector in various phantom materials, from a ~1 mCi ^{125}I source (model 6702). (From Meigooni et al., 1988)

Endovascular Brachytherapy Sources

Liquid-filled balloon: ^{90}Y, ^{32}P, ^{188}Re

Balloons: 20 to 40 mm length, 2 to 4 mm outside diameter
Polyethylene walls: 0.04 to 0.05 mm thick

$^{90}Sr/^{90}Y$ seeds

Emitting core: 2.3 mm length, 0.54 mm diameter
($\rho = 2.6$ g/cm^3)
Encapsulation: 2.5 mm length, 0.64 mm diameter
($\rho = 8.1$ g/cm^3 steel)
Seed train: 12 seeds, with Au marker seeds at ends

^{32}P wire

Emitting core: 27 mm length, 0.24 mm diameter
($\rho = 1.1$ g/cm^3)
Encapsulation: 27 mm length, 0.46 mm diameter
($\rho = 6.5$ g/cm^3 NiTi)

^{192}Ir seeds

Emitting core: 3 mm length, 0.1 mm diameter
($\rho = 22$ g/cm^3 Pt-Ir alloy)
Encapsulation: 3 mm length, 0.5 mm diameter
($\rho = 8.1$ g/cm^3 steel)
Ribbon: 0.8 mm diameter ($\rho = 1.1$ g/cm^3 nylon)

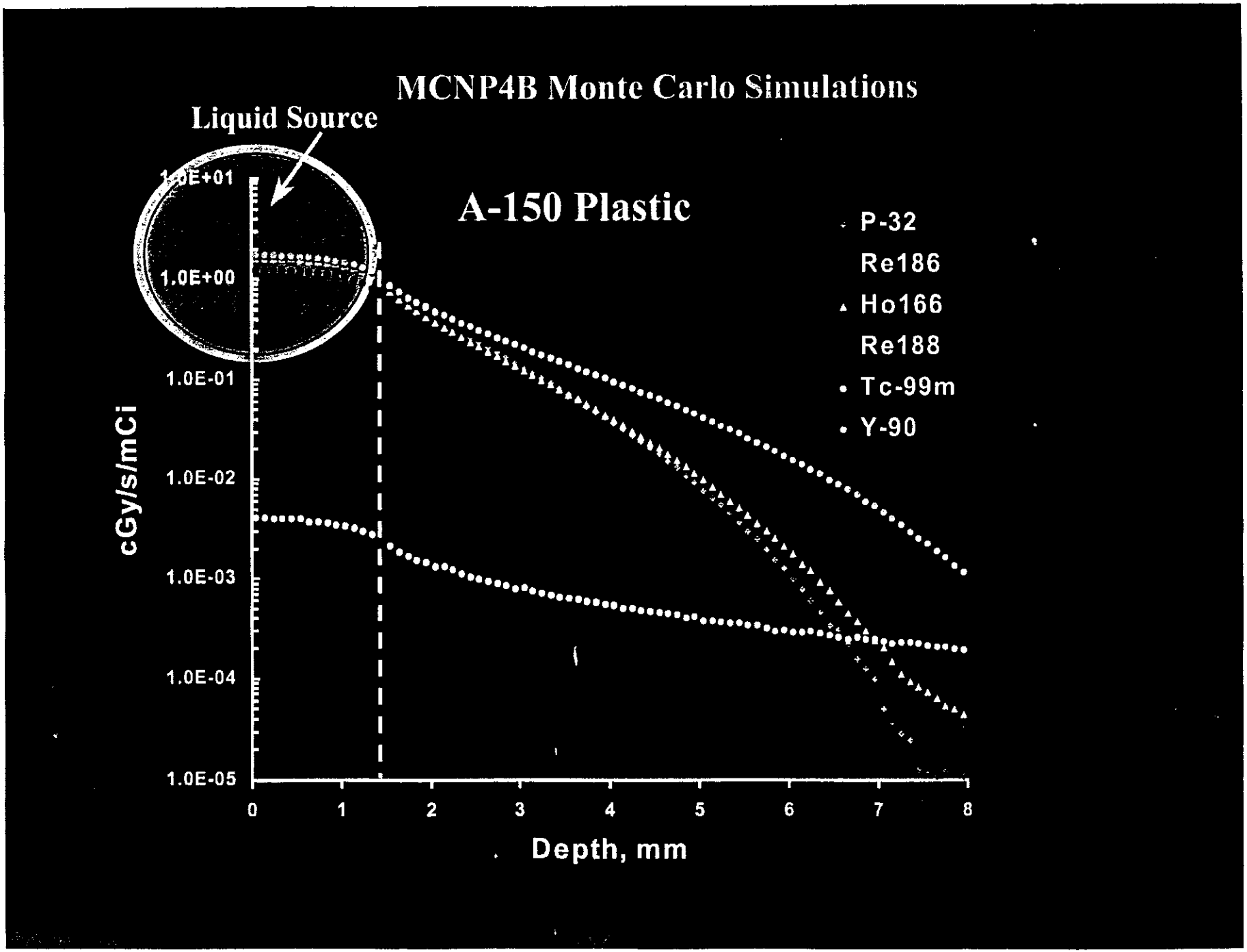
MCNP4B Monte Carlo Simulations
Liquid Source
A-150 Plastic
P-32
Re186
Ho166
Re188
Tc-99m
Y-90
cGy/s/mCi
1.0E+01
1.0E+00
1.0E-01
1.0E-02
1.0E-03
1.0E-04
1.0E-05
0
1
2
3
4
5
6
7
8
Depth, mm

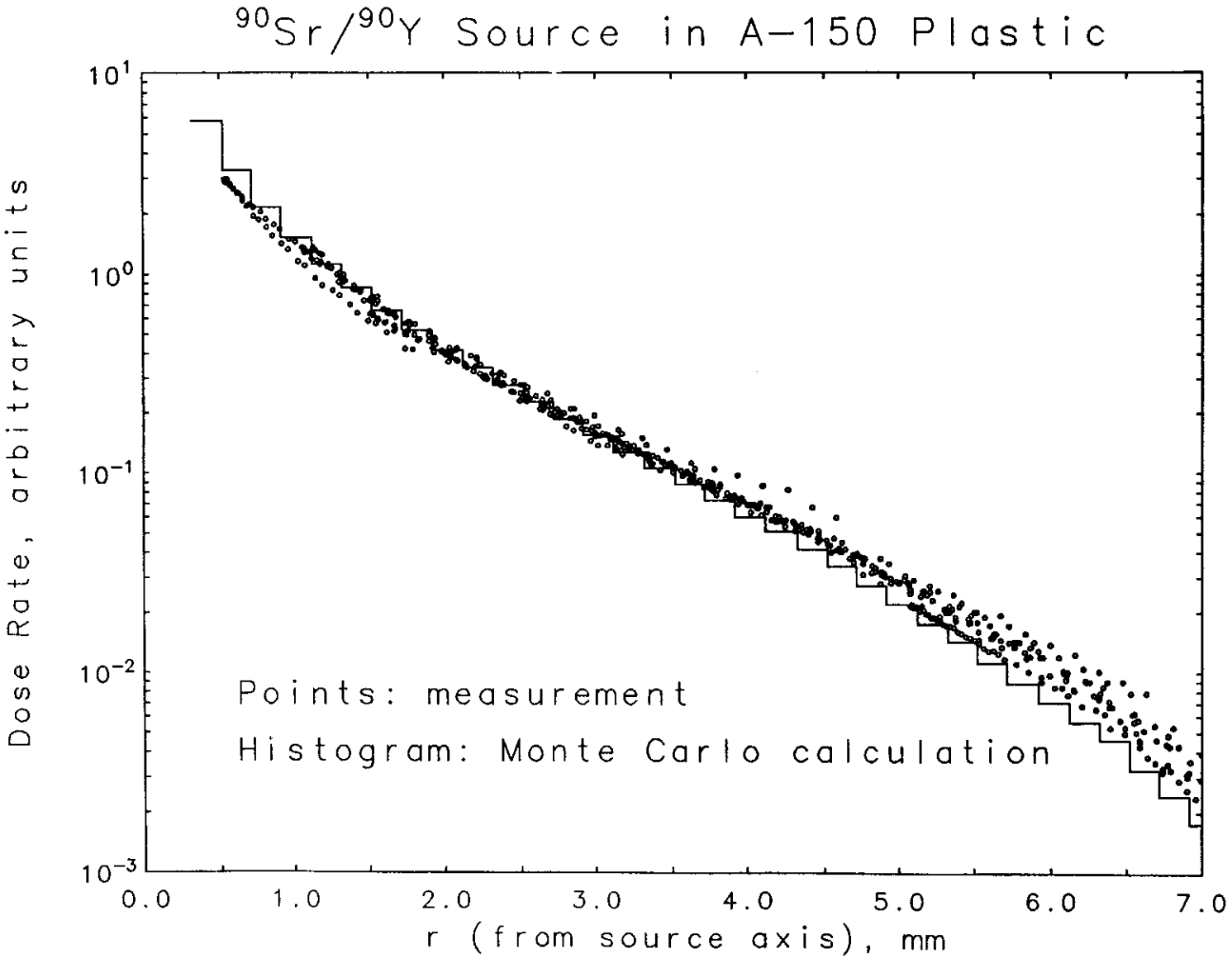
$^{90}Sr/^{90}Y$ Source in A-150 Plastic
Dose Rate, arbitrary units
10^{1}
10^{0}
10^{-1}
10^{-2}
10^{-3}
Points: measurement
Histogram: Monte Carlo calculation
0.0
1.0
2.0
3.0
4.0
5.0
6.0
7.0
r (from source axis), mm

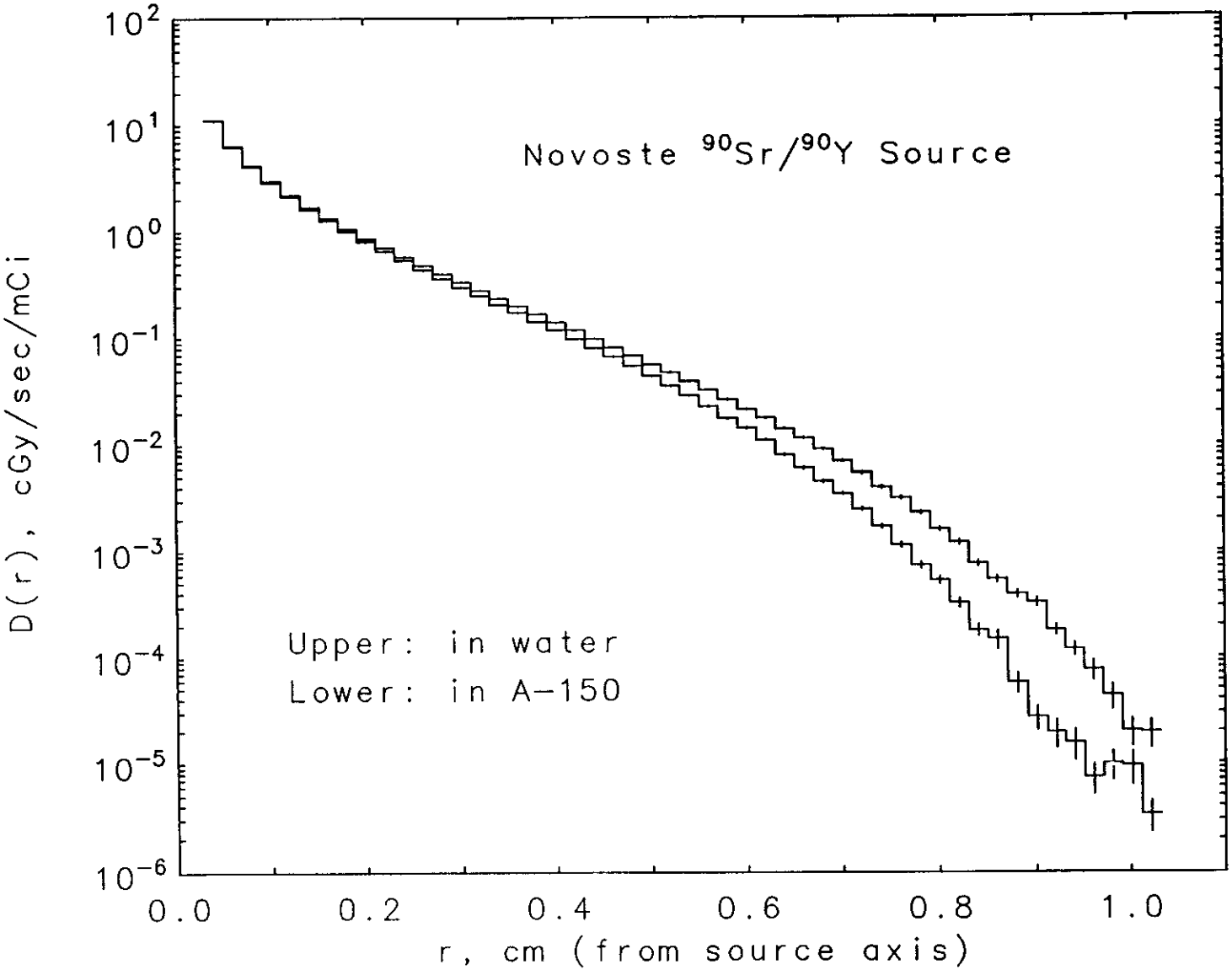
Novoste $^{90}Sr/^{90}Y$ Source
Upper: in water
Lower: in A-150
D(r), cGy/sec/mCi
r, cm (from source axis)
10^{2}
10^{1}
10^{0}
10^{-1}
10^{-2}
10^{-3}
10^{-4}
10^{-5}
10^{-6}
0.0
0.2
0.4
0.6
0.8
1.0

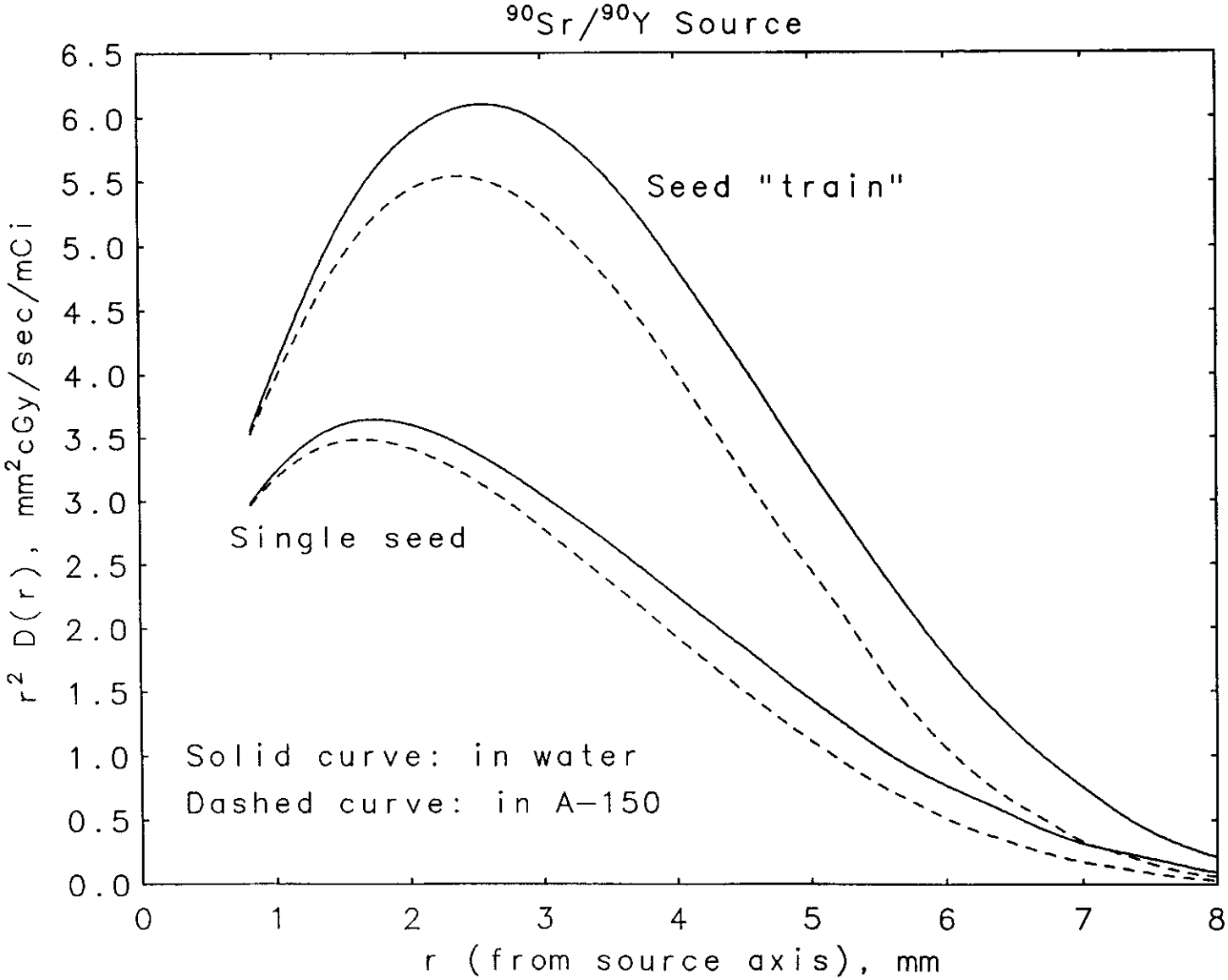
$^{90}Sr/^{90}Y$ Source
r^2 D(r), mm^2cGy/sec/mCi
6.5
6.0
5.5
5.0
4.5
4.0
3.5
3.0
2.5
2.0
1.5
1.0
0.5
0.0
0
1
2
3
4
5
6
7
8
r (from source axis), mm
Seed "train"
Single seed
Solid curve: in water
Dashed curve: in A-150

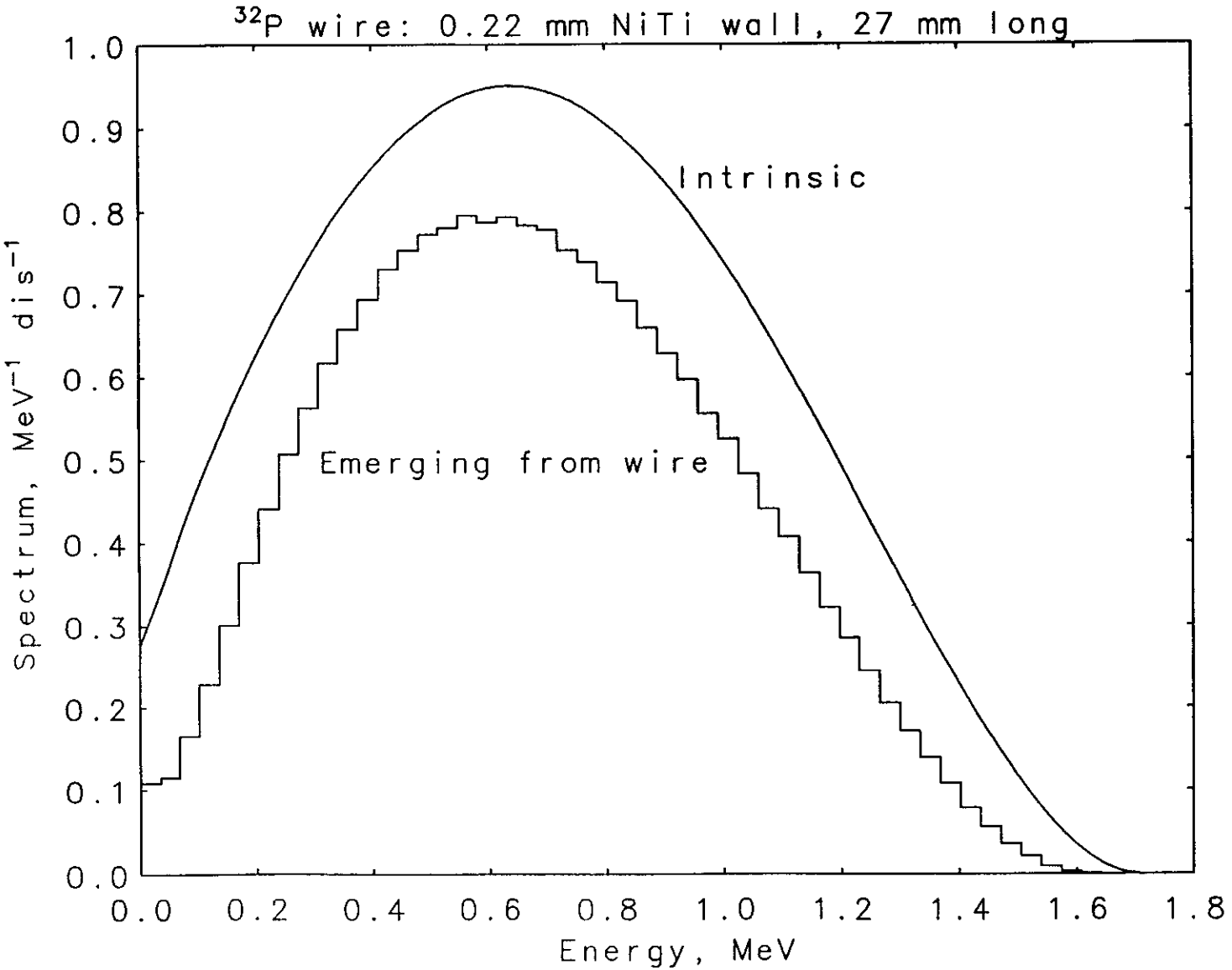
^{32}P wire: 0.22 mm NiTi wall, 27 mm long
Intrinsic
Emerging from wire
Spectrum, MeV^{-1} dis^{-1}
Energy, MeV
0.0
0.1
0.2
0.3
0.4
0.5
0.6
0.7
0.8
0.9
1.0
0.0
0.2
0.4
0.6
0.8
1.0
1.2
1.4
1.6
1.8

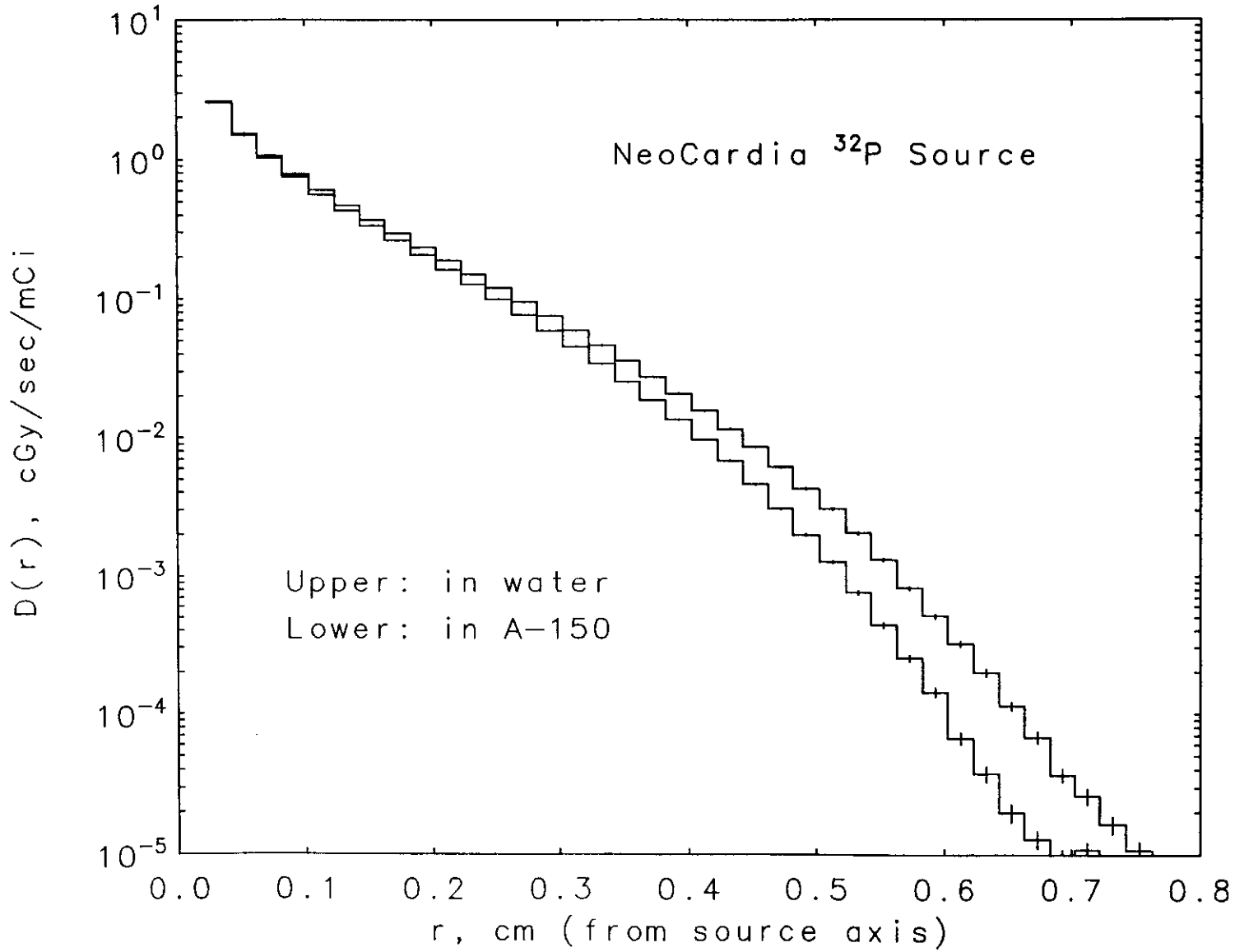
NeoCardia 32P Source
Upper: in water
Lower: in A-150
D(r), cGy/sec/mCi
r, cm (from source axis)
10^1
10^0
10^-1
10^-2
10^-3
10^-4
10^-5
0.0
0.1
0.2
0.3
0.4
0.5
0.6
0.7
0.8

Codes Compared

- Monte Carlo N-Particle transport code (MCNP4B)
- CYLTRAN from the Integrated Tiger Series codes (ITS v.3)
- Electron Gamma Shower code (EGS4)

Codes Common Ground

- ^{32}P energy spectrum from data provided by Stephen Seltzer, NIST
- Scoring bins up to 6 mm away from the wire center (0.1 mm thick x 15 mm long)
- Geometry and material composition of wire and catheter provided by Sam Lott, Guidant Inc.

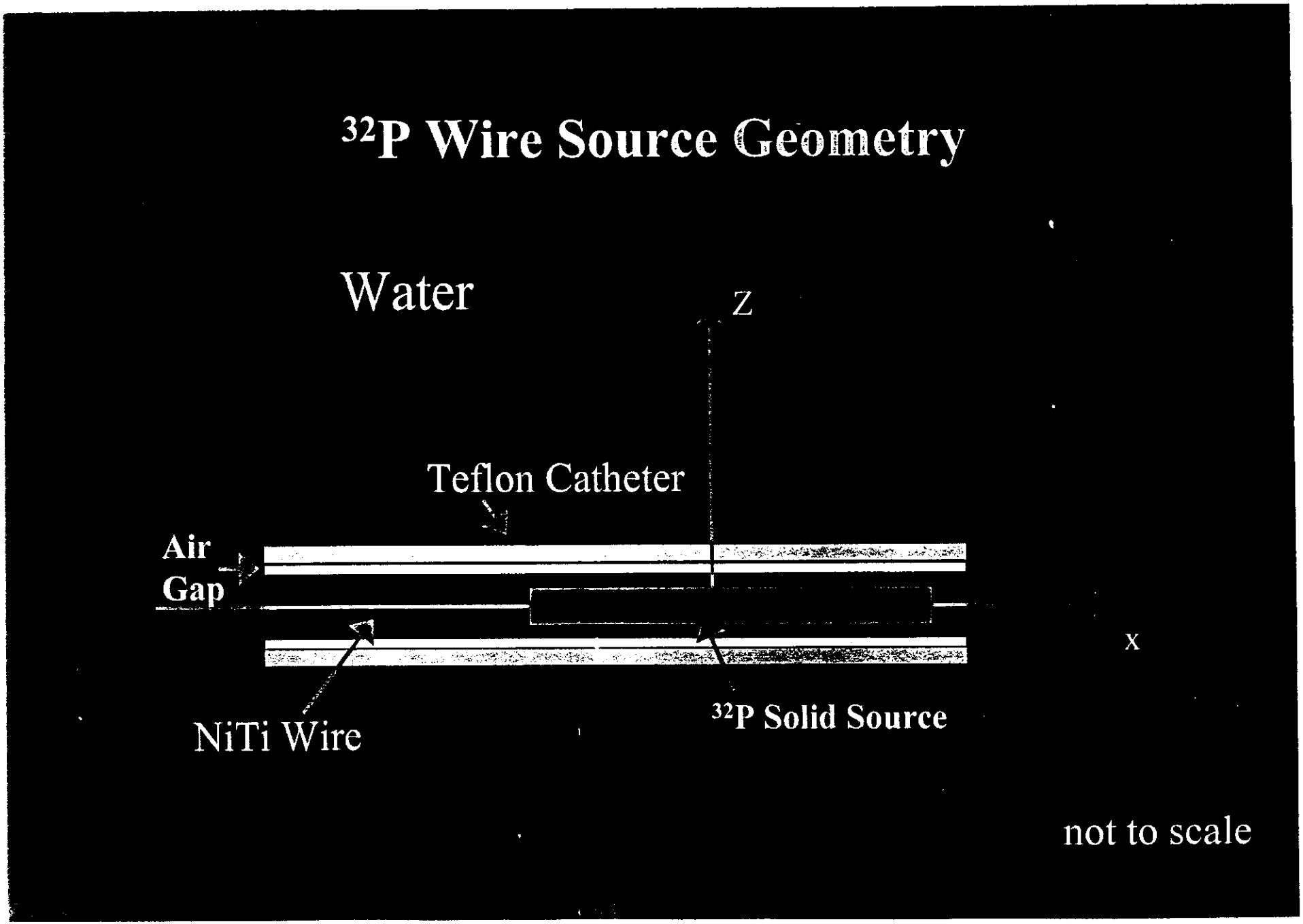
^{32}P Wire Source Geometry
Water
z
Teflon Catheter
Air
Gap
x
NiTi Wire
^{32}P Solid Source
not to scale

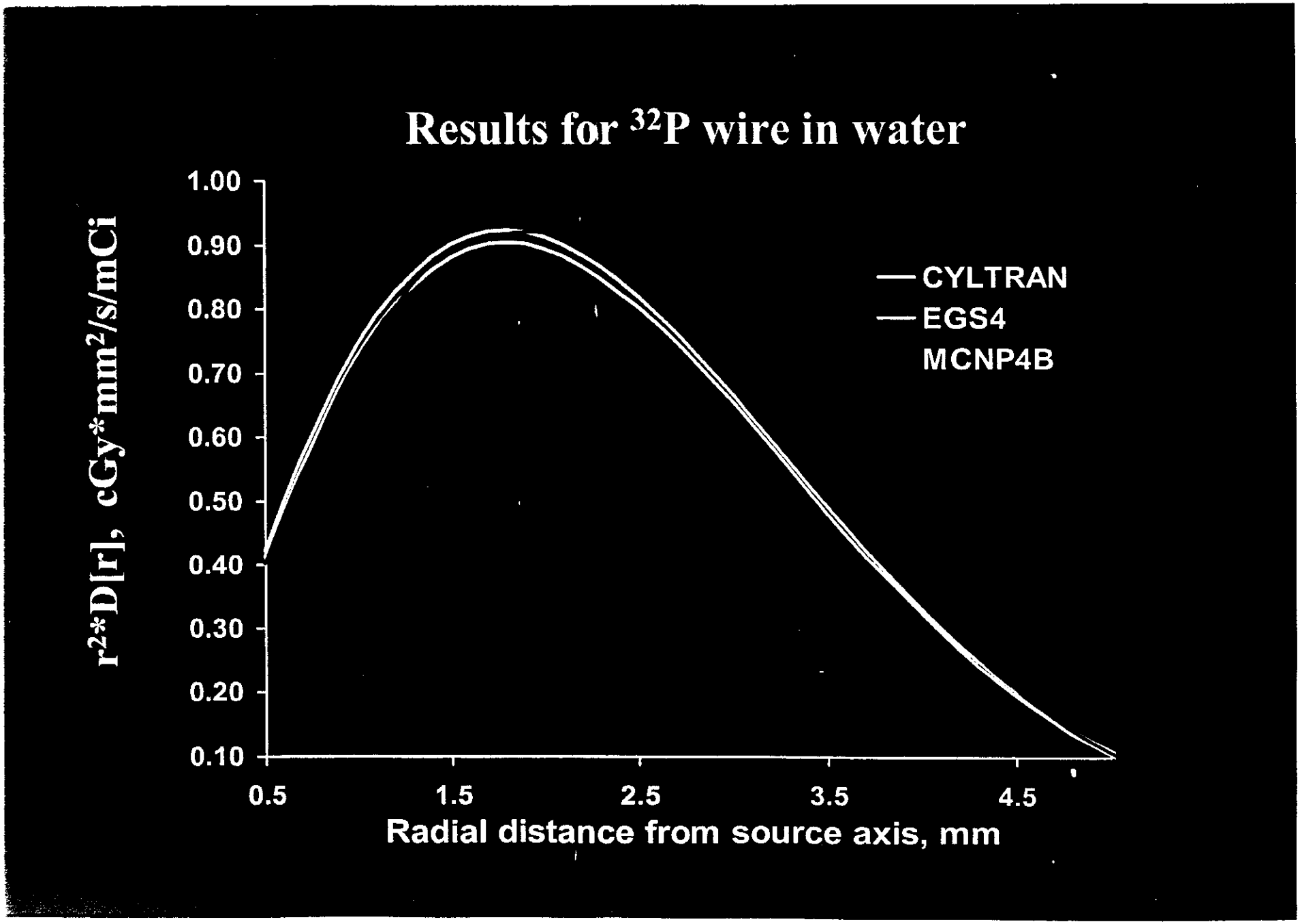
Results for ^{32}P wire in water
$r^2*D[r]$, cGy*mm^2/s/mCi
1.00
0.90
0.80
0.70
0.60
0.50
0.40
0.30
0.20
0.10
0.5
1.5
2.5
3.5
4.5
Radial distance from source axis, mm
CYLTRAN
EGS4
MCNP4B

Point kernels

- describe the distribution of absorbed dose around a point, isotropic emitter (*e.g.*, a radioactive atom),
- in an infinite, homogeneous medium,
- and are usually expressed in some scaled form.
- are a function only of single spatial variable, r

Uses

- by superposition, can apply to source distributed in energy and/or space
- originally developed for nuclear medicine applications

Advantages

- very fast, semi-analytic with no statistical fluctuations

Disadvantages

- does not account for boundaries and inhomogeneities,

Point-Kernel Method: Electrons

- Point kernel for monoenergetic electrons in water

$$F_o(r) = 4\pi r^2 \rho_w D_o(r) / E_o$$

- Point kernel for a beta spectrum in water

$$F(r) = \int_0^{E_{max}} (E_o / E_{av})\, S(E_o)\, F_o(r)\, dE_o$$

- Dose (or dose rate) from uniform volume source (per electron)

$$D(r) = \frac{E_{av}}{4\pi\rho V} \int_V \frac{F(|\vec{r}-\vec{r}'|)}{|\vec{r}-\vec{r}'|^2}\, dV$$

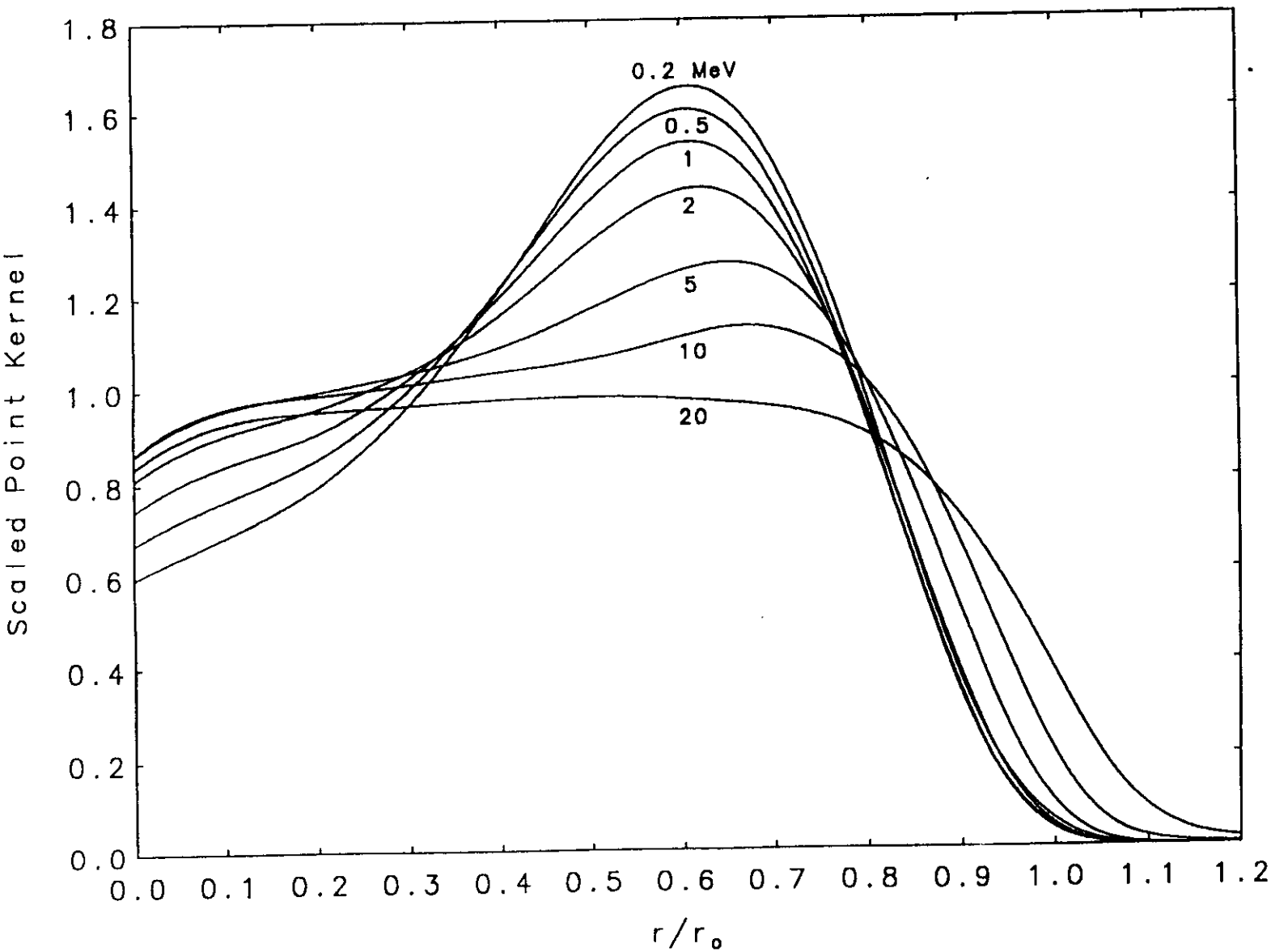
Scaled Point Kernel
1.8
1.6
1.4
1.2
1.0
0.8
0.6
0.4
0.2
0.0
0.2 MeV
0.5
1
2
5
10
20
0.0 0.1 0.2 0.3 0.4 0.5 0.6 0.7 0.8 0.9 1.0 1.1 1.2
r/r₀

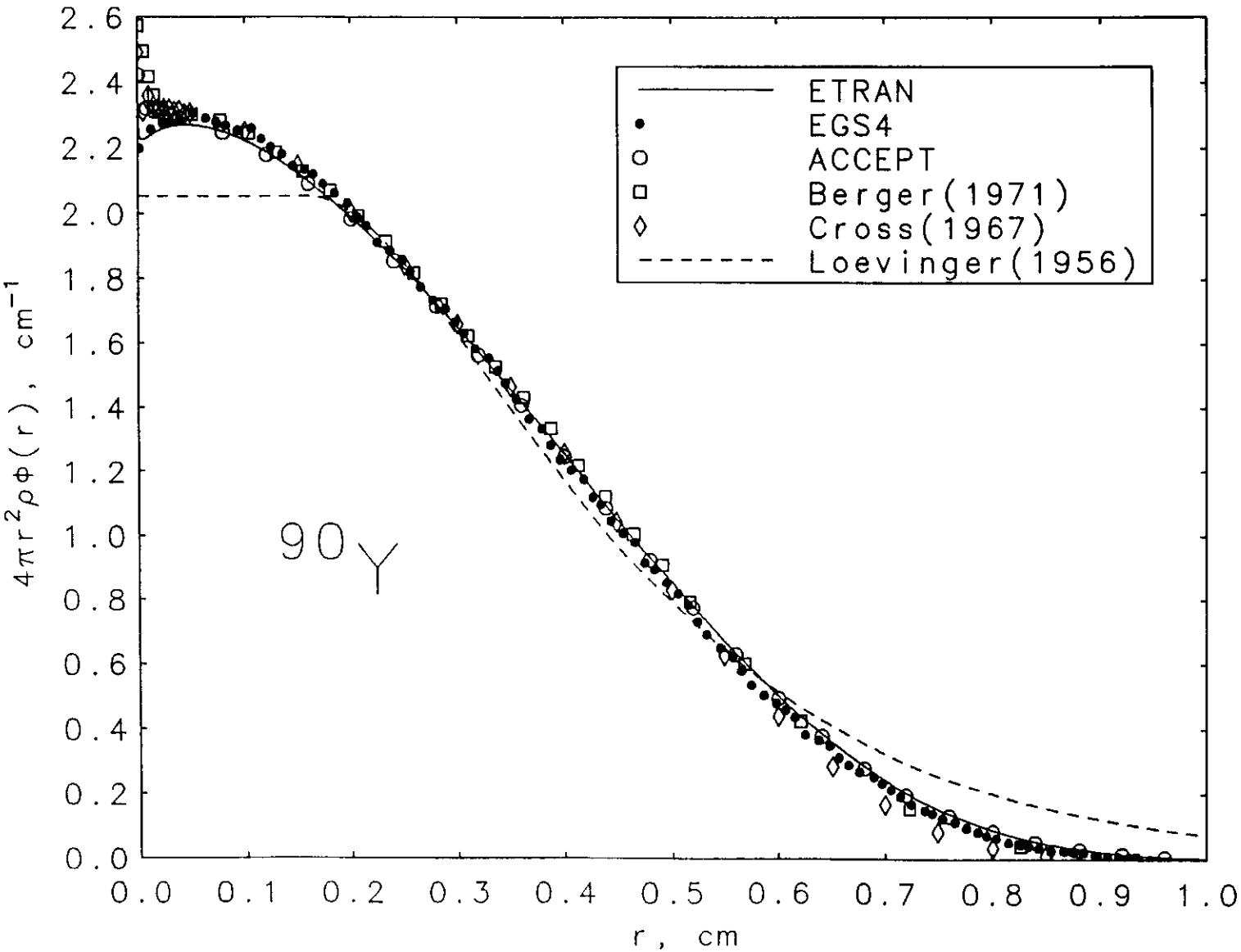
ETRAN
EGS4
ACCEPT
Berger(1971)
Cross(1967)
Loevinger(1956)
90Y
$4\pi r^2 \rho \Phi(r)$, cm^{-1}
r, cm
0.0
0.2
0.4
0.6
0.8
1.0
1.2
1.4
1.6
1.8
2.0
2.2
2.4
2.6
0.0
0.1
0.2
0.3
0.4
0.5
0.6
0.7
0.8
0.9
1.0

Point-Kernel Method: Electrons

- Include non-water materials along each ray *r*-*r*' by scaling approximation

$$F(r) = \eta\, F_w(\eta\, r\, \rho / \rho_w)$$

where $\eta = \eta(Z_{eff})$, and $Z_{eff} = [\Sigma\omega_i Z_i^2/A_i] \,/\, [\Sigma\omega_i Z_i/A_i]$.

- The scaling parameter for a range of applications has been developed by Cross (ICRU Report 56).

- Simple density scaling: $\eta = 1$.

Scaling parameters:

$$\eta_{Cross} = \left[0.777 + \langle Z \rangle (0.03756 - 0.00066\langle Z \rangle)\right] \frac{r_0^{water}(500\,keV)}{r_0^{med}(500\,keV)}$$

$$\eta_{Berger} = \left[1 + 0.02252(\langle Z \rangle - 6.60)\right] \frac{S_{med}(200\,keV)}{S_{water}(200\,keV)}$$

where S is mass collision stopping power

Material	<Z>	ρ (g/cm^3)	η (Cross)	η (Berger)
polyethylene	4.75	0.924	0.997	1.018
nylon 12	5.16	1.01	0.980	0.997
polystyrene	5.29	1.06	0.936	0.950
A150	5.49	1.127	0.968	0.982
polyurethane	5.74	1.09	0.965	0.975
PMMA	5.85	1.19	0.948	0.957
WT1	5.95	1.02	0.957	0.966
kapton	6.22	1.42	0.903	0.909
mylar	6.24	1.40	0.918	0.924
tissue (ICRU 4 component)	6.50	1.0	0.984	0.988
water	6.60	1.0	1.0	1.0
air	7.36	0.001205	0.901	0.899
5%Xe+95%CO_2	12.78	0.005992	0.968	0.956
Ni/Ti alloy	25.36	6.5	0.908	0.978
stainless steel (302)	25.71	8.06	0.896	0.970
plaque (0% apatite)	5.01	1.07	0.979	0.997
plaque (10% apatite)	5.82	1.14	0.985	0.993
plaque (20% apatite)	6.65	1.23	0.987	0.992
plaque (30% apatite)	7.50	1.34	0.989	0.988

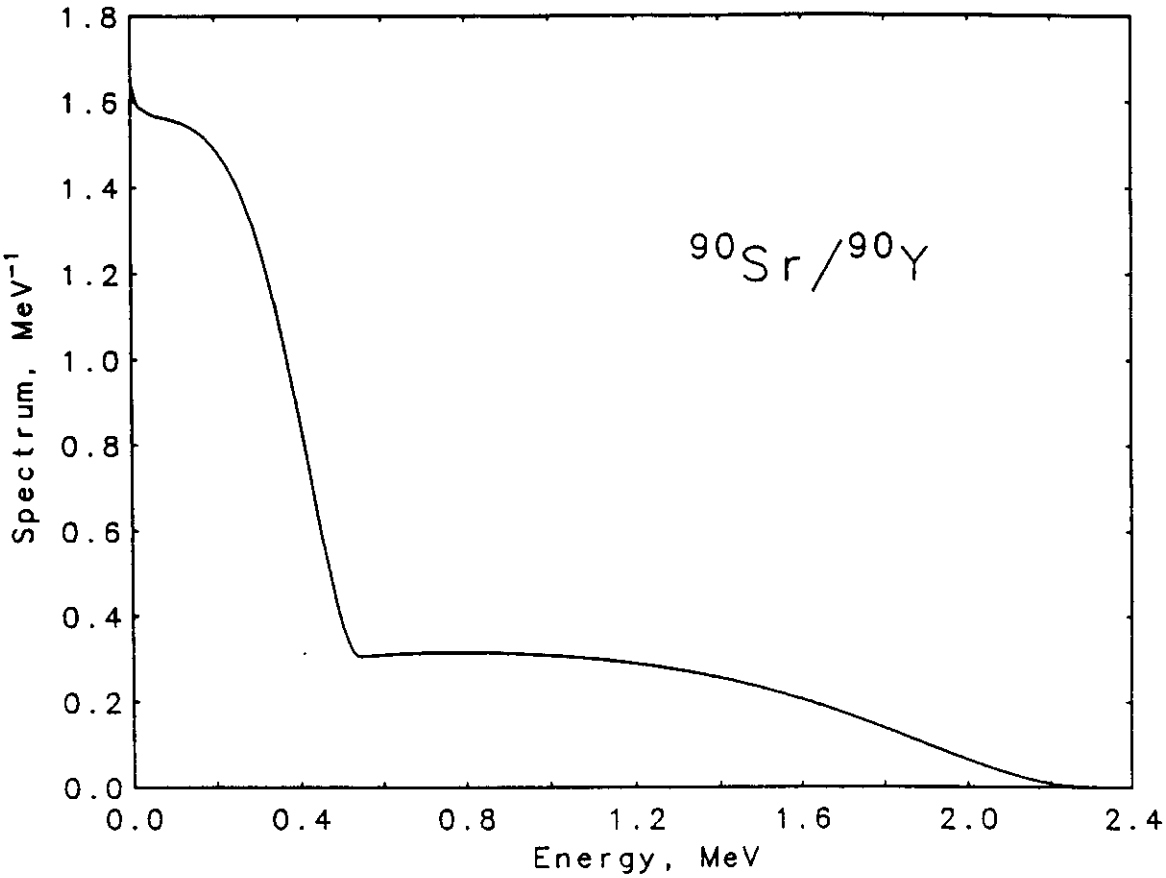
1.8
1.6
1.4
1.2
1.0
0.8
0.6
0.4
0.2
0.0
Spectrum, MeV^{-1}
^{90}Sr/^{90}Y
0.0
0.4
0.8
1.2
1.6
2.0
2.4
Energy, MeV

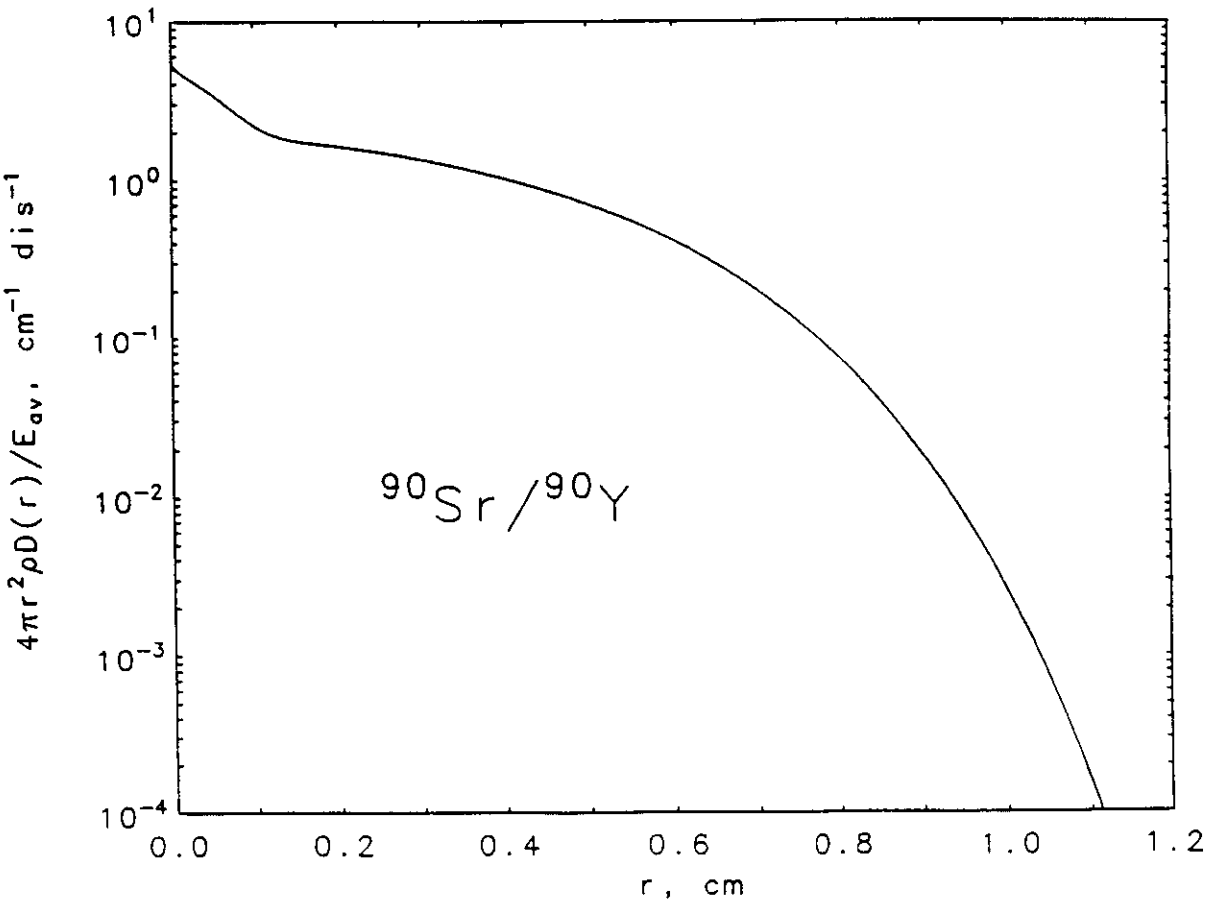
10^{1}
10^{0}
10^{-1}
10^{-2}
10^{-3}
10^{-4}
$4\pi r^2 \rho D(r)/E_{av}$, cm^{-1} dis^{-1}
^{90}Sr/^{90}Y
0.0
0.2
0.4
0.6
0.8
1.0
1.2
r, cm

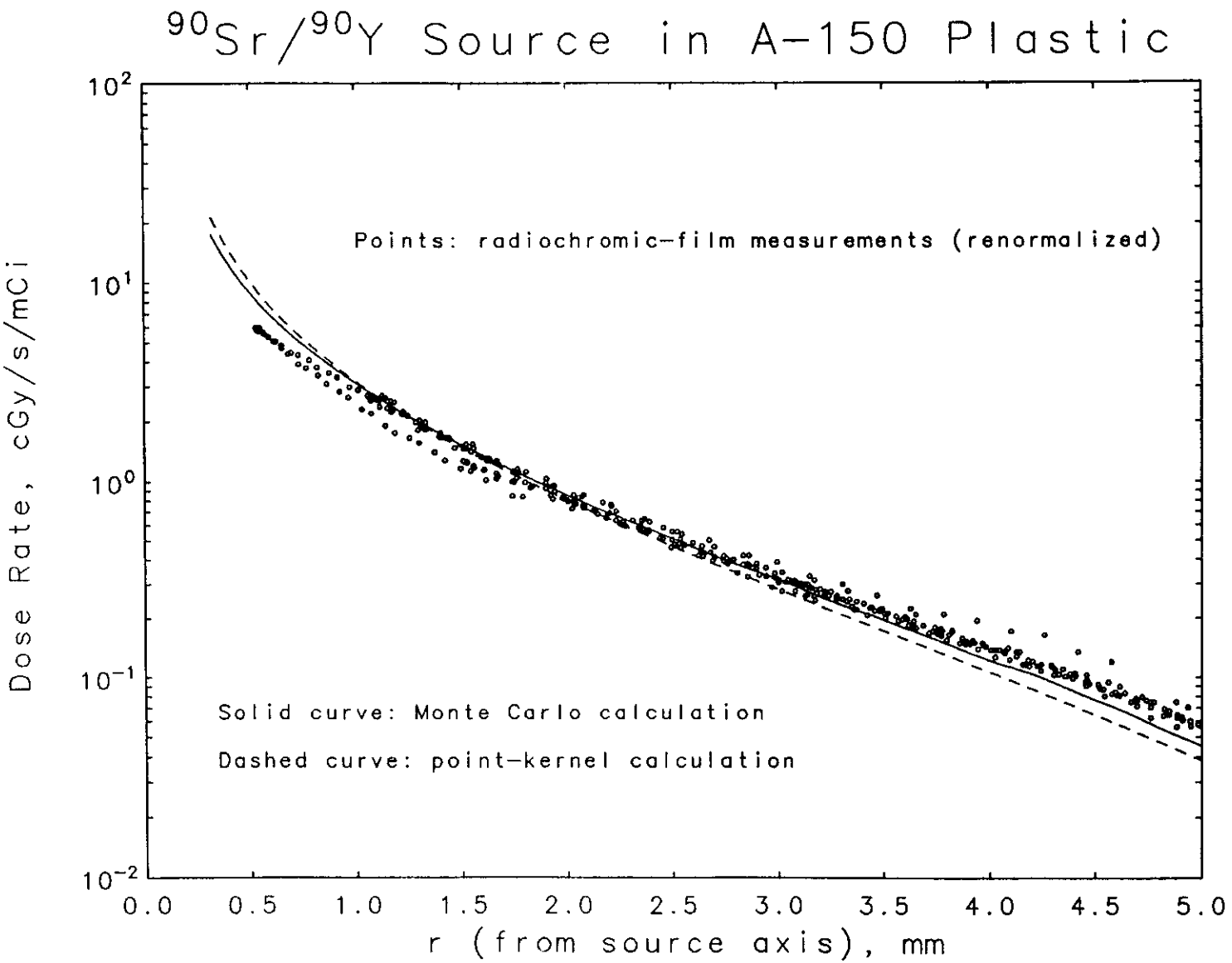
$^{90}Sr/^{90}Y$ Source in A-150 Plastic
Points: radiochromic-film measurements (renormalized)
Solid curve: Monte Carlo calculation
Dashed curve: point-kernel calculation
Dose Rate, cGy/s/mCi
10^{2}
10^{1}
10^{0}
10^{-1}
10^{-2}
0.0
0.5
1.0
1.5
2.0
2.5
3.0
3.5
4.0
4.5
5.0
r (from source axis), mm

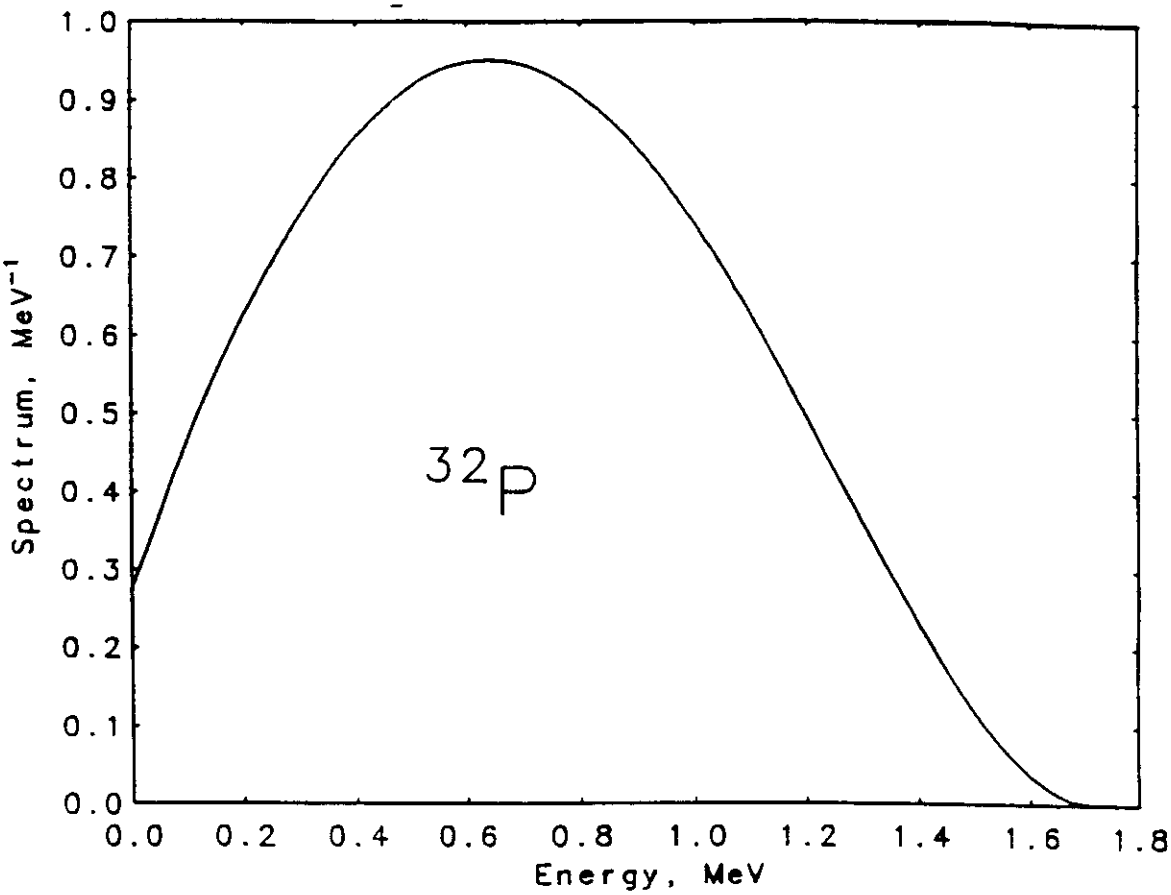
1.0
0.9
0.8
0.7
0.6
0.5
0.4
0.3
0.2
0.1
0.0
Spectrum, MeV^{-1}
^{32}P
0.0
0.2
0.4
0.6
0.8
1.0
1.2
1.4
1.6
1.8
Energy, MeV

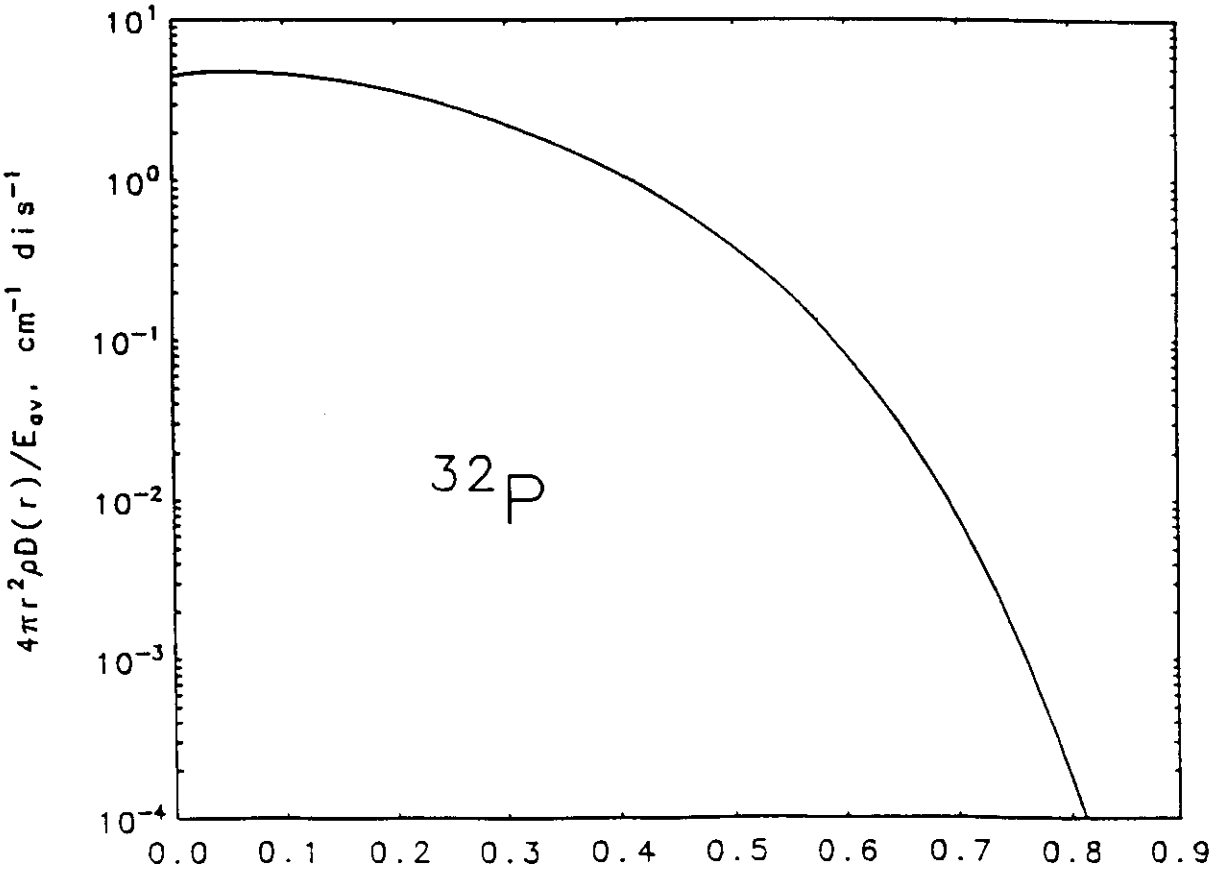
10^{1}
10^{0}
10^{-1}
10^{-2}
10^{-3}
10^{-4}
$4\pi r^2 \rho D(r)/E_{av}$, cm^{-1} dis^{-1}
^{32}P
0.0
0.1
0.2
0.3
0.4
0.5
0.6
0.7
0.8
0.9

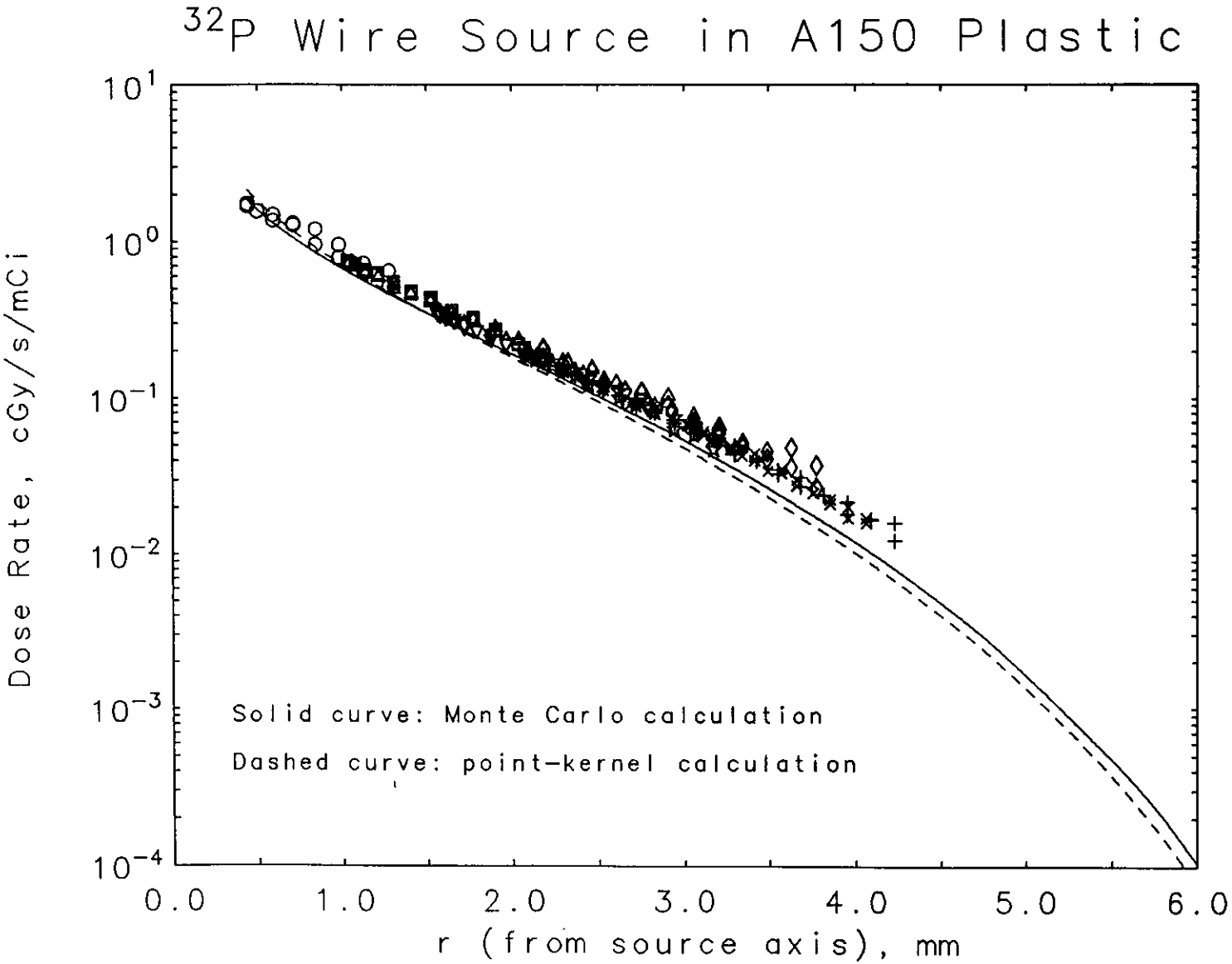
^{32}P Wire Source in A150 Plastic
Dose Rate, cGy/s/mCi
10^{1}
10^{0}
10^{-1}
10^{-2}
10^{-3}
10^{-4}
0.0
1.0
2.0
3.0
4.0
5.0
6.0
r (from source axis), mm
Solid curve: Monte Carlo calculation
Dashed curve: point-kernel calculation

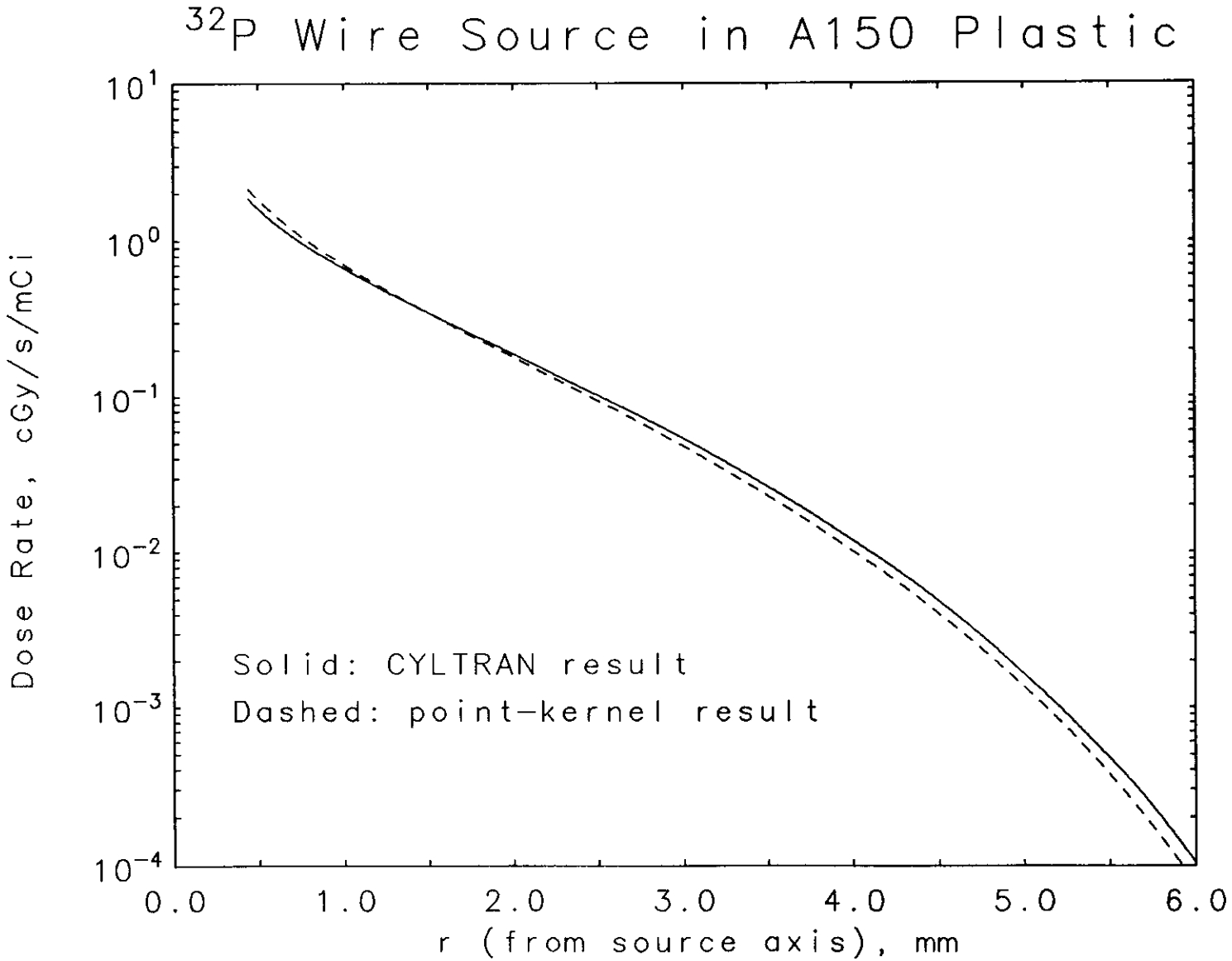
^{32}P Wire Source in A150 Plastic
Dose Rate, cGy/s/mCi
10^{1}
10^{0}
10^{-1}
10^{-2}
10^{-3}
10^{-4}
Solid: CYLTRAN result
Dashed: point-kernel result
0.0
1.0
2.0
3.0
4.0
5.0
6.0
r (from source axis), mm

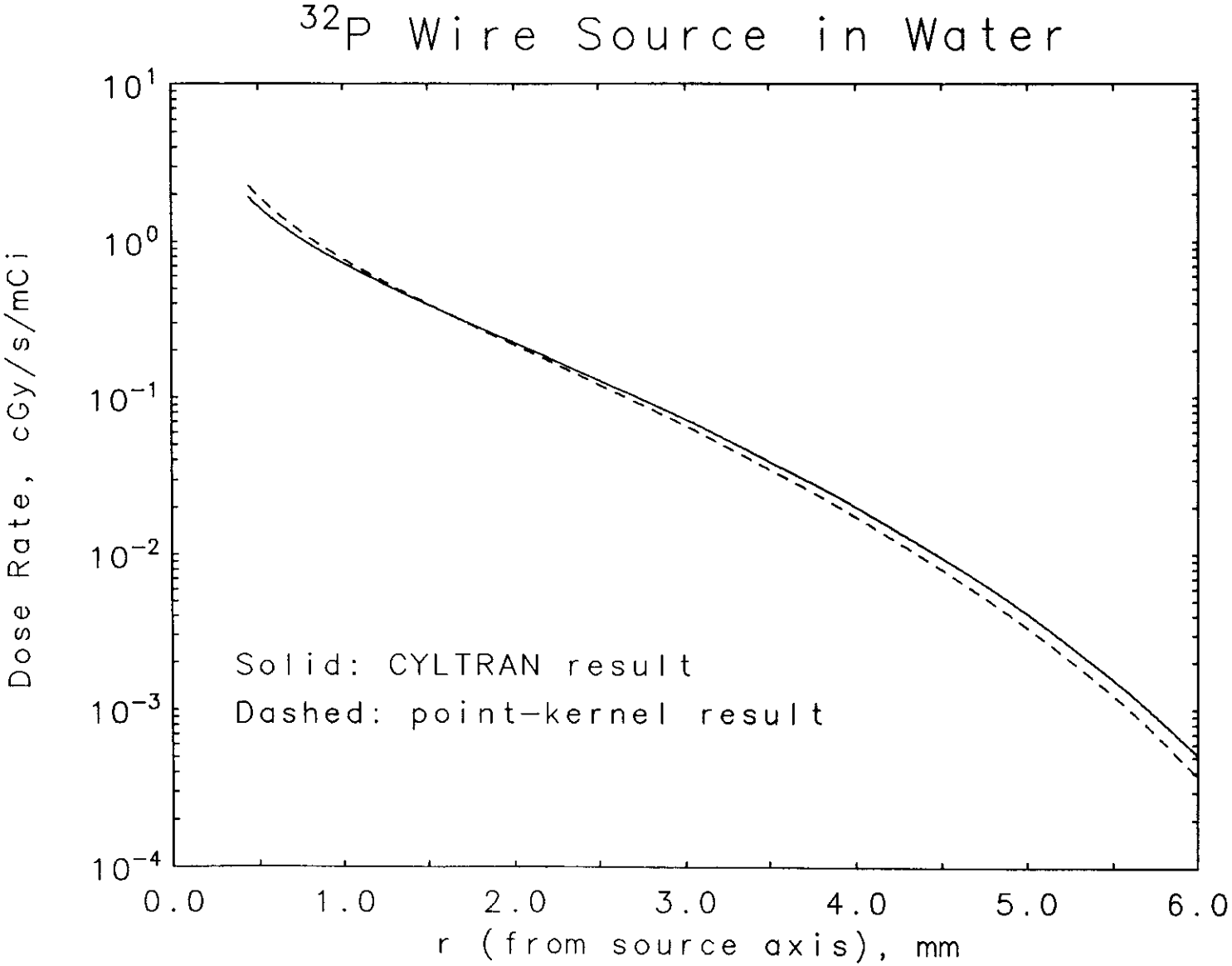
^{32}P Wire Source in Water
Dose Rate, cGy/s/mCi
10^{1}
10^{0}
10^{-1}
10^{-2}
10^{-3}
10^{-4}
Solid: CYLTRAN result
Dashed: point-kernel result
0.0
1.0
2.0
3.0
4.0
5.0
6.0
r (from source axis), mm

Point-Kernel Method: Photons

- Dose (or dose rate) from uniform volume source (per photon of energy E)

$$D(r) = \frac{E\,\mu_{en}(E)}{4\pi\rho V}\int_V T(E,|\vec{r}-\vec{r}'|)\;B_{en}(E,\mu(E)\,|\vec{r}-\vec{r}'|)\;\frac{e^{-\mu(E)\,|\vec{r}-\vec{r}'|}}{|\vec{r}-\vec{r}'|^2}\,dV$$

where B_{en} is the energy-absorption build-up factor for water.

- Include non-water materials along each ray r-r' by taking into account appropriate attenuation coefficient μ

$$\mu(E)\,r = \sum_j \mu_j(E)\,r_j$$

and using simple density scaling for $T(r)$, the transition-to-electronic-equilibrium function for water.

- Transition function $T(r)$ is assumed to be a universal function of $r/r_{eff}(E)$, where $r_{eff}(E)$ is the weighted average of the maximum csda ranges of the secondary electrons produced in the interaction.

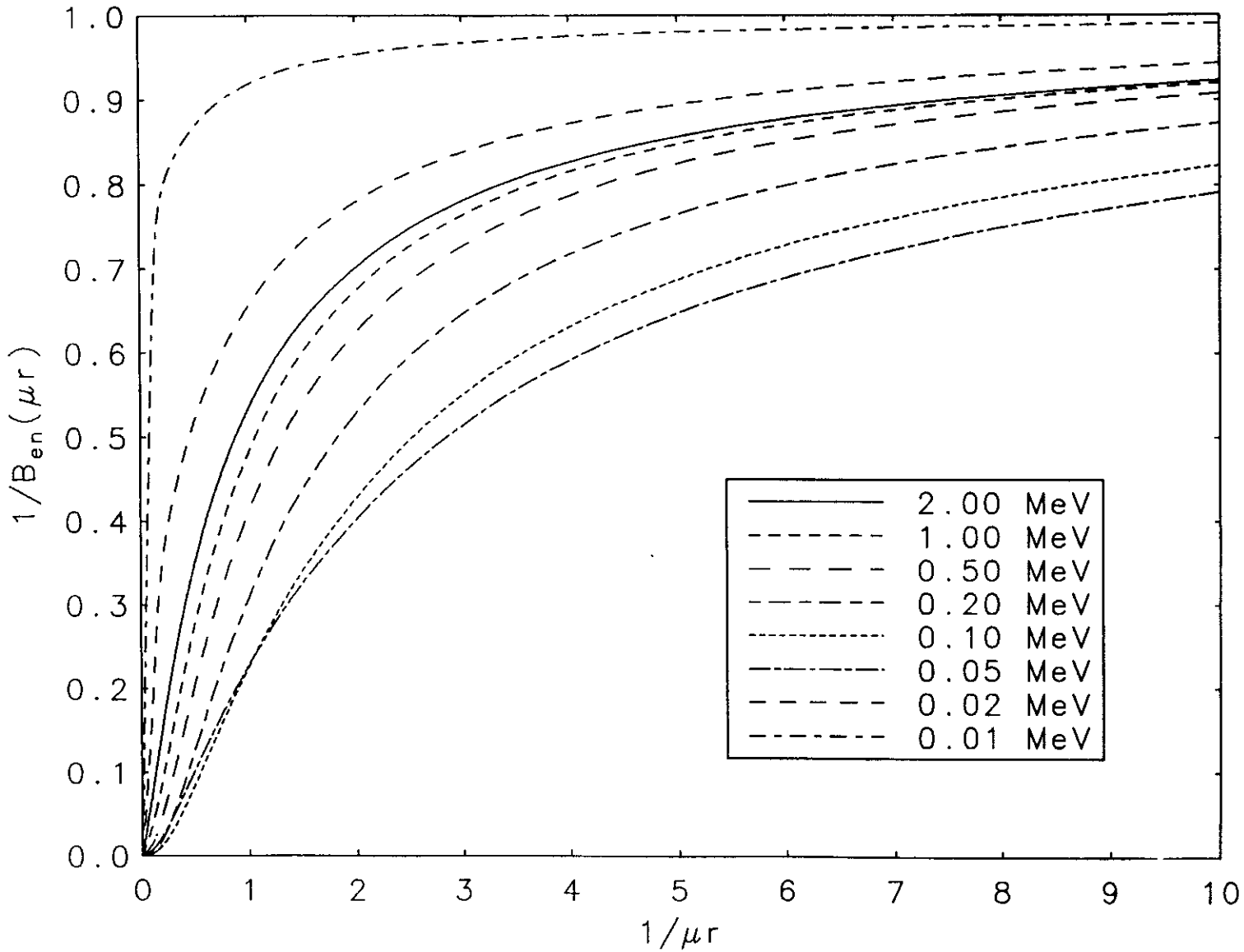
1.0
0.9
0.8
0.7
0.6
0.5
0.4
0.3
0.2
0.1
0.0
1/Ben(μr)
0
1
2
3
4
5
6
7
8
9
10
1/μr
2.00 MeV
1.00 MeV
0.50 MeV
0.20 MeV
0.10 MeV
0.05 MeV
0.02 MeV
0.01 MeV

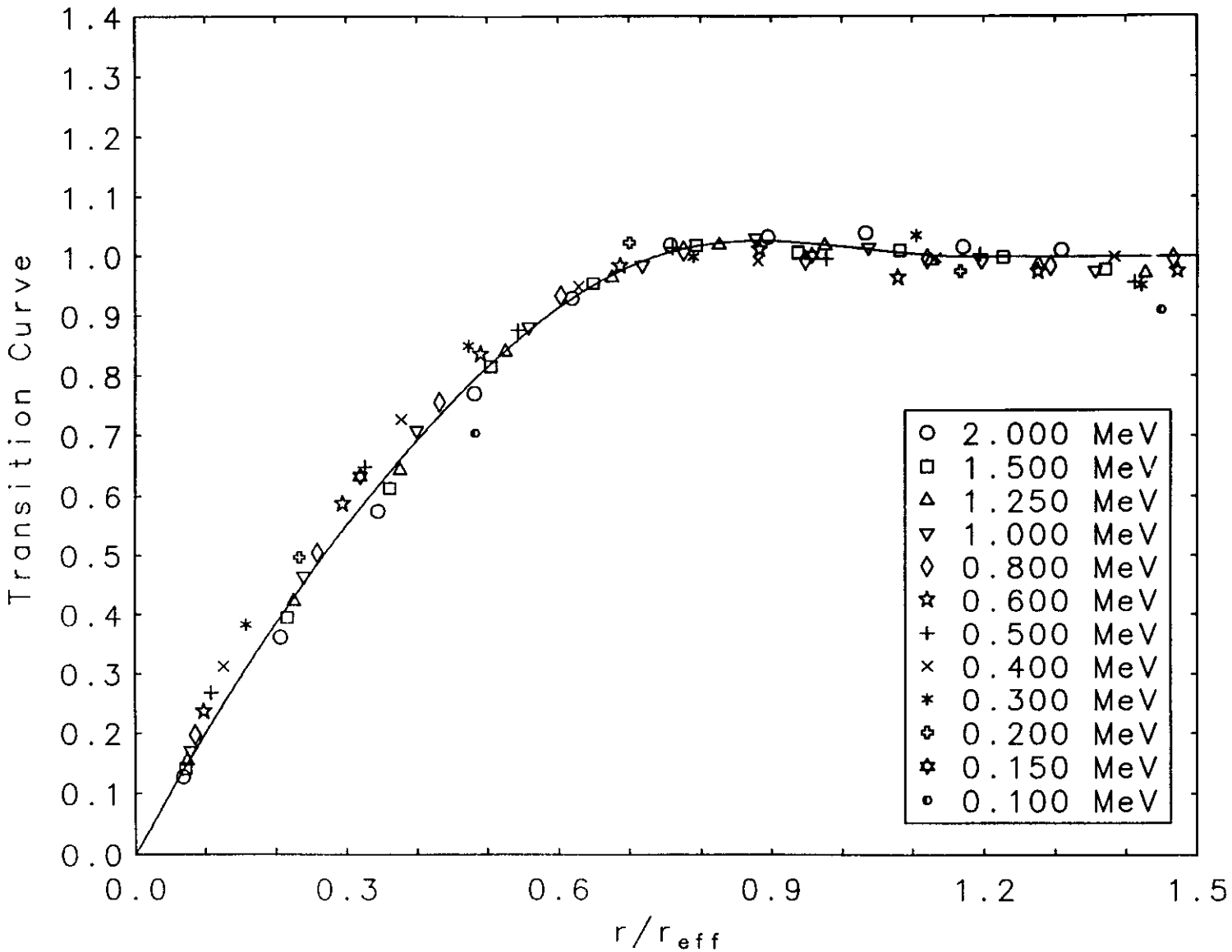
Transition Curve
1.4
1.3
1.2
1.1
1.0
0.9
0.8
0.7
0.6
0.5
0.4
0.3
0.2
0.1
0.0
0.0
0.3
0.6
0.9
1.2
1.5
r/r_eff
2.000 MeV
1.500 MeV
1.250 MeV
1.000 MeV
0.800 MeV
0.600 MeV
0.500 MeV
0.400 MeV
0.300 MeV
0.200 MeV
0.150 MeV
0.100 MeV

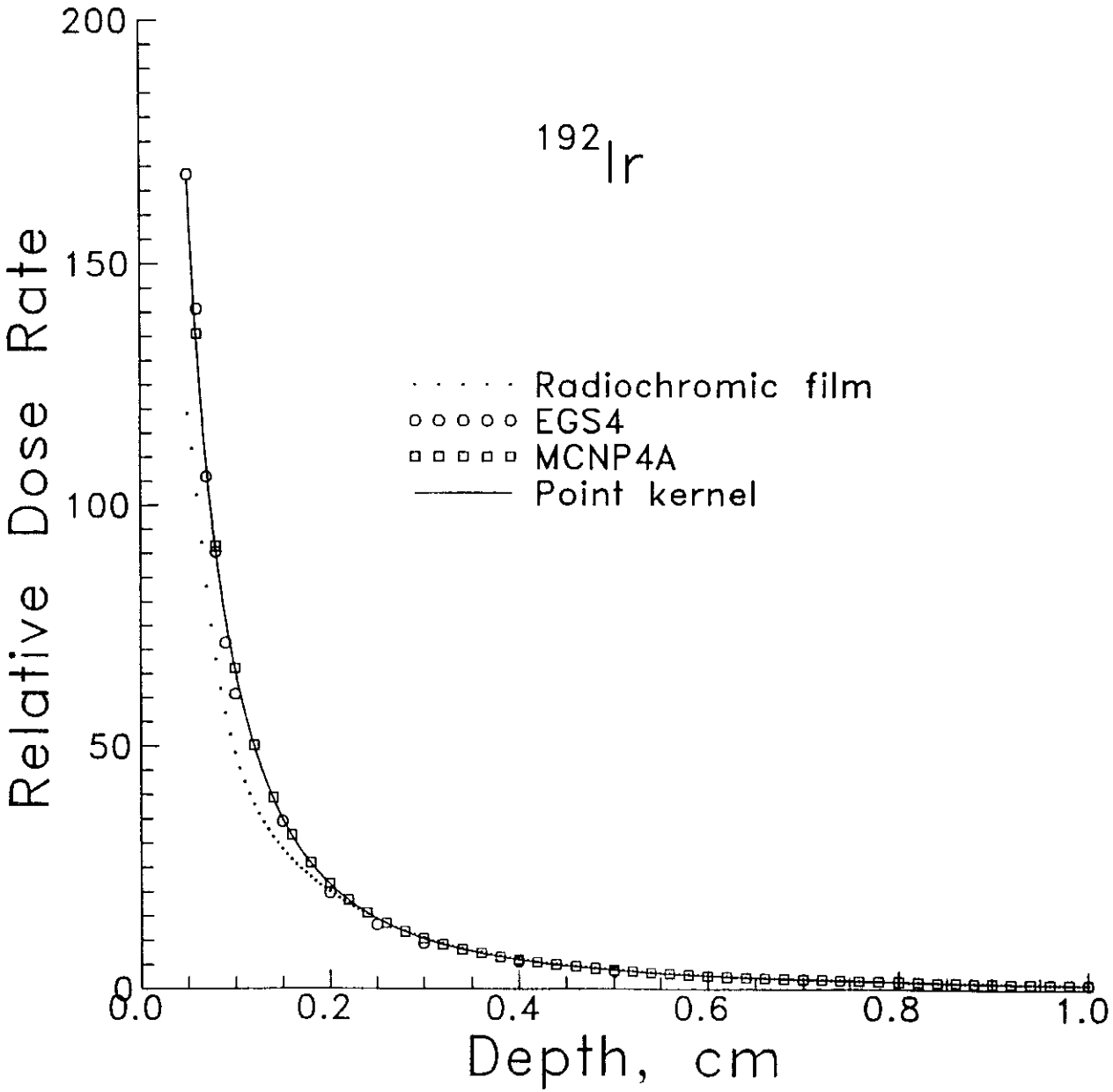
^{192}Ir
Radiochromic film
EGS4
MCNP4A
Point kernel
Relative Dose Rate
200
150
100
50
0
0.0
0.2
0.4
0.6
0.8
1.0
Depth, cm

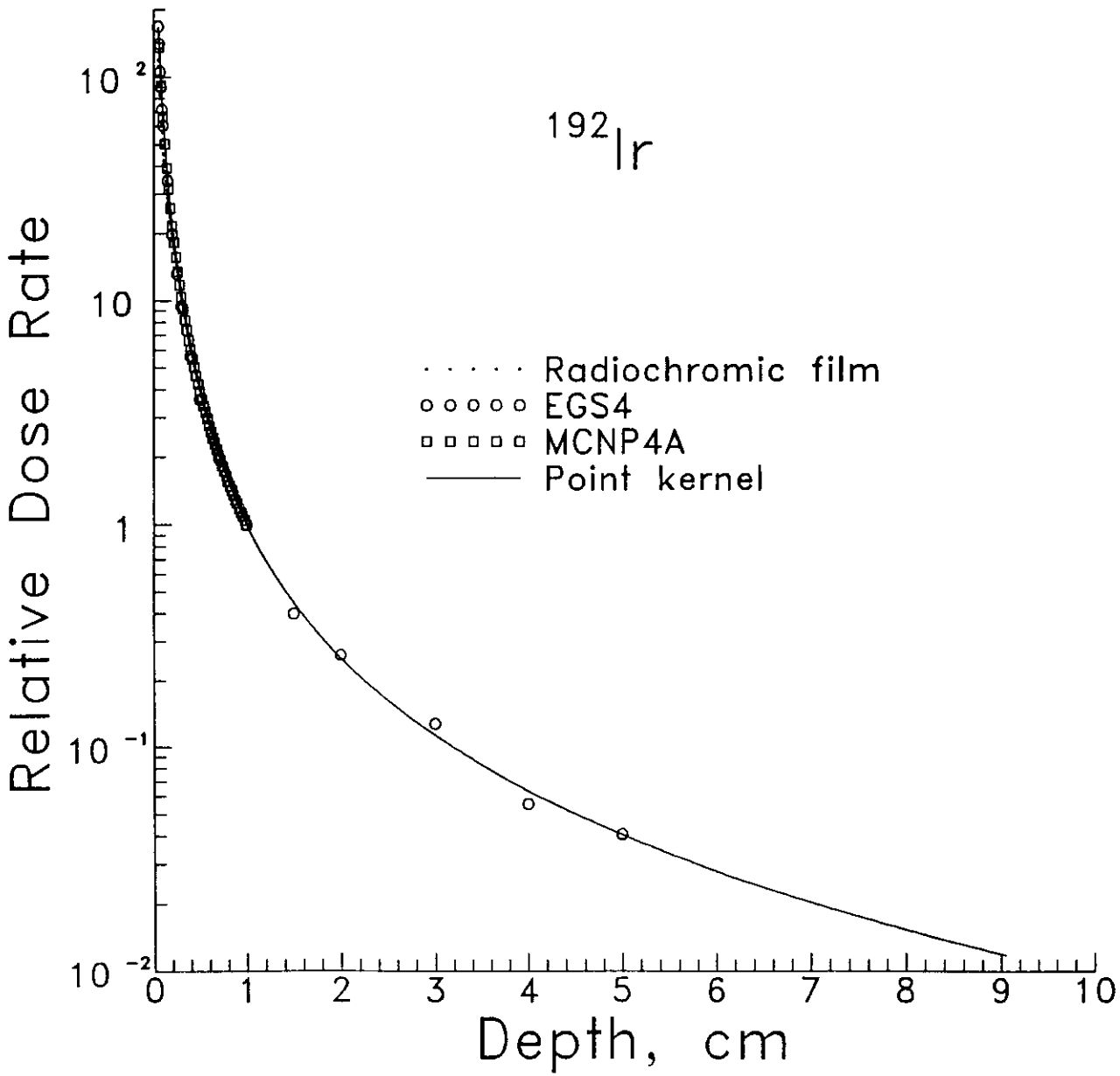
^{192}Ir
Relative Dose Rate
10^{2}
10
1
10^{-1}
10^{-2}
Radiochromic film
EGS4
MCNP4A
Point kernel
0
1
2
3
4
5
6
7
8
9
10
Depth, cm